DESIGN OF A TRAVERSE SYSTEM FOR THE CHARACTERIZATION OF A LARGE-SCALE WIND TUNNEL

A THESIS SUBMITTED TO
THE GRADUATE SCHOOL OF NATURAL AND APPLIED SCIENCES
OF
MIDDLE EAST TECHNICAL UNIVERSITY

BY

TUNAHAN ULU

IN PARTIAL FULFILLMENT OF THE REQUIREMENTS
FOR
THE DEGREE OF MASTER OF SCIENCE
IN
AEROSPACE ENGINEERING

SEPTEMBER 2022

Approval of the thesis:

DESIGN OF A TRAVERSE SYSTEM FOR THE CHARACTERIZATION OF A LARGE-SCALE WIND TUNNEL

submitted by **TUNAHAN ULU** in partial fulfilment of the requirements for the degree of **Master of Science** i**n Aerospace Engineering, Middle East Technical University** by,

Prof. Dr. Halil Kalıpçılar
Dean, Graduate School of **Natural and Applied Sciences** _____

Prof. Dr. Serkan Özgen
Head of the Department, **Aerospace Engineering** _____

Asst. Prof. Dr. Mustafa Perçin
Supervisor, Aerospace Engineering, METU _____

Examining Committee Members:

Prof. Dr. Oğuz Uzol
Aerospace Engineering, METU _____

Asst. Prof. Dr. Mustafa Perçin
Aerospace Engineering, METU _____

Prof. Dr. Mehmet Metin Yavuz
Mechanical Engineering, METU _____

Prof. Dr. Mehmet Şerif Kavsaoğlu
Airframe and Powerplant Maintenance Eng, ESTU _____

Asst. Prof. Dr. Onur Baş
Mechanical Engineering, TEDU _____

Date: 02.09.2022

I hereby declare that all information in this document has been obtained and presented in accordance with academic rules and ethical conduct. I also declare that, as required by these rules and conduct, I have fully cited and referenced all material and results that are not original to this work.

Name Last name : Tunahan, Ulu

Signature :

ABSTRACT

DESIGN OF A TRAVERSE SYSTEM FOR THE CHARACTERIZATION OF A LARGE-SCALE WIND TUNNEL

Ulu, Tunahan
Master of Science, Aerospace Engineering
Supervisor: Asst. Prof. Dr. Mustafa Perçin

September 2022, 97 pages

This study presents the design and simulations of a traverse system and preliminary characterization measurements of the RÜZGEM large-scale wind tunnel. In the first phase of the study, the traverse system was simulated aerodynamically using computational fluid dynamics (CFD) tools. The effects of the rectangular, whole profile and partial profile traverse mechanisms on the measurements were examined. The probe lengths were studied in detail to determine the most suitable length. According to the simulations, the expected maximum error is 1.3% for velocity measurement. In the second phase of the study, the simulated traverse system is integrated to wind tunnel test sections. The dynamic stability was measured as ±9% in the boundary layer test section (BLTS) at a freestream of 14.8 m/s, which is at the same level as the uncertainty range of the pressure scanner. The dynamic stability in the aeronautical test section (ATS) was obtained as ±1% and ±0.5% at freestream velocities of 35.1 m/s and 70.9 m/s, respectively. The velocity distribution in the measured plane of BLTS and ATS shows that 60% and 5% variation from the center to the wall are expected for test sections, respectively. In terms of angularity in test sections of RÜZGEM, 4° pitch angle in BLTS and 3° pitch angle in ATS were measured. In order to assess the effect of the traverse system on the angularity measurements, 2D simulations and measurements with a strut-type support system were performed. The results of the simulations revealed that the lateral support of

the traverse system causes 3° of flow deviation in the five-hole probe position. This is also justified by the decreasing measured pitch angle obtained in the measurements with a strut-type support system. These results suggest that the traverse system influences flow angularity measurements in the wind tunnel and should be re-configured for proper characterization measurements.

Keywords: Wind Tunnel Test, Wind Tunnel Characterization, Experimental Aerodynamics, Five-Hole Probe Measurements

ÖZ

BÜYÜK ÖLÇEKLİ RÜZGAR TÜNELİ KARAKTERİZASYON ÖLÇÜMLERİ İÇİN TRAVERS SİSTEMİ TASARIMI

Ulu, Tunahan

Yüksek Lisans, Havacılık ve Uzay Mühendisliği
Tez Yöneticisi: Dr. Öğr. Üyesi Mustafa Perçin

Eylül 2022, 97 sayfa

Bu çalışma, RÜZGEM büyük ölçekli rüzgâr tüneli travers sistem tasarımını, simülasyonlarını ve karakterizasyon ölçümlerini sunmaktadır. Çalışmanın ilk aşamasında, travers sistem, hesaplamalı akışkanlar dinamiği (HAD) araçları kullanılarak aerodinamik olarak simüle edilmiştir. Dikdörtgen, tam profil ve kısmi profil travers mekanizmalarının ölçümler üzerindeki etkileri incelenmiştir. Uygun prob uzunluğunu belirlemek için farklı konumları prob uzunlukları detaylı olarak incelenmiştir. Simülasyon sonuçlarına göre hız ölçümünde beklenen en yüksek hata %1.3'tür. Çalışmanın ikinci aşamasında, simülasyonları tamamlanmış travers sistemi rüzgâr tüneli test kesitlerine entegre edilmiştir. Dinamik kararlılık, 14.8 m/s'lik bir serbest akışta sınır tabaka test kesiti (TK2) için ±%9 olarak ölçülmüştür. Bu değer ölçümlerde kullanılan basınç tarayıcının belirsizliği ile benzer seviyelerdedir. Havacılık test kesiti (TK1) için 35.1 m/s ve 70.9 m/s'lik serbest akışlarda dinamik kararlılık ±%1 ve ±%0.5 olarak ölçülmüştür. TK2 ve TK1'in ölçüm kesitindeki hız dağılımı, test kesitleri için hızın merkezden duvara sırasıyla %60 ve %5 değiştiğini göstermektedir. Tünelin test kesitlerinde serbest akış açısı açısından TK2'de 4°, TK1'de 3° dikey yönde açı ölçülmüştür. Travers sisteminin açı

ölçümleri üzerindeki etkisini incelemek için iki boyutlu sayısal simülasyonlar ve dikme tipi destek sistemi ile ölçümler yapılmıştır. Sayısal simülasyonların sonuçları, travers sisteminin alt desteğinin, beş delikli prob konumunda akışta 3° sapma olduğunu ortaya koymuştur. Bu aynı zamanda, dikme tipi destek sistemi ile yapılan ölçümlerde elde edilen azalan ölçülen akış açısı ile de doğrulanmaktadır. Bu sonuçlar, travers sisteminin tünel test kesiti içerisinde ölçümleri etkilediğini ve uygun karakterizasyon ölçümleri için yeniden yapılandırılması gerektiğini göstermektedir.

Anahtar Kelimeler: Rüzgâr Tüneli Testi, Rüzgâr Tüneli Karakterizasyonu, Deneysel Aerodinamik, 5-Delilkli Prob Ölçümleri

Zordur,

En ufak bir bilgiye ulaşmak

Emek harcamak, başarmak,

Kendine güvenmek bazen, ne yapacağından emin olmadan

Zordur,

Doğru sonuca ulaşmak,

Çabalamak, başarmak

Tekrarlamak bazen, ne yapacağından emin olmadan

Tüm zorlukları daha kolay hale getirelim..

Oğlum Yavuz Ulu, Ağustos 2022'de aramızda..

ACKNOWLEDGMENTS

I would like to thank my supervisor Asst. Prof. Dr. Mustafa Perçin for his guidance, patience and support.

I would like to express my sincere gratitude to Osman Yılmaz on behalf of Turkish Aerospace for supporting this thesis.

Also, I wish to thank to Dr. Anas Abdulrahim, Dr. Aytaç Şanlısoy, Onur Öktem, Batuhan Doğan and Mehmet Şahbaz for their endless patience.

Finally, I would like to express my thankful to my wife Esma for her love and support.

TABLE OF CONTENTS

LIST OF TABLES

TABLES

LIST OF FIGURES

FIGURES

LIST OF ABBREVIATIONS

METU-RÜZGEM	Middle East Technical University – Center for Wind Energy Research
CFD	Computational Fluid Dynamics
DOF	Degree of Freedom
PIV	Particle Image Velocimetry
PSP	Pressure Sensitive Paint
NWTC	National Wind Tunnel Complex
AMRL	Aeronautical and Maritime Research Laboratory
TDT	Transonic Dynamics Tunnel
ABLWT	Atmospheric Boundary Layer Wind Tunnel
TI	Turbulence Intensity
BL	Boundary Layer
ATS	Aeronautical Test Section
BLTS	Boundary Layer Test Section
OJTS	Open Jet Test Section
TSS	Test Section Start
TSE	Test Section End
TVR	Turbulence Viscous Ratio
FHP	Five-hole Probe
CFL	Courant Number

CP	Pressure coefficient
Q	Dynamic pressure
Q_∞	Free-stream dynamic pressure
ρ	Density
ρ_∞	Free-stream density
V	Velocity
V_∞	Free-stream velocity
U_X	Velocity along the X axis
U_Y	Velocity along the Y axis
U_Z	Velocity along the Z axis
$\overline{U}$	Mean velocity
u'	Velocity fluctuations
${u_X}'$	Velocity fluctuation along the X axis
${u_Y}'$	Velocity fluctuations along the Y axis
${u_Z}'$	Velocity fluctuations along the Z axis
M	Mach number
PT	Total pressure
PS	Static pressure
TT	Total temperature
TS	Static temperature
R	Universal gas constant
γ	Specific heat ratio

CHAPTER 1

INTRODUCTION

Wind tunnels are ground facilities that are used to investigate the effects of air flow on solid bodies. Wind tunnel tests are defined as activities performed in wind tunnels using specified and controlled flow conditions to analyze the impact of flow on a vehicle and/or a vehicle component. Generally, the objectives of wind tunnel tests are to generate aerodynamic forces, moment, and pressure database, to understand and assess the flow field characteristics, to simulate high-speed and low-speed conditions, to provide input for design activities, to support aerodynamic design studies and to validate the computational fluid dynamic simulations.

In this chapter, the type and definitions of wind tunnels, characterization requirements, details of the RÜZGEM large-scale wind tunnel, characterization plan and methods are given in detail. Finally, the scope and purpose of the thesis are presented.

1.1 Wind Tunnels

Wind tunnels are defined as facilities that are designed and built for the simulation of air flows around solid objects in a controlled manner. Mostly a scaled model of an actual body is used as a test model (sometimes referred as test article) in wind tunnel applications. Wind tunnels serve different industries such as the aviation industry, the automotive industry, the development of wind turbines/propellers/rotors, the simulation of atmospheric flows about bridges/buildings and also for the sports industry. Herein, Figure 1.1 give an overview to illustrate the effectiveness of wind tunnel testing.

Figure 1.1 Wind tunnel testing examples [1,2,3,4,5,6]

As a detailed example to emphasize the significance of wind tunnels, Figure 1.2 and Figure 1.3 show the position of wind tunnel testing in the development of the F-22 aircraft and the history of wind tunnel test hours for major programs, respectively.

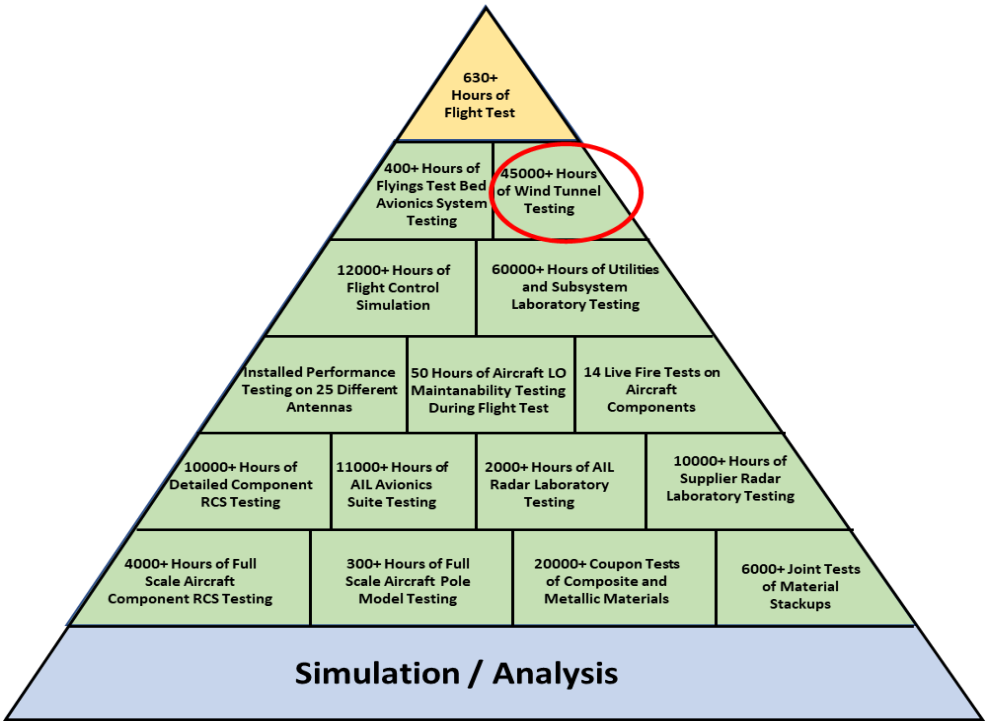

Figure 1.2 History of wind tunnel test hours for major aircraft programs [7]

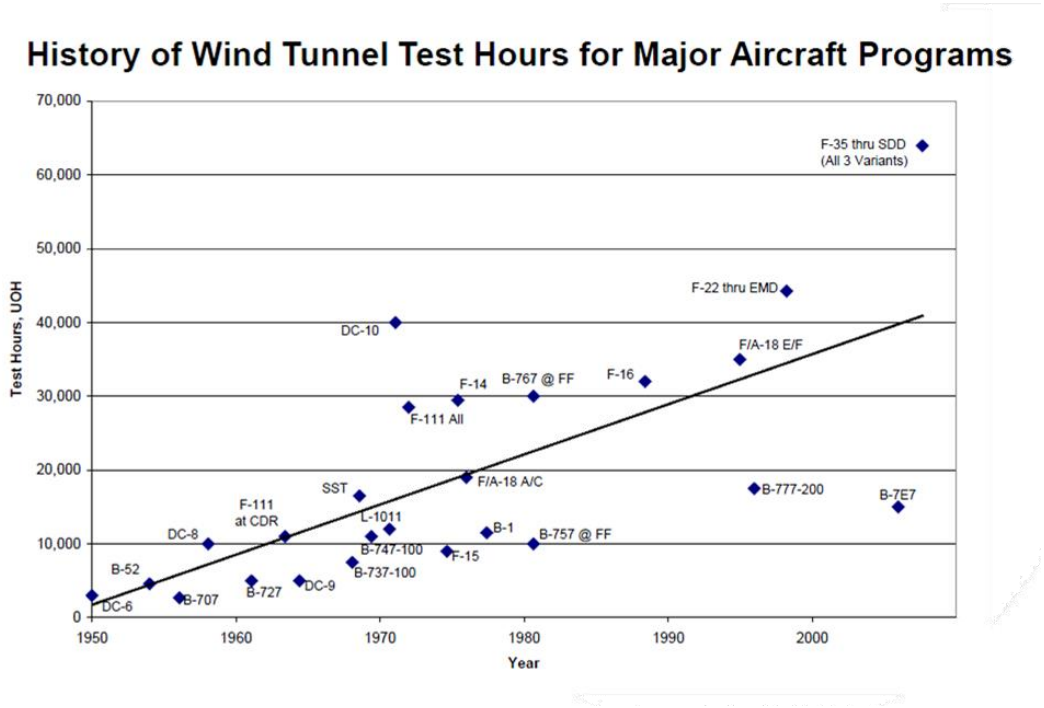

Figure 1.3 Wind tunnel test hours in some major aircraft development programs in history [8]

1.1.1 Types of Wind Tunnels

Wind tunnels are categorized based on flow regimes and structural designs. Mach number is a non-dimensional parameter and is defined as the ratio between free stream velocity and speed of sound. Based on the Mach number range, wind tunnels are categorized as low subsonic, high subsonic, transonic, supersonic and hypersonic. Figure 1.4 summarizes the wind tunnel flow regimes.

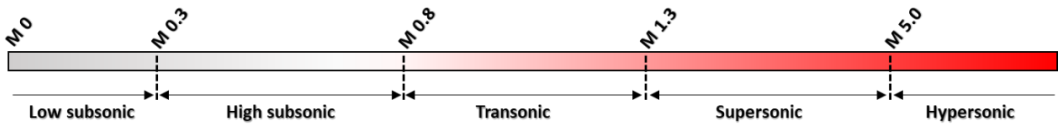

Figure 1.4 Mach number regimes for wind tunnels [9]

Based on the structural design, which also can be considered the flow generation principle, wind tunnels are categorized as closed-circuit, open-circuit and blowdown types [9]. The following figures present the structural layouts of the tunnels.

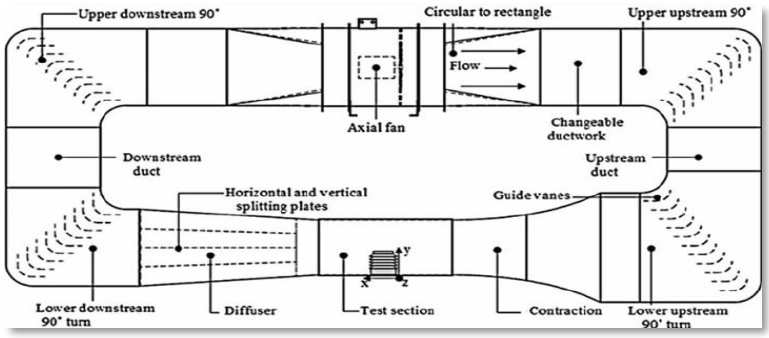

Figure 1.5 Closed-circuit types wind tunnel concept [10]

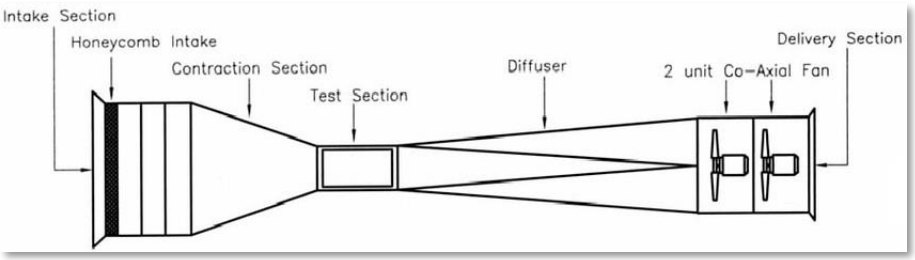

Figure 1.6 Open-circuit types wind tunnel concept [11]

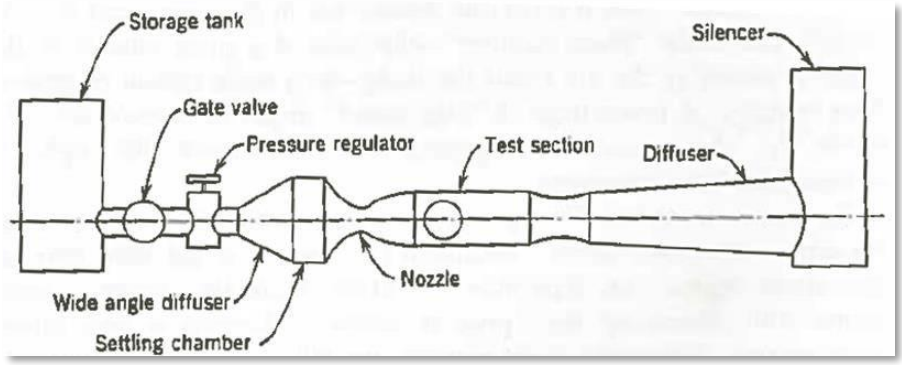

Figure 1.7 Blowdown types wind tunnel concept [12]

For closed circuit wind tunnels, the air moves in a closed environment with little or no exchange in flow. There are different variations of wind tunnel constructions and each of them has its advantages and disadvantages. As a general concept, the flow is generated by a fan or a set of fans that are driven by a motor(s), and the flow is initiated. A diffuser downstream of the fan decelerates the airflow, and then air passes from the turning vanes and reaches the settling chamber, which is upstream of the test section with a wider area. The flow characteristics, mainly turbulence and angularity, are improved in this section with the help of turbulence screens and honeycombs or flow straighteners. Moreover, the contraction ratio between the settling chamber and test section plays a role in further reducing the turbulence level [9]. The contraction accelerates the air and the maximum speed is reached at the test section where the test model and related instrumentations are placed. After that, the air passes through the diffuser and turning vanes again, and reaches the fan. Closed circuit wind tunnels can be atmospheric or pressurized in an aspect of the operational condition. The details of the wind tunnel operating conditions are given in [9]. Figure 1.8 shows the static pressure distribution along the wind tunnel components for an atmospheric wind tunnel in which air breathers are placed at the end of the test section and provides information about the losses and effects of closed-circuit wind tunnel components.

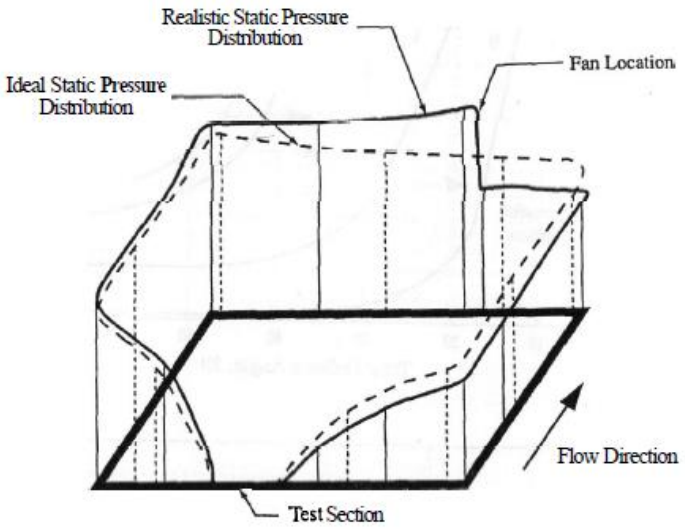

Figure 1.8 Pressure variations along a closed-circuit wind tunnel [9]

For open circuit wind tunnels, as a general concept, the flow is created by a fan which is placed at the end of the wind tunnel and air is sucked from the environment. The ambient air goes through the settling chamber of an open circuit wind tunnel. In this section, flow is straightened with the same principles as the closed-circuit settling chamber and reaches the test section. Downstream of the test section, there is generally a diffuser section and then the air exhausts into the atmosphere passing through the fan.

For blowdown wind tunnels, flow is generated using pressurized air stored in vessels or suction tanks at the end of wind tunnel construction. Mass flow is controlled by a pressure regulation valve placed upstream of the settling chamber. A high-pressure difference is created to obtain the desired flow conditions in the test section. Downstream of the pressure regulation valve, there is a settling chamber and the flow is conditioned there. After passing the settling chamber, the air reaches the test section and goes through the diffuser. After that, the air is released into the ambient.

Each type of wind tunnel serves different industries due to its advantages and disadvantages, which are summarized in Table 1.1. Based on the test requirements and intended schedule, the most suitable one is preferred for tests.

Table 1.1 Wind tunnel advantages and disadvantages [9]

Wind Tunnel Type	Advantages	Disadvantages
Closed Circuit	• Flow quality is independent of weather conditions • High utilization, less energy consumption • Less environmental noise • Achievement of various total pressure at the same Mach number	• Higher initial cost • Purging problem, after combustion tests • Additional cooling system requirement
Open Circuit	• Low initial cost • No smoke purging	• Additional screens at the inlet to get high-quality flow. • Inefficient utilization due to energy consumption • Noise
Blowdown	• Low initial cost • Flow quality is independent of weather conditions • Achievement of high Mach numbers. • Achievement of various total pressure at the same Mach number	• Additional area requirement due to vessel size • Low utilization • Limited test duration

In summary, the figure below gives the overall idea about wind tunnels. The METU-RÜZGEM large-scale wind tunnel, which is the main subject of this thesis, is a

closed-circuit, low-subsonic aeronautical/environmental wind tunnel with interchangeable open and closed test sections.

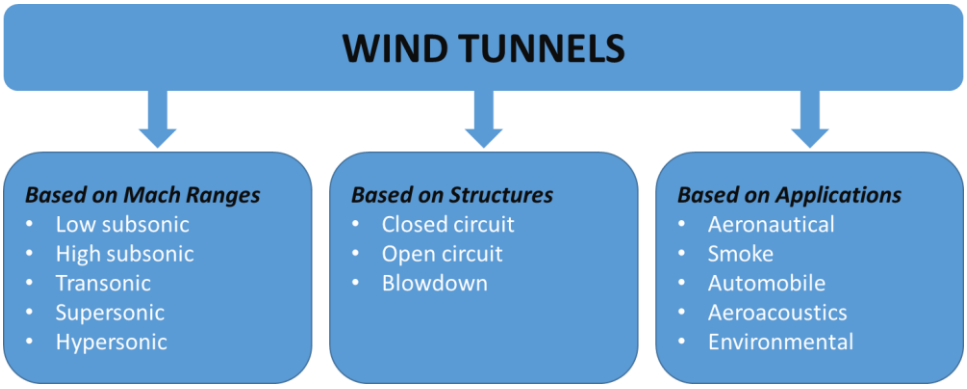

Figure 1.9 Wind tunnel classification [9]

1.1.2 Flow Similarity in Wind Tunnels

Wind tunnels are utilized to simulate the flow physics to answer the several questions in the design phase of vehicles where aerodynamics is of relevance. Viscosity, inertia, elasticity and gravity are the main parameters resulting in forces for a solid body moving through a fluid [9]. To obtain the flow similarity, these parameters are taken into consideration together with the reference length, area and/or volume of the non-scaled model to obtain some non-dimensional quantities. However, some models have to be scaled down due to size restrictions of wind tunnels. For instance, a typical wind turbine cannot be tested at full scale in a wind tunnel due to its vast size hence necessity of scaling arises.

The Mach and Reynolds numbers are the vital non-dimensional numbers in order to satisfy the dynamic similarity in aerodynamic tests [9]. Moreover, the geometric and the kinematic similarities between the actual prototype and the wind tunnel model have to be satisfied to ensure similarity between the actual and the wind tunnel conditions. Further details regarding the flow similarity and scaling laws can be found in [9] and [13] respectively.

1.1.3 Wind Tunnel Measurements

Various types of tests can be performed in wind tunnels. These tests are generally performed in order to:

- generate a database of aerodynamic forces and moments;
- understand and assess the flow field characteristics around the test article;
- simulate high-speed performance and low-speed conditions;
- provide input for design teams;
- support aerodynamic design studies;
- validate CFD simulations.

In this scope, the following measurements can be performed during a wind tunnel test:

- Six degree-of-freedom (DOF) force and moment measurements using an internal strain-gauged balance or an external balance;
- Steady and unsteady pressure measurements using pressure scanners and high response pressure instruments;
- Acceleration measurements using an accelerometer;
- Angle measurements using an inclinometer;
- Bending/torsion/hinge moment and force measurements using strain gauges;
- Flow angle measurements using multi-hole probes;
- Boundary layer measurements using total pressure probe rakes;
- Flow visualization using the Schlieren, PIV, PSP, oil flow, tuft, smoke, sublimation and infrared measurements

1.1.4 Wind Tunnel Data Reduction Basics

Wind tunnels are operated at specifically defined flow conditions to simulate the flow. The flow parameters in the test section are either calculated or directly

measured via related instrumentations. Here, the test section flow parameters and generally the calculated parameters are summarized Table 1.2 [14].

Table 1.2 Data reduction basics for a wind tunnel

Parameter at the test section	Basics
Total pressure	Measured at the settling chamber and during calibration
Static pressure	Measured at the test section or plenum and during calibration
Dynamic pressure	Calculated using isentropic flow equations
Total temperature	Measured at the settling chamber and during calibration
Static temperature	Calculated using isentropic flow equations
Density	Calculated using isentropic flow equations
Reynolds number	Calculated using isentropic flow equations
Mach number	Calculated using isentropic flow equations
Velocity	Calculated using isentropic flow equations

Test section total pressure:

The total pressure in the settling chamber is measured, and a relation between the total pressure values in the settling chamber and the test section is obtained during the characterization phase. Ideally, the total pressure in the test section is expected to be the same as that in the settling chamber.

Test section static pressure:

Test section static pressure is measured using reference pressure ports inside the test section or plenum chamber. The static pressure of the reference ports/test section pressure is calibrated during the characterization phase. Ideally, the reference ports

can be used directly for subsonic regimes, but calibration is a must for supersonic test sections.

Test section total temperature:

The total temperature in the settling chamber is measured and the settling chamber/test section total temperature is calibrated during the characterization phase. Ideally, the total temperature in the test section is expected to be the same as that in the settling chamber.

The rest of the parameters can be calculated using the isentropic flow equations [13].

1.2 Wind Tunnel Characterization

Ideally, the flow in the test section is expected to be uniform along the test section, parallel to the walls and with zero turbulence [15]. Since the flow deviates from this ideal condition due to the effectiveness of the flow conditioning components (i.e., honeycomb, screens, etc.), the boundary layer development along the walls and the swirl induced by the fan downstream, characterization/calibration tests are performed to investigate and assess the flow field quality in the test section.

1.2.1 Types of Wind Tunnel Characterization

Mainly the calibration can be considered as either a check calibration or a full calibration [14]. Check calibration tests are short tests to provide information about the health of the wind tunnel and measurement devices with a limited number of measurements before the start of an actual test. On the other hand, full calibration tests are detailed measurements in the test section to investigate the flow field. The calibration tests are performed in an empty test section to exclude the effect of any test article. The full calibration tests can be performed at a single point, on a plane, or in a volume. Figure 1.10 gives an idea about the point, planar and volume calibration methods.

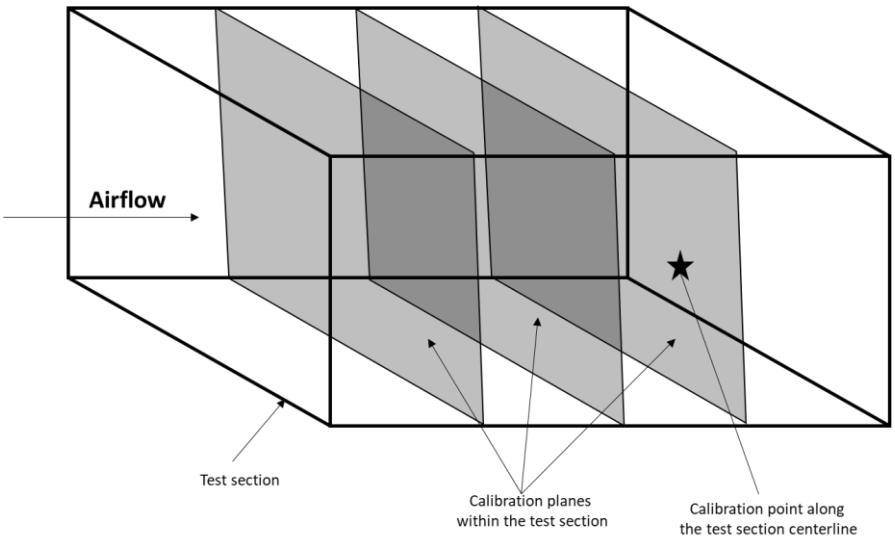

Figure 1.10. Characterization types [14]

Point calibration tests relate the flow conditions at a single measurement station, whereas planar calibration tests deal with plane measurements in the test section. Testing at different planes along the test section is defined as volume calibration. The easiest method is the measurement at a single point, but it does not provide detailed flow information of the test section.

1.2.2 Wind Tunnel Characterization Requirement

The calibration and reporting of the results are important aspects for a wind tunnel to ensure accurate measurements. Based on the AIAA recommended practice [14], the significance of the characterization is summarized as follows:

- Required for the understanding of the flow in the test section and ensuring the quality of the test data. Well-documented test-section flow information is used to understand whether the results are facility related or test article related.

- The calibration results are valuable for customers. According to the test goals, knowledge of uncertainty in the flow parameters is precious, especially in the case of high accuracy requirements.
- Aerodynamic and propulsion are tests mostly affected by flow field characteristics.
- CFD simulations require the flow field and boundary condition parameters for better simulations. Uncertainties ensure the evaluation of differences between measurements and simulations.
- Provides a stronger basis for the extrapolation of test data to actual flight conditions.

Furthermore, the calibration of a wind tunnel facilitates tunnel-to-tunnel data comparisons and identification of test data anomalies. Each tunnel has its own flow quality and there is not any standard rule of thumb that defines flow parameters. In 1994, the list in Figure 1.11 was published [16] for a national subsonic wind tunnel operating from low pressures up to 5 atm, and these parameters are considered suitable in the aspect of the evaluation of the wind tunnel flow field. Also, the adopted goals of NWTC flow quality characterization in Figure 1.12 is presented to have an assessment criterion for wind tunnel flow quality [16].

Parameter	Low speed	Transonic
Volume for flow quality	Fully encompasses model	Fully encompasses model
Total temperature distribution (°F)	±1.5	±1.0
Turbulence	<0.08%, (10–40 kHz)	<0.07% (laminar flow tests) <0.2%, with <0.1% variation (aerodynamic testing)
Noise, rms	53.3 dB[1] (1.25–40 kHz) (acoustic testing) 70 dB (1.25–40 kHz) (aerodynamic testing)	95.0 dB[2] (1.25–40 kHz) (laminar flow testing) 104–120 dB (1–30 kHz) (aerodynamic testing)
Stream angle deviation (deg)	<±0.03	<±0.1
Dynamic pressure distribution (%)	±0.1	
Total pressure distribution (%)	±0.1	±0.05
Mach number distribution		±0.001

Figure 1.11 Flow field parameters [16]

Parameter	Low speed (closed jet)	Low speed (open jet)	Transonic
Volume for flow quality	Fully encompasses model	Fully encompasses model	Fully encompasses model
Total temperature distribution (°F)	±1.0	±1.0	±1.0
Turbulence	0.04 longitudinal	0.2 longitudinal	0.04 longitudinal
	0.08 vertical	0.12 vertical	0.08 vertical
	0.08 lateral	0.12 lateral	0.08 lateral
Noise, rms (dB)	59.4	59.4	95.0
Stream angle deviation	$<\pm 0.1°$	TBD	$<\pm 0.1°$
Stream angle gradient	0.01°/ft, any line	TBD	0.01°/ft, any line
Mach number distribution	±0.001 centerline	TBD	±0.001 ($M<1$); ±0.01 ($M>1$) centerline
	±0.001 in cross-section at model rotation center		±0.001 in cross-section at model rotation center
	±0.0005/ft along centerline		±0.0005/ft along centerline
Tunnel stability	±1 psf over 10 s	±1 psf over 10 s	±1 psf over 10 s
	±0.5 °F over 10 s	±0.5 °F over 10 s	±0.5 °F over 10 s
	±0.0005 Mach over 10 s	±0.0005 Mach over 10 s	±0.0005 Mach over 10 s
Acoustic levels	None given	Specified over 100–20 kHz	Specified over 100–20 kHz

Figure 1.12. NWTC Flow quality characterization goals [16]

1.2.3 Wind Tunnel Characterization Basics and Examples

During the calibration of wind tunnels, different types of measurements are performed. Measurements of total pressure and static pressure are performed in the test section for the mean velocity calibration. For this purpose, Pitot tubes or Pitot-static tubes are mainly used. These measurements can be performed using a traverse system or rakes. Figure 1.13 and Figure 1.14 present the usage of both rake and traverse mechanisms in the low-speed wind tunnel at Aeronautical and Maritime Research Laboratory (AMRL) [15].

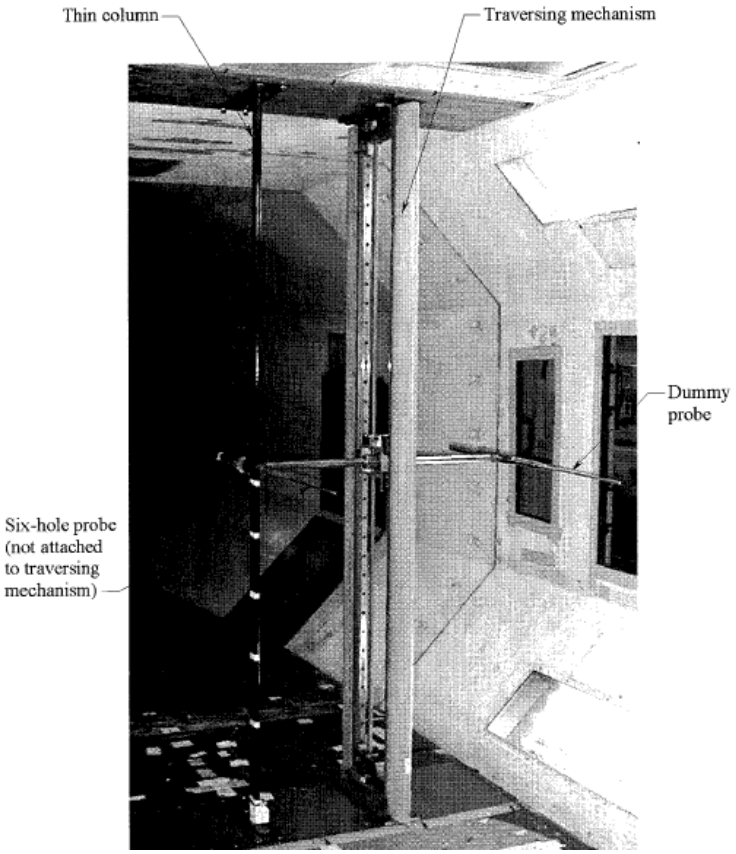

Figure 1.13 Traverse system in the low-speed wind tunnel at AMRL [15]

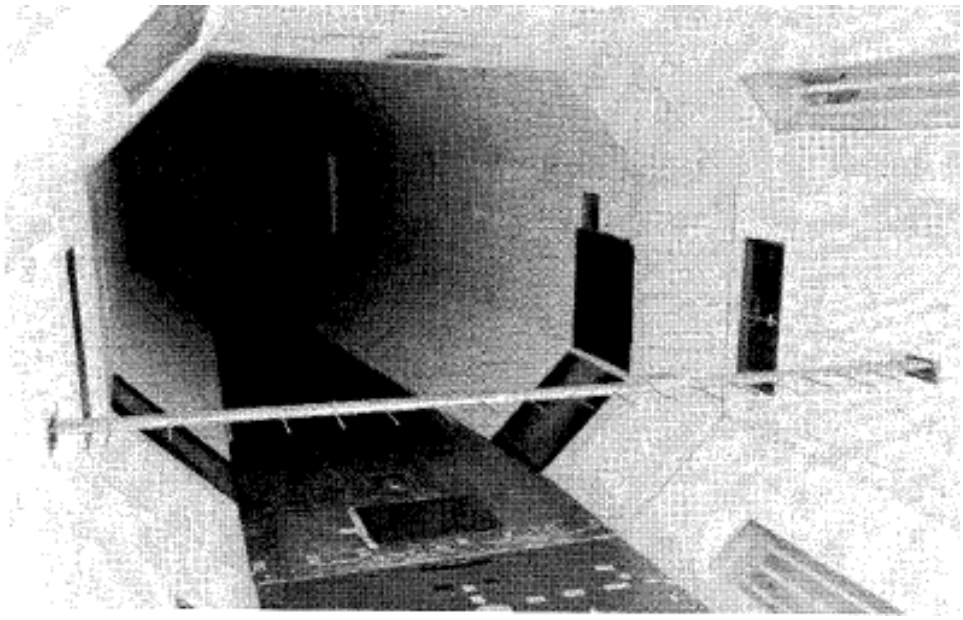

Figure 1.14 Rake system in the low-speed wind tunnel at AMRL [15]

The traverse mechanism and the rake system allow multiple measurements without any start/stop requirement. The axial static pressure gradient variation along the test section is one of the parameters that must be measured during the characterization phase. Regarding the results of the pressure gradient variation along the test section, required buoyancy corrections are taken into consideration for wind tunnel corrections [14] if a pressure gradient is observed along the test section. The second parameter is the measurement of the flow angles or flow angularity. The flow angularity in a cross-section of the test section needs to be obtained. The best-known technique is the use of multi-hole probes. An example of the measurement of the flow angularity in the NASA-Langley Transonic Dynamics Tunnel is given in Figure 1.15 [17]. The results at the Mach number of 0.5 (see Figure 1.16) show the possible outputs. The local flow angle throughout the test volume is then used to correct the true flow angles on the model since it affects the lift and drag forces on the model [14].

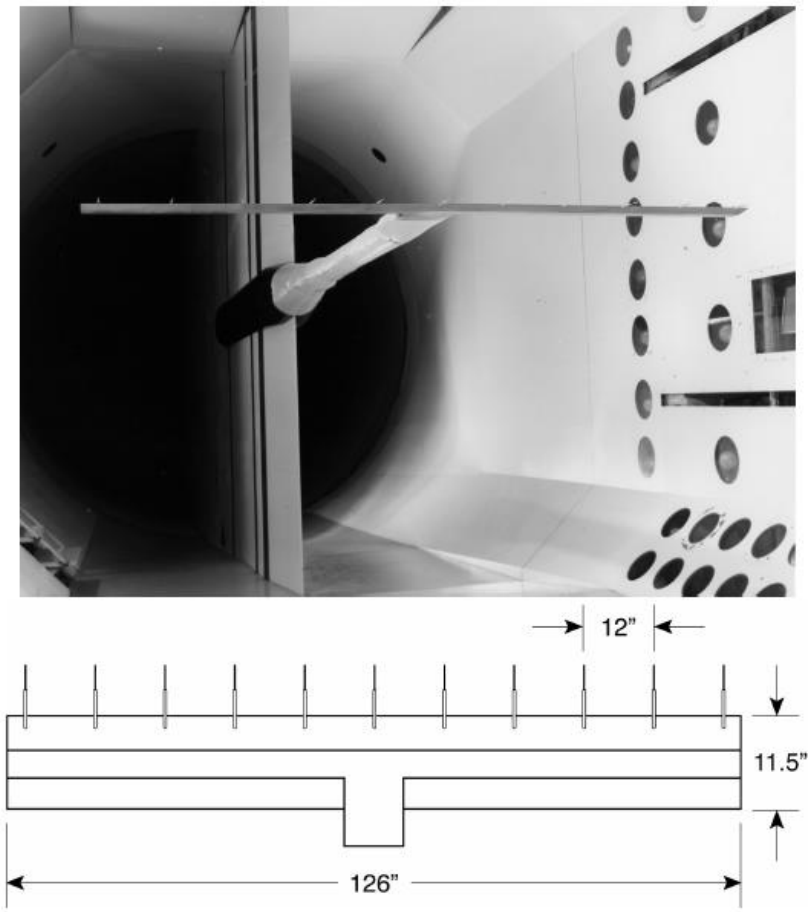

Figure 1.15 NASA-Langley TDT 5-hole probe usage [17]

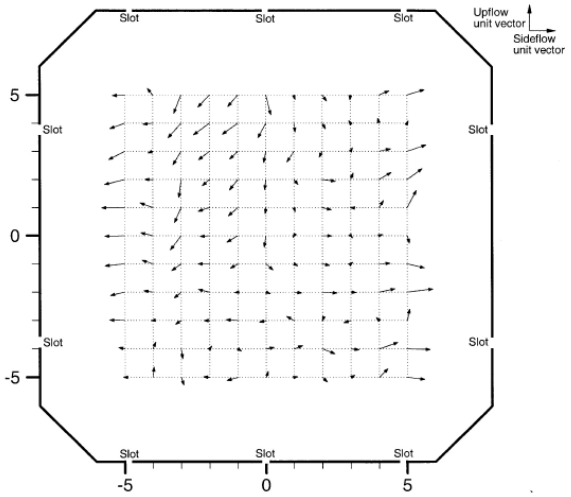

Figure 1.16 Angularity measurements in NASA-Langley Transonic Dynamics Tunnel (TDT) at Mach 0.5 [17]

Another important characterization parameter is the turbulence intensity. The turbulence intensity distribution in (a) cross-section(s) is obtained during the characterization phase. Generally, the settling chamber flow straighteners and the contraction are used to decrease the turbulent fluctuations within the test section. The turbulence intensity is an important parameter for the considerations of boundary layer transition, flow separation, shock-boundary layer interaction, buffet onset, and skin friction drag [14]. Although the results of turbulence intensity measurements are not directly implemented as a wind tunnel correction, they are used as input for numerical simulations. Constant temperature anemometry techniques are mostly preferred for measuring the turbulence intensity levels. Figure 1.17 displays a hot-wire measurement in a wind tunnel and a typical result.

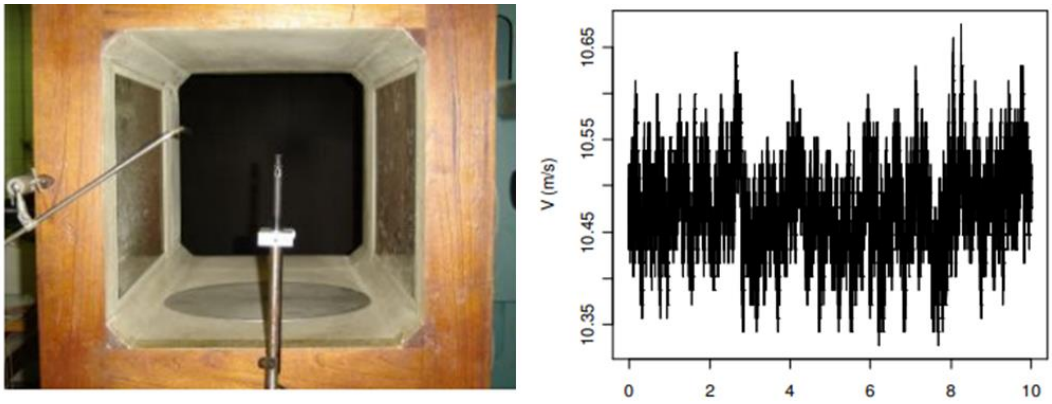

Figure 1.17 Usage of hot-wire anemometer, wind tunnel of the Institute for Technological Research (IPT) in Brazil [18]

General characteristics of wind tunnels are presented in the table in Figure 1.18 [16] Table includes measurement techniques and acoustic/turbulence characteristics based on Mach number to allow for a systematic comparison of the results.

Facility description	Measurement method	Freestream conditions	Frequency range (Hz)	Turbulence level (%)	Comments
Langley 8-ft transonic	Hot wire	$M = 0.2–0.8$	0.1–25,000	0.1–0.4	AIAA 94-2503
	p' probe, p'/p		0.1–5000	0.007–0.35	AGARD CP 348
Langley LTPT	Hot wire	$M = 0.05–0.3$	0.1–5000	0.02–0.08	AIAA 84-0621
					AIAA 94-2503
					AGARD CP 348
Langley 0.3 m transonic cryogenic	Hot wire	$M < 0.4$	0.1–5000	0.04–0.2	AIAA 94-2503
					AGARD CP 348
ONERA F1 pressurized subsonic	Hot wire, microphone,	$M < 0.4$	?	0.04–0.1	@1.1 bar p'/q
				1–4	ICAS 1980
RAE 5 m	Hot wire	$M < 0.3$	16–3150	0.15–0.3	RAE report 1978
DFVLR NWB 3.25 m × 2.8 m	Hot wire, microphone	< 100 m/s	1.6–12,800	0.05–0.2	DFVLR report 1986
				?	
DFVLR 3 m × 3 m (NWG)	Hot wire, microphone	< 100 m/s	1.6–12,800	0.38–0.75	DFVLR 1986
				?	
DNW	Hot wire, microphone	< 100 m/s	1.6–12,800	0.03–0.22	DFVLR 1986
				?	
Ames 12 ft	Hot wire, p' probe, p'/p	$M = 0.26–0.82$	0.1–25,000	0.04–0.2	AGARD CP 348
PWT			0.1–5000	0.01–0.2	AIAA 96-2204
LaRC 4 m × 7 m (VSTOL)	Hot wire		0.1–5000	0.35–4	AGARD CP 348
ONERA T2	Hot film, microphone, Tt probe	$M = 0.7–0.85$	10–10,000	0.1	Mass flux
Cryogenic		100–300 K		0.3	P'/q
				0.02–0.15	Tt'/Tt
					ICIASF 1997
Lewis 9 × 15 ft^2 low speed	Hot wire, hot film	$M = 0.05–0.2$	?–10,000	1.5–2.5	AIAA 95-2390
Ames 11 × 11-ft^2 TWT	Hor wire	$M = 0.2–0.95$	1–16,000	0.05–0.5	AIAA 2000-2681
	Acoustic probe, $C_{p_{rms}}$		1–10,000	0.1–0.6	
				Slots taped	
ETW	Hot film	$M = 0.3–0.85$	20–12,000	0.15–0.25	AIAA 2000-2206
	Acoustic probe, $C_{p_{rms}}$		?–?	0.4–0.6	

Figure 1.18 Turbulence and acoustic characteristics of wind tunnels [16]

Lastly, boundary layer development in the test section is investigated as a part of the characterization process. The boundary layer thickness should be characterized along the test section since it determines the effective measurement area and can be used as a reference for the positioning of the models within the test section. A motorized probe or a boundary layer rake are mostly used for such measurements.

1.2.4 Characterization Measurement Methods

In this section, guidelines and methods that are used for the characterization of a wind tunnel are provided for the test section flow parameters such as velocity, static pressure, dynamic pressure, temperature, flow angularity, boundary layer, and turbulence intensity.

1.2.4.1 Static and Total Pressure Measurements

Static pressure distribution along the longitudinal axis of a wind tunnel affects mainly the drag force calculations of solid bodies. It is suggested that less than 0.002 ΔC_P/m can be corrected using standard buoyancy correction methods [19]. Based on this, the axial pressure gradient was defined as 0.002 ΔC_P/m. Moreover, the axial distance for the measurements was planned as 0.5m considering the data of centreline probe of the Korea Air Force Academy Subsonic Wind Tunnel given in Figure 1.19.

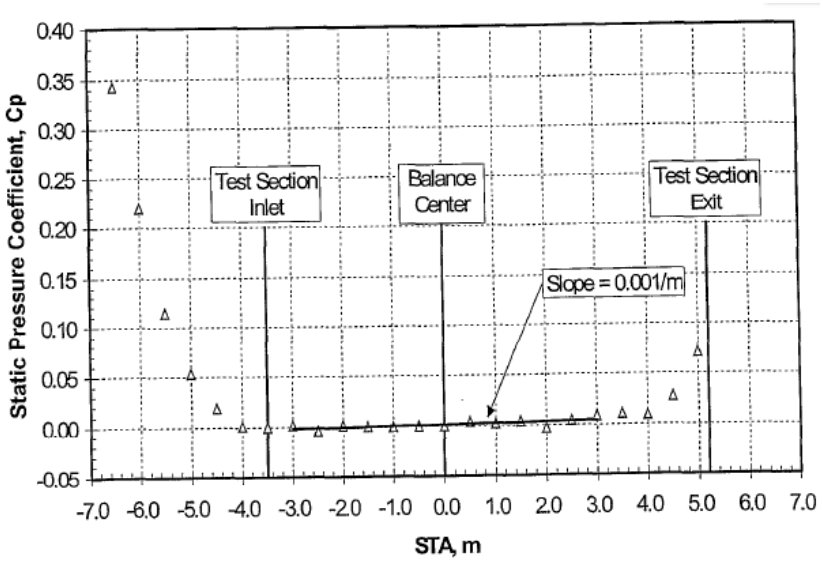

Figure 1.19 Axial pressure gradient at 74 m/s [19]

Another example to present the usage of centerline probes in a subsonic wind tunnel [20] is given in Figure 1.20. The centerline probe is preferred and mainly used for axial pressure measurement. However, the pressure data at different axial locations of test sections of RÜZGEM large scale wind tunnel are planned to be measured using the axial movement capability of the traverse system.

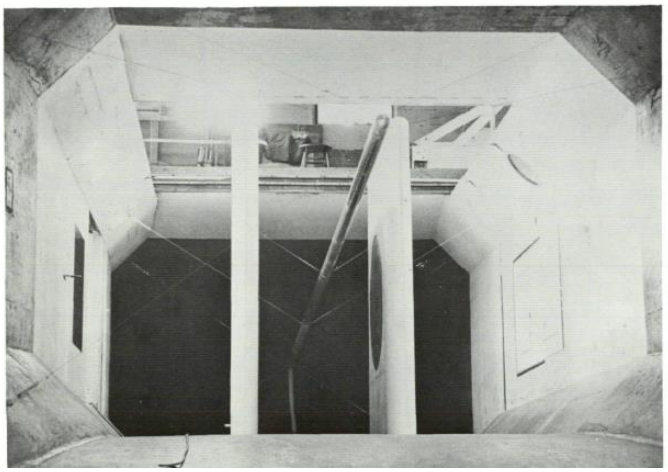

Figure 1.20 Static pressure pipe usage [20]

Static and total pressure measurements are performed using static or Pitot-static probes as shown in Figure 1.21. Heely [21] provides detailed information about the working principles of measurement equipment and sensors.

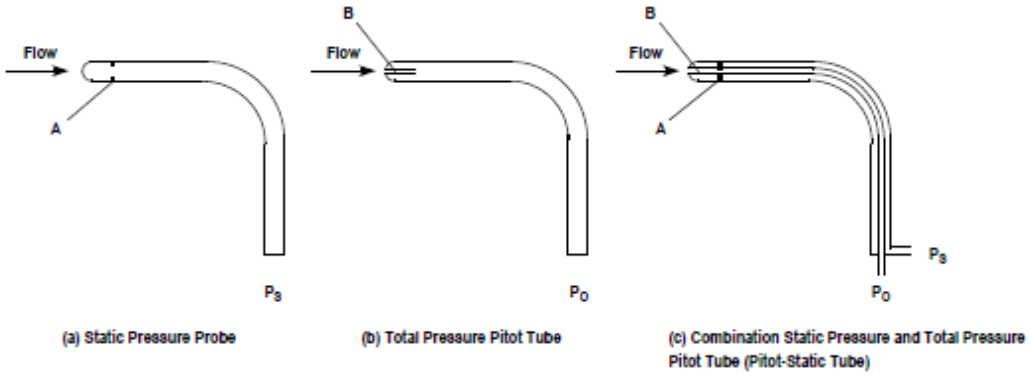

Figure 1.21 Various pressure probes [21]

1.2.4.2 Dynamic Pressure Measurements

Dynamic pressure is a moving quantity of particles calculated using total pressure and static pressure measurements. Dynamic pressure is defined based on the equation below and is used in all flows, from incompressible to hypersonic flows [13]

$$Q = \frac{1}{2} \times \rho \times V^2 \tag{1.1}$$

Specifically, for incompressible flows, dynamic pressure is defined as the difference between total pressure and static pressure.

$$Q = P_T - P_S \tag{1.2}$$

If the Mach number is higher than 0.3, the dynamic pressure definition is mostly defined based on the Mach number and static pressure as shown in equation 1.3. The details of compressible and incompressible flow can be found in [22].

$$Q = \frac{\gamma}{2} \times M^2 \times P_S \tag{1.3}$$

The compressible flow equations can also be used for the incompressible regime, and it is suggested to calculate all parameters with the use of compressible flow equations. The method for the calculation of the dynamic pressure is given as follows:

1. Measure the total and static pressures via suitable probes
2. Calculate the Mach number using the below formula

$$M = \sqrt{\left(\left(\frac{P_T}{P_S}\right)^{\frac{\gamma-1}{\gamma}} - 1\right) \times \frac{2}{\gamma-1}} \tag{1.4}$$

3. Calculate the dynamic pressure using the compressible dynamic pressure formula (equation 1.3)

The dynamic pressure at the center of the tunnel test section at various velocity conditions is to be reported to evaluate the dynamic stability characteristics of the tunnel. The ±0.5% standard deviation value for the dynamic pressure change is recommended in [9] and ±0.1% distribution is recommended in [16].

1.2.4.3 Temperature Measurements

Static temperature is not easy to measure for a flow since the probes should be moving at the same velocity as the air to be able to measure the static temperature according to its definition [15]. Therefore, the stagnation temperature is measured and the static temperature is calculated accordingly as a function of the Mach number. Total temperature measurement probe examples are given below in Figure 1.22.

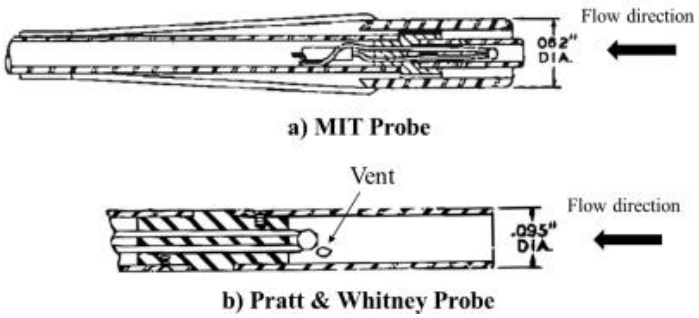

Figure 1.22 Total temperature probe design examples [23]

After the measurement of the total temperature, the following formula is used to calculate the static temperature.

$$T_S = T_T \times \left(1 + \frac{\gamma - 1}{2} \times M^2\right)^{-1} \tag{1.5}$$

It is stated in [19] that the aerodynamic coefficients are insensitive to temperature variations less than 1 °C. Furthermore, variations less than ±1.5 °F is recommended in [16].

1.2.4.4 Velocity Measurements

Velocity can be measured directly in the flow field using the hot wire anemometry technique [24] or can be calculated using the relation between temperature and the Mach number [22]. The steps given below are followed to calculate the velocity

1. Measure total pressure, static pressure, and total temperature via suitable probes
2. Calculate the Mach number using equation 1.4
3. Calculate the static temperature using equation 1.5
4. Calculate the velocity using the equation 1.6

$$V = M \times \sqrt{\gamma \times R \times T_S} \tag{1.6}$$

1.2.4.5 Flow Angularity Measurements

For the measurement of flow angularity, multi hole probes are generally used. A five-hole probe (FHP) provides pitch and yaw angles. Static pressure holes/orifices on five-hole probes are used to acquire the static pressure simultaneously. The deviation for the angularity is recommended to be less than ±0.03 degree in [16] and stated as acceptable for less than ±0.1 degree in [19].

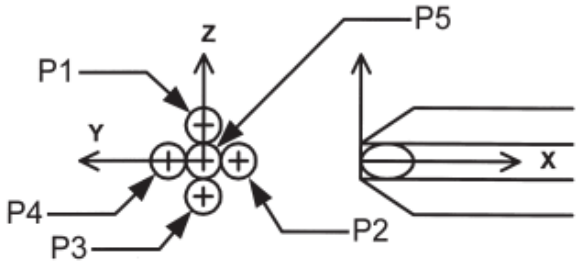

Figure 1.23 Five-hole probe (FHP) example [25]

To acquire the pitch and the yaw angles in the test section:

1. Install a five-hole probe on the traverse system.
2. Acquire the P1, P2, P3, P4, and P5 pressures of the five-hole probe.
3. Calculate the following coefficients, [25] [26].

$$C_{p,yaw} = \frac{P_2 - P_3}{P1 - \bar{P}} \tag{1.7}$$

$$C_{p,pitch} = \frac{P_5 - P_4}{P1 - \bar{P}} \tag{1.8}$$

$$C_{p,tot} = \frac{P_1 - P_{tot}}{P1 - \bar{P}} \tag{1.9}$$

$$C_{p,st} = \frac{\bar{P} - P_{st}}{P1 - \bar{P}} \tag{1.10}$$

$$\bar{P} = \frac{P_2 + P_3 + P_4 + P_5}{4} \tag{1.11}$$

4. Calculate the flow angles using the coefficients and the calibration data of FHP.

1.2.4.6 Turbulence Intensity Measurements

Turbulence intensity measurement is performed using the hot wire anemometry technique in the test section. Various types of hot wires provide different directional measurements [24]. Here, it is aimed to acquire turbulence intensity of the flow in three axes. Hence, a 3-dimensional wire probe hot wire anemometry is recommended for the measurement.

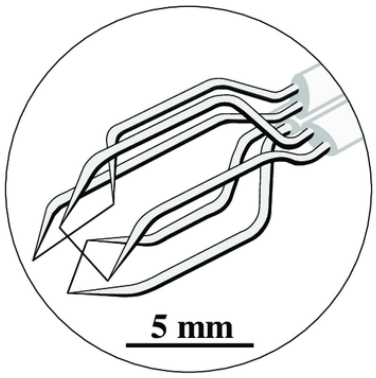

Figure 1.24 General 3-dimensional wire probe [27]

The principle:

1. Install a 3 axial hot wire probe on the traverse system
2. Acquire U_X, U_y, U_z data
3. Calculate turbulence intensity using the below formula, details in [224].

$$TI = \frac{u'}{U} = \frac{Velocity\ fluctuations}{Mean\ velocity} \tag{1.12}$$

$$U = \sqrt{\overline{U_X}^2 + \overline{U_Y}^2 + \overline{U_Z}^2} \tag{1.13}$$

$$u' = \sqrt{\frac{1}{3} \times \left(u_X'^2 + u_Y'^2 + u_Z'^2\right)} \tag{1.14}$$

1.2.4.7 Boundary Layer Measurements

The boundary layer thickness inside a wind tunnel test section changes the effective area of the test section and it should be defined. For this purpose, boundary layer rakes are used to measure the boundary layer thickness.

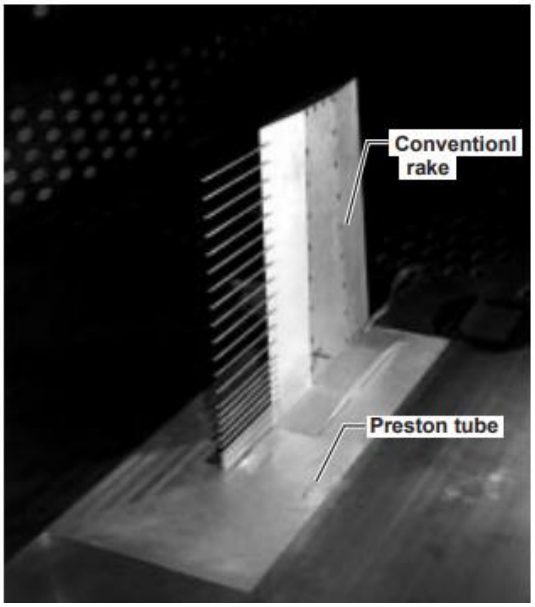

Figure 1.25 Conventional BL rake [28]

Boundary layer rake is placed to the defined locations and P_T data are acquired. After that, the boundary layer thickness is defined using probe locations on rake and measurements Boundary layer thickness is defined when the following criterion is met. [29].

$$u = U \times 99\% \tag{1.15}$$

1.3 RÜZGEM Large Scale Wind Tunnel

The RÜZGEM large-scale multi-purpose wind tunnel facility was constructed in 2020 and aimed to serve several industries with three interchangeable test sections [30].

- The aeronautical test section (ATS) is 2.5 m by 2.5 m with a length of 10 m. The maximum speed of this test section is 100 m/s. The turbulence intensity was aimed at <0.1% and the measurements were performed. This test section is useful for force and moment tests of air vehicles, missiles, and wind turbines.
- The boundary layer test section (BLTS) is 3 m by 7 m with a length of 20 m. The maximum speed of this test section is 30 m/s. The turbulence intensity was aimed at <2%. This test section is mainly considered for the investigation of the atmospheric flows around buildings, bridges, etc.
- The open-jet (OJ) test section has a 3 m diameter and the maximum speed of this section is 70 m/s. The turbulence intensity was aimed at <0.3%. Relatively big models which are not suitable for the aeronautical test section can be tested in this test section.

A general schematic of the tunnel is given in Figure 1.26 [31]. The tunnel is driven by six 400 kW motors and the blades of fans are designed by the RÜZGEM personnel. These motors are placed on an isolated concrete floor to eliminate the effect of vibrations. Furthermore, there is a 750-kW heat exchanger to maintain constant temperature of the air during the extended tests.

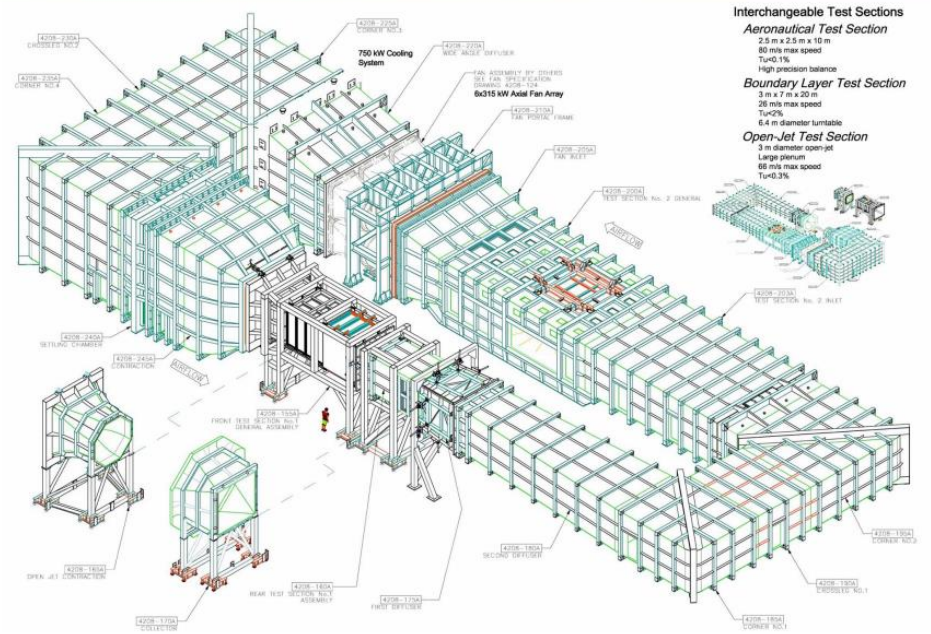

Figure 1.26. RÜZGEM Large scale wind tunnel [31]

1.4 Scope and Aim

In previous sections, the required measurements and purposes of characterization were explained clearly.

In this work the followings are aimed:

1. Performing aerodynamic analysis and conceptual design of a traverse system to be used during the characterization of the RÜZGEM large scale wind tunnel.
2. Performing preliminary characterization of the BLTS and the ATS of RÜZGEM large scale wind tunnel.

For this purpose, a traverse system was designed and simulated aerodynamically. The designed traverse system was then manufactured and a set of preliminary measurements were acquired using a five-hole probe.

CHAPTER 2

CONCEPTUAL DESIGN OF THE TRAVERSE SYSTEM

2.1 Traverse System Design and Considerations

2.1.1 Conceptual Design Considerations

Traverse systems and rakes are mainly preferred to perform tunnel characterization along the test sections at various flow conditions. Although the traverse system allows more data point measurements in the test section compared to the rake system, it brings design disadvantages due to its blockage and induced effects. The characterization tests are performed to obtain the flow characteristics of the wind tunnel. Hence, the measurement system must match the requirements such that characterization measurements are not affected by the presence of the traverse system. For this purpose, the traverse system is designed by taking into consideration both manufacturability and aerodynamics in this study.

The first conceptual design, which was the starting point of the traverse system, is given below in Figure 2.1 and Figure 2.2.

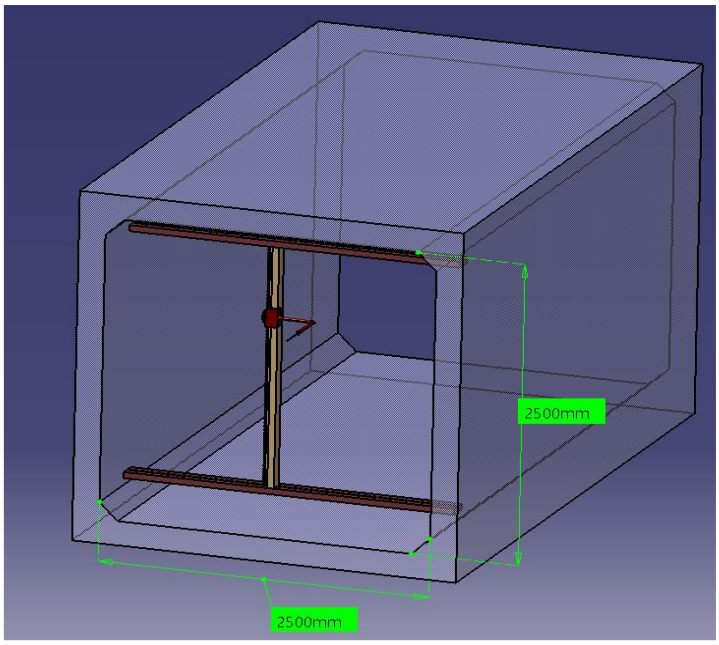

Figure 2.1 RÜZGEM large scale wind tunnel traverse concept for ATS

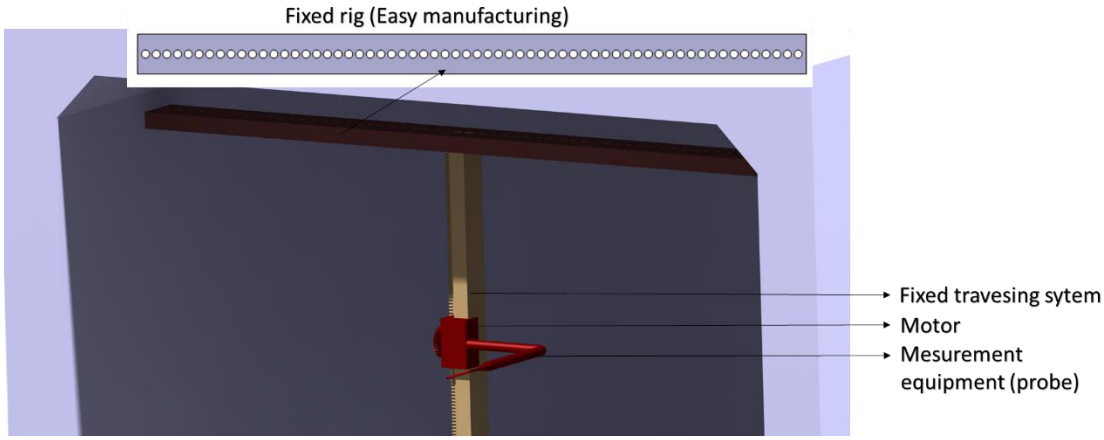

Figure 2.2 Details of the RÜZGEM large-scale wind tunnel traverse system conceptual design

This design allows the movement of one probe autonomously for vertical measurement points on a plane; however, it should be moved manually in the other directions.

The design was changed due to a single probe that can be attached to the system and manual movement in two directions which will increase the total measurement time. The use of three probes to acquire the data at a time was evaluated for a rectangular and profile-shape support system. It should be noted that the support system should be stiff so as not to cause any vibrations and should not cause extreme back pressure due to the generated blockage so that the data will not be altered due to the presence of the traverse system. It is expected that the profile support system should present less blockage effect on pressure and velocity distribution around the probe measurement points which is to be proven using numerical flow simulations. The purpose of this first comparison is to observe the blockage effect of the considered support systems.

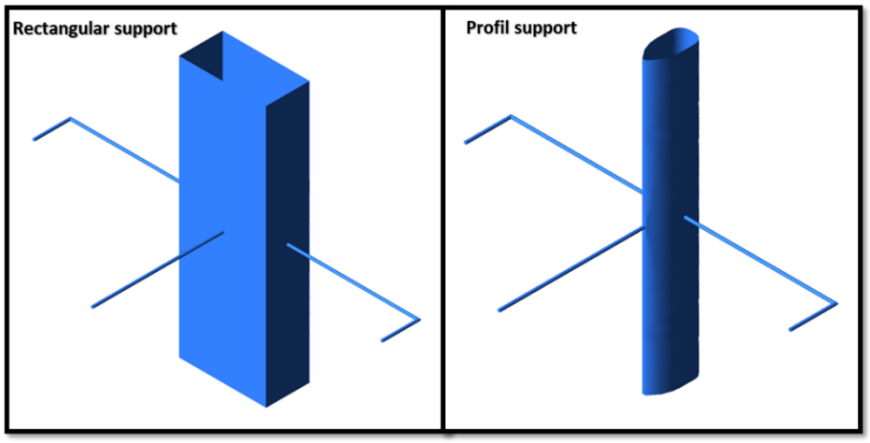

Figure 2.3 Rectangular and profile support system geometries

2.1.2 Conceptual Design Simulations

The conceptual designs are compared in numerical simulations, which were performed by use of the commercial CFD solver ANSYS FLUENT. The purpose is to compare the effect of rectangular and profile support systems. The actual size of the aeronautical test section is 2.5 m by 2.5m. In the simulations of the conceptual designs, a height of 0.6 m is adopted with symmetry boundary conditions defined for the upper and lower walls. It does not completely simulate the effect of upper and

lower walls however provides required information regarding the effect of the support. The domain includes 3.3 million mesh elements and y+ is lower than 1.

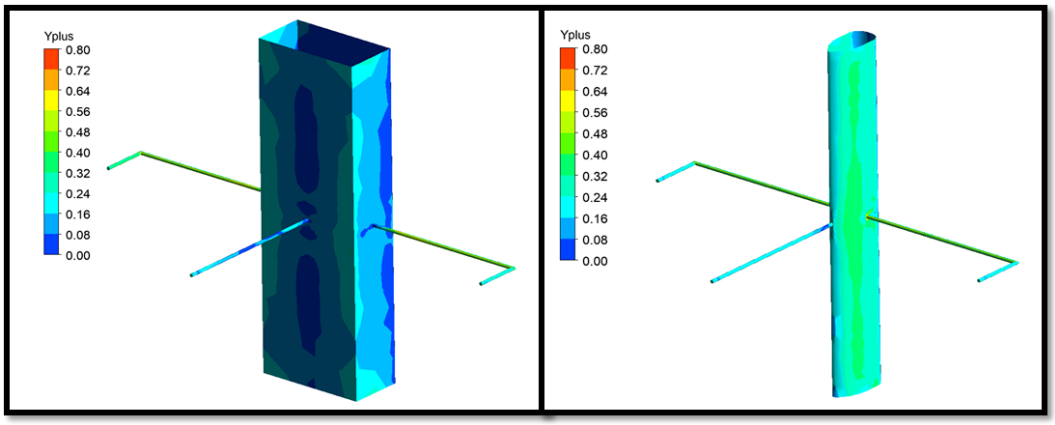

Figure 2.4 y+ Distribution of Analysis

The freestream velocity should be caught upstream of the support system in ideal consideration. However, a pressure field of the support system, which also affects the upstream flow field, is an expected issue in the subsonic flow regime. As a result, an acceptable effect of the support system should be defined, and the required lengths for the probes should be chosen accordingly.

Before the simulations, it was already estimated that the rectangular profile would cause excessive perturbation in the flow field. However, still, the simulations were performed with this geometry to assess its effect on the flow field since rectangular profiles are available components in the laboratory. Contours of pressure coefficient are presented in Figure 2.5 for the two geometries. The pressure coefficient is calculated using equation 2.1 as follows;

$$C_p = \frac{P - P_\infty}{Q_\infty} \tag{2.1}$$

It is clear that the rectangular profile influences the pressure field significantly, and probe lengths should be increased excessively to move out of the influence zone of

the support system. On the other hand, the support with an elliptical profile creates a relatively small disturbance in the flow field, allowing for more accurate measurements of the freestream pressure values with the defined probe lengths. The simulations for these two concepts reveal that the support system should have a slender geometry for proper characterization measurements. The probe lengths are a vital evaluation parameter for both rectangular and profile support systems, not neglecting the effect of probe vibrations due to lengths. In the beginning of simulations, a representative probe length was chosen to be analysed. After the decision of which probe will be used, the probe length was updated and the difference is examined.

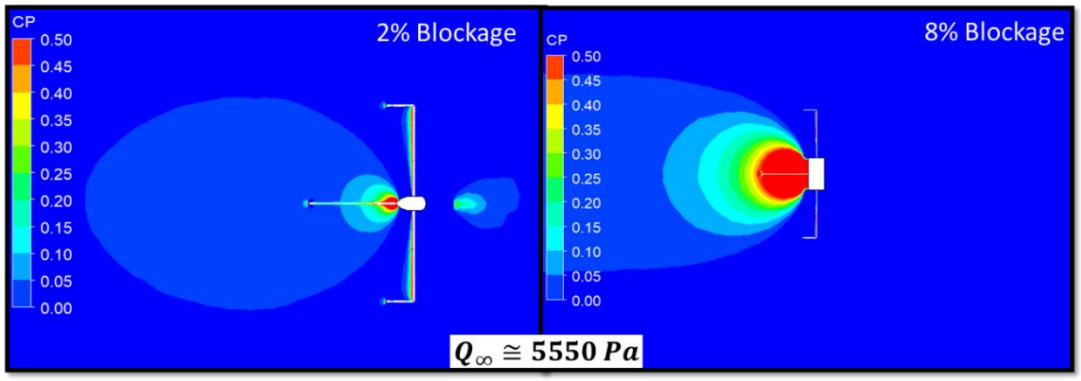

Figure 2.5 C_p Distribution obtained from the numerical simulations of the conceptual designs. Profile-shape support (left) and rectangular support (right)

The rectangular support system has a noticeable effect on the velocity distribution along the X axis on the mid-probe stagnation point (see Figure 2.6). However, the effect of arm's length could not be clearly observed.

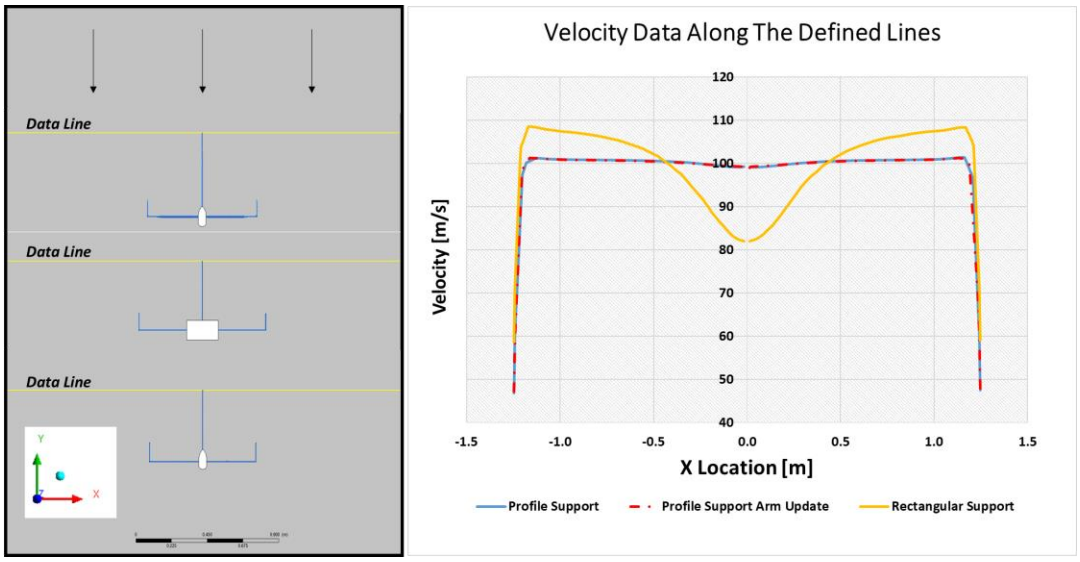

Figure 2.6 Velocity distributions for the different concepts

2.2 Detailed Design of the Traverse-Probe System

2.2.1 Empty Test Section Characteristics

For the numerical flow simulations of the detailed traverse-probe system, first, the flow in the empty aeronautical test section (ATS) of the RÜZGEM large-scale wind tunnel is solved. The ATS test section is arranged as CFD domain. Here, ATS has an increasing area along the test section to avoid static pressure deviation, which is named the buoyancy effect and should be corrected in post-processing data if observed [14]. The region mentioned in orange in Figure 2.7 is removed from the CFD domain since this section is an extension of the contraction part of the tunnel. This section can be modelled with the contraction part but note that the purpose of this work is to observe the effect of the traverse system on the flow in the test section. For this reason, this section together with the contraction is excluded from the numerical simulations and it is assumed that a uniform velocity profile is present at the exit of the contraction.

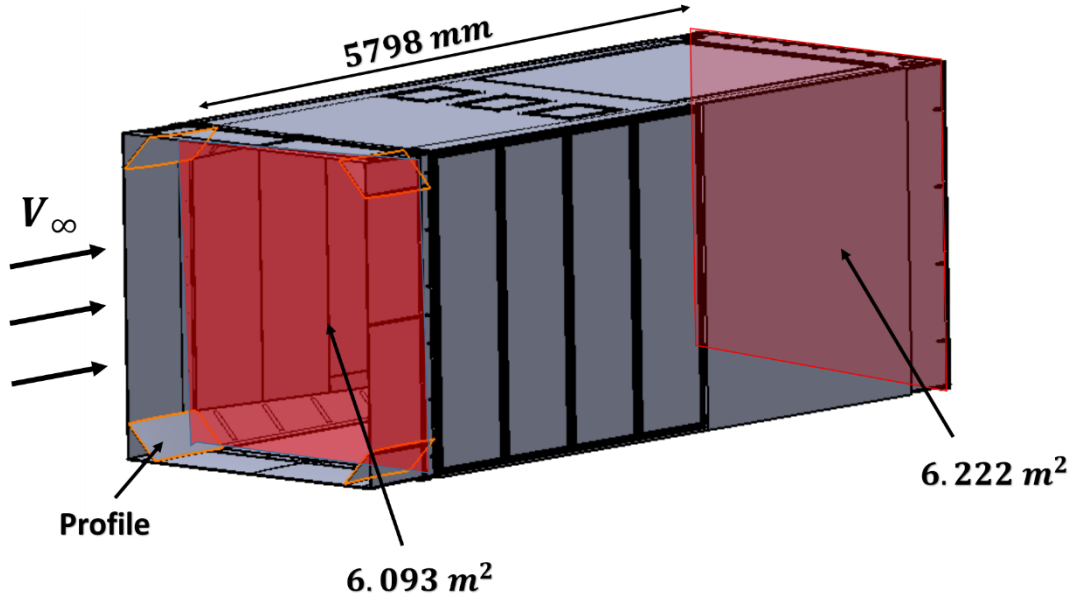

Figure 2.7 A 3D model of the Test Section 1 (ATS) of the RÜZGEM large- scale wind tunnel

The CFD domain is extended 5 m upstream and 10 m downstream from the inlet and outlet of the test section, respectively, without any area variation to ensure a developed flow at the inlet of the test section.

In the beginning, only the wind tunnel is analysed to check the boundary conditions and static pressure distribution along the test section. The domain is meshed with quad-elements due to the simplicity of the geometry (see Figure 2.8). The solution grid has 3.1×10^6 elements with a maximum skewness value of 0.88. The maximum y+ is 0.6 in this analysis (see Figure 2.9).

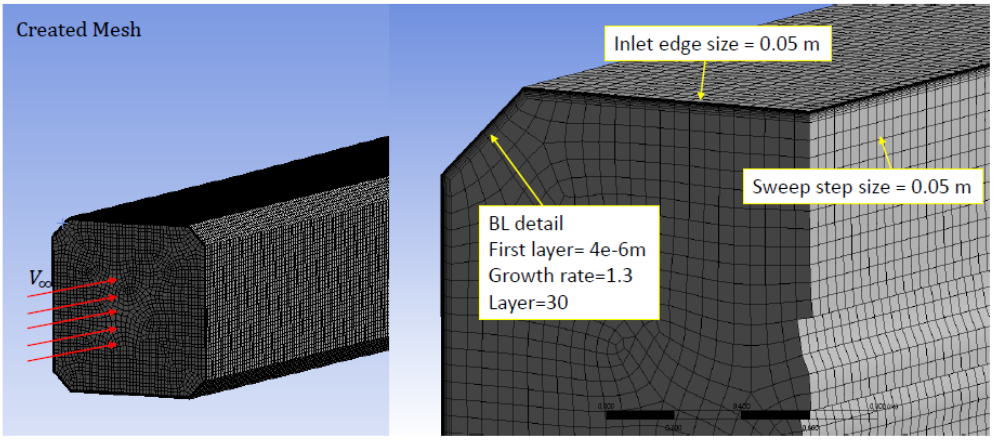

Figure 2.8 Meshing of empty wind tunnel

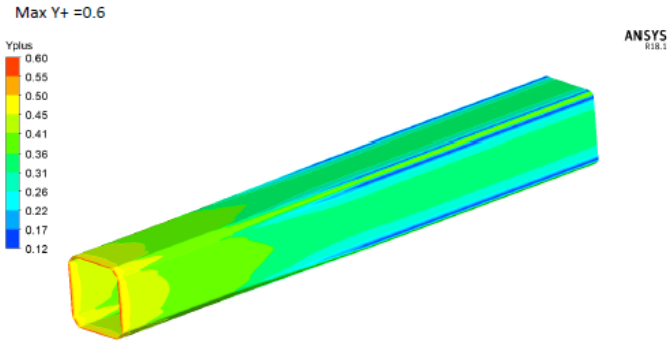

Figure 2.9 y+ distribution for empty test section numerical simulations

This analysis reveals the presence of the axial pressure gradient along the test section (Figure 2.10). The analysis was performed with a 5m upstream domain. The constant upstream will not represent the actual boundary layer profile completely. This analysis is only to reflect the effect of the support system. Note that the "U" velocity sign is negative due to the X-axis being positive towards the inlet. As a result of this analysis, the following observations are noted for the 100 m/s inlet condition.

- 120 Pa static pressure difference between the inlet and the outlet of the empty test section is expected (see Figure 2.10).
- 5 mm boundary layer increment is observed along the test section (see Figure 2.11)

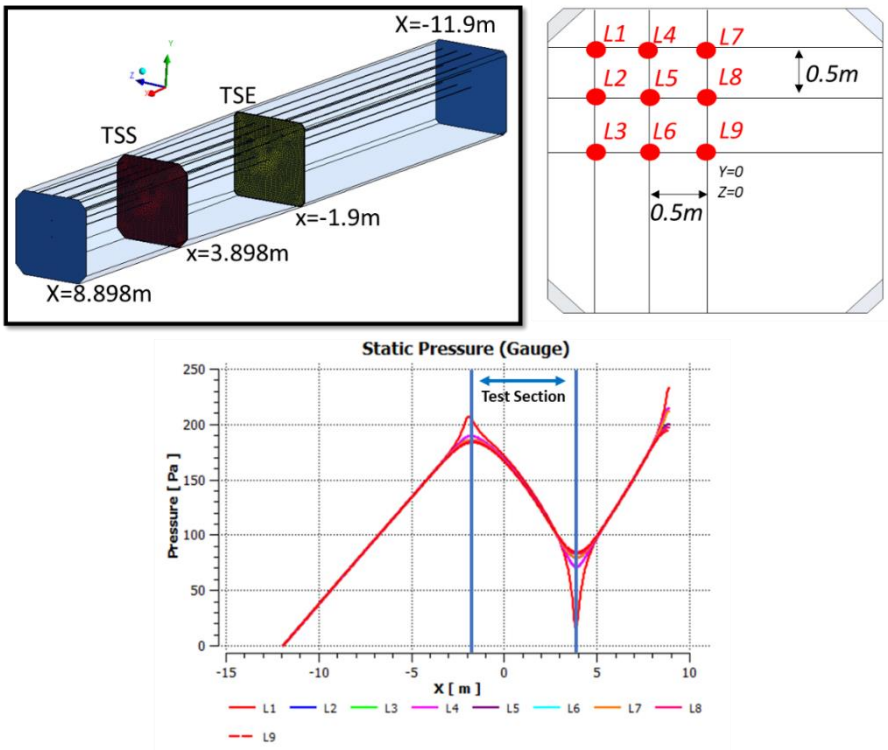

Figure 2.10 Static pressure variation along the aeronautical test section (ATS) at the freestream velocity of 100 m/s (The flow is in the negative X direction)

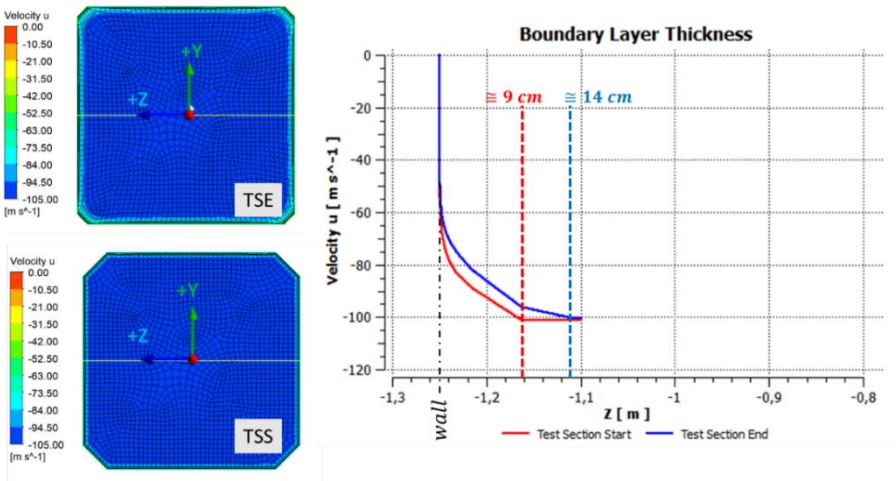

Figure 2.11 Growth of the boundary layer in the empty aeronautical test section (ATS) at the freestream velocity of 100 m/s

2.2.2 Traverse System Simulations

In the conceptual design simulations, two different support sections are compared, and it is found that a support section with an aerodynamic profile is needed to mitigate the effects of the traverse system on the measurements. In this section, numerical simulations of the flow in the empty aeronautical test section of the RÜZGEM Large-Scale wind tunnel are performed first. Then, detailed traverse design concepts are implemented in the numerical simulations to assess their aerodynamic performance in terms of causing minimum perturbation in the flow.

2.2.2.1 Numerical Models

The general view of the traverse system is given in Figure 2.12. For the traverse system, two L-shaped and a straight probe are planned to be used. The probes' dimensions can be seen in Figure A.1 and Figure A.2 respectively in the appendix section. It should be noted that the figures represent the dimensions of the probes, and additional connectors or extensions can come down between the traverse system and probes resulting in changes in the total dimension of the probes. After investigating the empty test section characteristics of ATS, the traverse system, excluding the moving system, seen in the Figure 2.13 as simplified, was modelled.

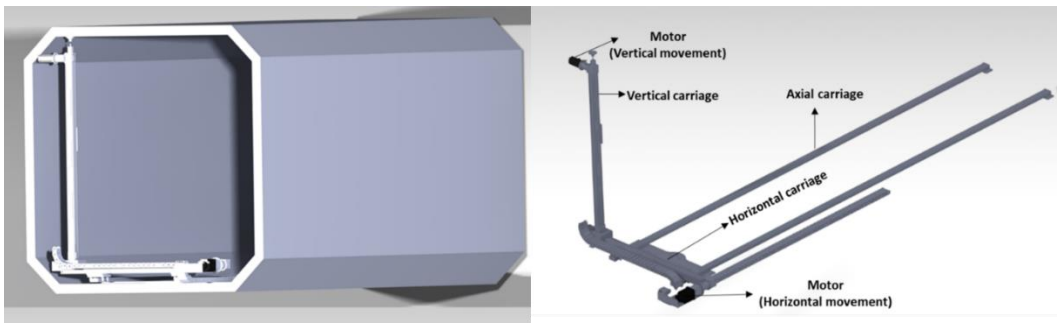

Figure 2.12 Traverse system representation

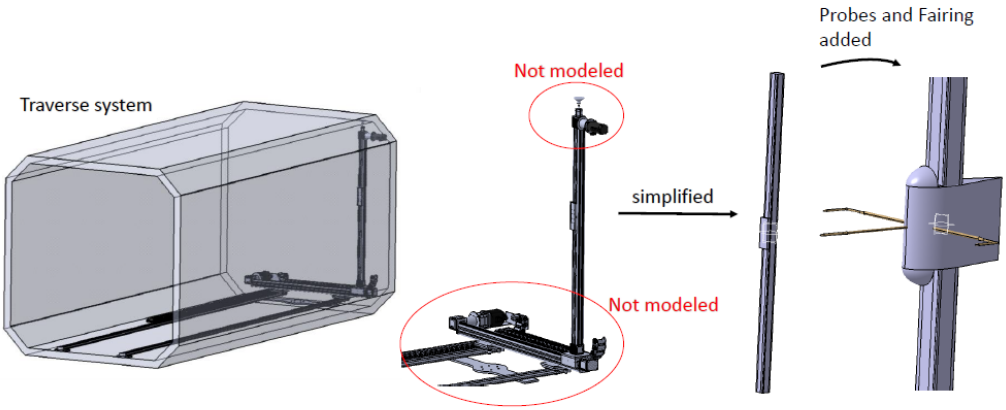

Figure 2.13 Traverse system simplification

The first design of the support system is a standard, off-the-shelf rectangular profile. The disadvantages of rectangular shapes are investigated in detail previously as they are preferred mainly due to ease of manufacturing and advantages for the motion of the probes. A carriage was considered assembled on the model, and an interface was required for probe connections. After that, a fairing is integrated to reduce the negative effects of the rectangular profile.

EPPLER 862 Strut symmetrical airfoil was chosen as the fairing of support system and carriage since it is a suitable profile for support system. The blockage with and without faring is 4.68 and 3.20 percent, respectively. Figure 2.14 and Figure 2.15 give the dimensions and blockage of fairing.

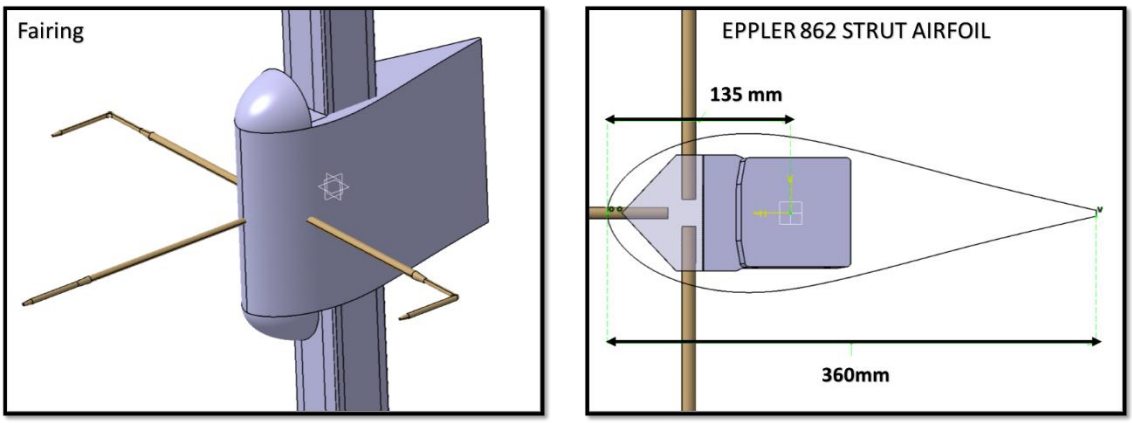

Figure 2.14 Fairing geometry details

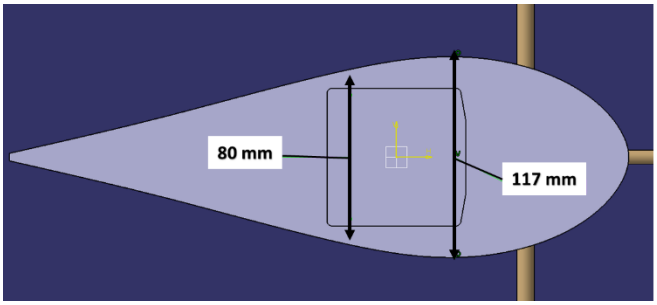

	Cross. Area (mm^2)	Blockage (%)
Rectangular support	80*2500	3.20
Profile support	117*2500	4.68

Figure 2.15 Cross sectional area comparison

Three different cases (see, Figure 2.16) with the same surface and volume mesh sizes were compared with each other to investigate the effect of the support system.

- Case1, Traverse system without any profile
- Case2, Traverse system with the partial airfoil support system
- Case3, Traverse system with the entire airfoil support system

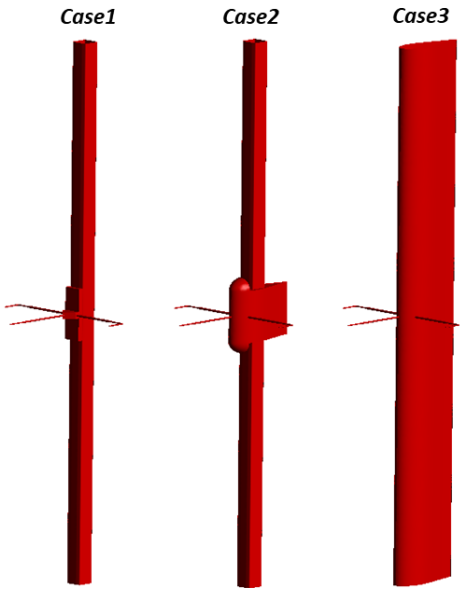

Figure 2.16 Case definitions of geometry

2.2.2.2 Solution Domain

Traverse system and CFD domain geometric parameters, which will be used for the investigation of the effect of the support system, are given below.

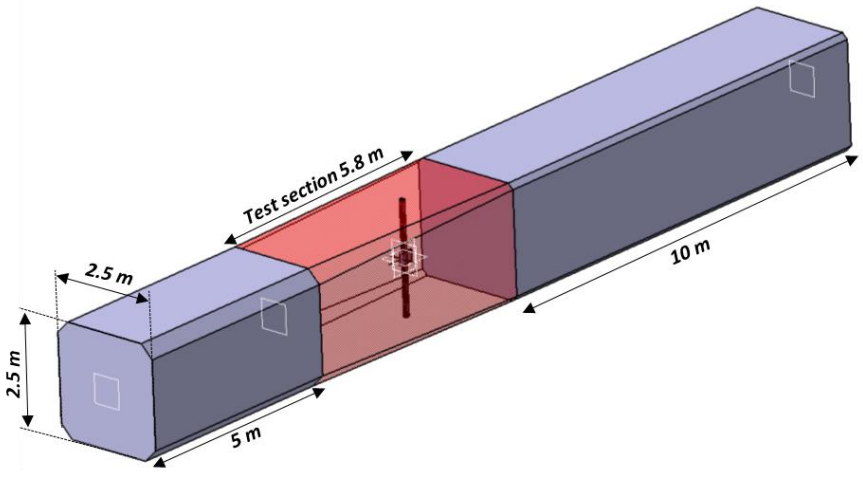

Figure 2.17 Traverse system and test section geometry

2.2.2.3 Solver Settings

The solver arrangements are provided below.

- The computational domain extends 5 m upstream and 10 m downstream of the support;
- Half domain with symmetry boundary condition is solved;
- Velocity inlet boundary condition with input properties of 100 m/s uniform velocity, 5% turbulence intensity and 300 K temperature;
- Pressure outlet boundary condition with an input property of 0 Pa gauge pressure
- The operating condition absolute static pressure value is arranged as 93000 Pa;
- ANSYS Fluent pressure-based solver is used;
- The ideal gas and the Sutherland viscosity laws are used;
- The k-omega SST turbulence model is used;
- Coupled, node based, second order solver is used
- y+ on the support system is kept lower than 1

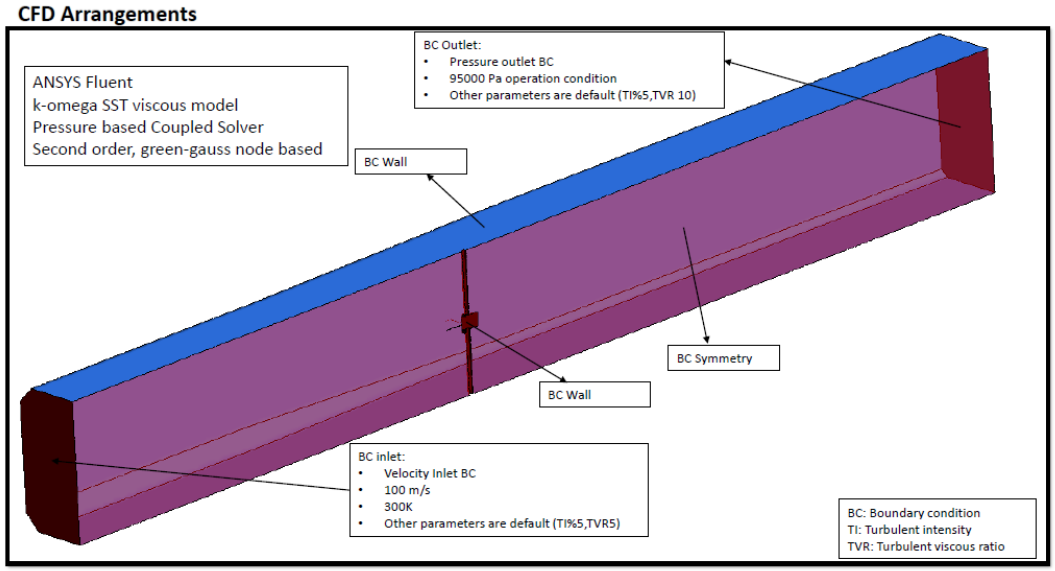

Figure 2.18 CFD Solver details for support system analyses

2.2.2.4 Mesh Independency

The wind tunnel domain has a width of 2.5 m, a height of 2.5 m, and a length of 20.5 m, which can be considered an enormous size to mesh. The half domain considering a symmetry condition is adopted in the numerical simulations.

Minimum mesh elements of 1 million were performed but could not be converged, and then minimum mesh elements of 7 million were chosen as start point after some trials. 4 different meshes were analysed for the 100 m/s freestream condition. The Table 2.1 gives the mesh details, including boundary layer, surface, and volume mesh sizes.

Table 2.1 Case definitions of mesh independency work

	Mesh 1	**Mesh 2**	**Mesh 3**	**Mesh 4**
Traverse System BL First Layer	5e-6m	**3e-6m**	3e-6m	3e-6m
Traverse System BL Growth rate	1.2	1.2	1.2	1.2
Traverse System BL Total Layer	30	30	30	30
Tunnel Wall BL First Layer	1e-5m	**45e-7m**	45e-7m	45e-7m
Tunnel Wall BL Growth rate	1.3	1.3	1.3	1.3
Tunnel Wall BL Total Layer	30	30	30	30
Min size	1e-3m	4e-4m	**2e-4m**	**1.5e-4m**
Proximity min size	1e-3m	4e-4m	**2e-4m**	**1.5e-4m**
Max face size	8e-2m	6e-2m	**3e-2m**	**2e-2m**
Max tet size	0.1m	8e-2m	**4e-2m**	**3e-2m**
Max Y+	1.99	0.98	0.98	0.98
Body of Influence	-	**3e-2m**	**1.5e-2m**	**1e-2m**
Max Skewness	0.9	0.88	0.89	0.94
Total element number (mil)	7.7	10.7	26.5	54.6

During the support system analyses, turbulence intensity and viscous ratio inputs were used as defaults of 5% and 5, respectively, and then updated as 0.3% and 3 for velocity inlet boundary conditions. For the detail simulations the updated turbulence intensity and viscous ratio values were used. It was noted during the previous analyses that continuity has a fluctuating characteristic, and the mesh size can affect

convergence history. Also, the following convergence thresholds (Table 2.2) were chosen to compare the results at the same residual conditions. The pressure coefficient along the midline can be shown in Figure 2.19.

Table 2.2 Converge criteria for residuals

Residuals	**Convergence Criteria**
Continuity	6×10^{-4}
X velocity	4×10^{-5}
Y velocity	1×10^{-6}
Z velocity	1×10^{-6}
Energy	1×10^{-6}
k	4×10^{-5}
omega	4×10^{-5}

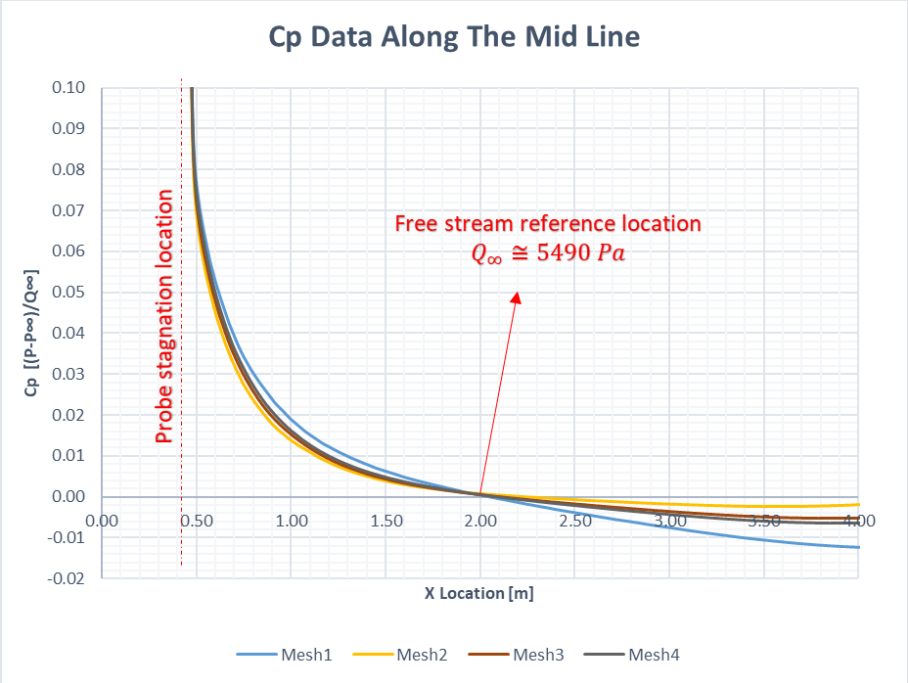

Figure 2.19 Midline C_P comparison for different mesh cases (X=0 is center of vertical support system and the flow is in the negative X direction)

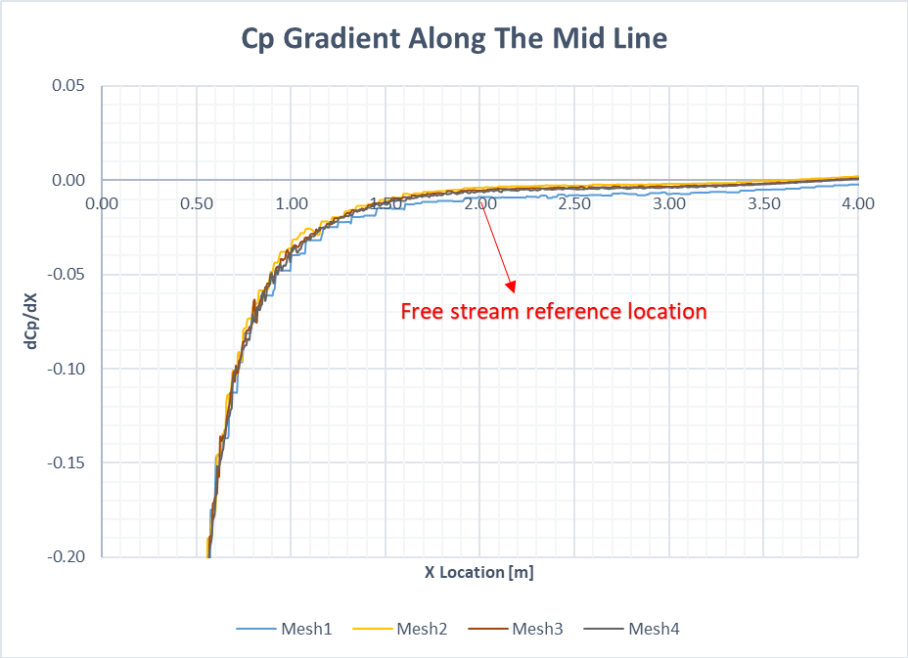

Figure 2.20 Midline C_P gradient comparison for different mesh cases (X=0 is center of vertical support system and the flow is in the negative X direction)

The results of Mesh2, Mesh3, and Mesh4 are nearly same up to X=2m location on the pressure coefficient data. However, the difference of Mesh1 can be noticed on Figure 2.20 clearly. According to the results, Mesh3 and Mesh4 are identical and can be concluded that the results converge for higher than 26 million mesh elements. The difference between Mesh2 and Mesh3 are in ignorable level around probe location. The 2 m upstream support system were used for the free stream static and dynamic pressure location to present the results, as shown Figure 2.20. During the mesh independency works, the first improvement was the arrangement of y+. It is lower than 1 for Mesh2, Mesh3 and Mesh4.

The parameters of Mesh2 were evaluated as suitable for simulations regarding both pressure data and computational time requirement related to the mesh elements. As a result, the mesh2 parameters were decided to be used for further analyses, and the domain mesh and parameters are provided below in Figure 2.21.

	Mesh
Traverse System BL First Layer	3×10^{-6} m
Traverse System BL Growth rate	1.2
Traverse System BL Total Layer	30
Tunnel Wall BL First Layer	45×10^{-7} m
Tunnel Wall BL Growth rate	1.3
Tunnel Wall BL Total Layer	30
Min size	4×10^{-4} m
Proximity min size	4×10^{-4} m
Max face size	6×10^{-2} m
Max tet size	8×10^{-2} m
Max Y+	0.98
Body of Influence	3×10^{-2} m
Max Skewness	0.88

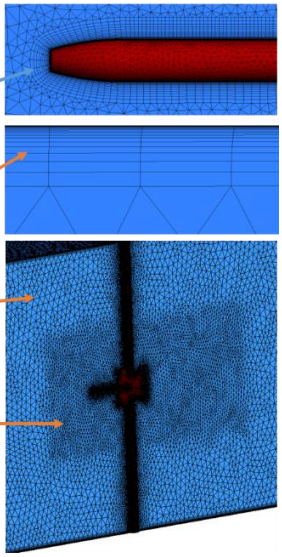

Figure 2.21 Computational mesh for the traverse system

2.2.2.5 Effects of the turbulence model

The arm length was fixed based on analyses performed using the k-omega SST turbulence model. In this section, k-epsilon standard, k-epsilon realizable, and k-omega SST models were performed to notice whether a difference occurs due to the turbulence model. C_P contour on a midplane and C_P data along the midline is provided in Figure 2.22 and Figure 2.23 respectively. C_P distribution is similar for different turbulence models. In the same C_P range, an area downstream of profile in Figure 2.22 for the k-epsilon standard solution is observed as different. According to the Figure 2.23, 0.003 C_P difference is observed for turbulence models. The Figure 2.24 provides the C_P distribution on probes for different turbulence models. The contours of three turbulence model are identical in this simulation.

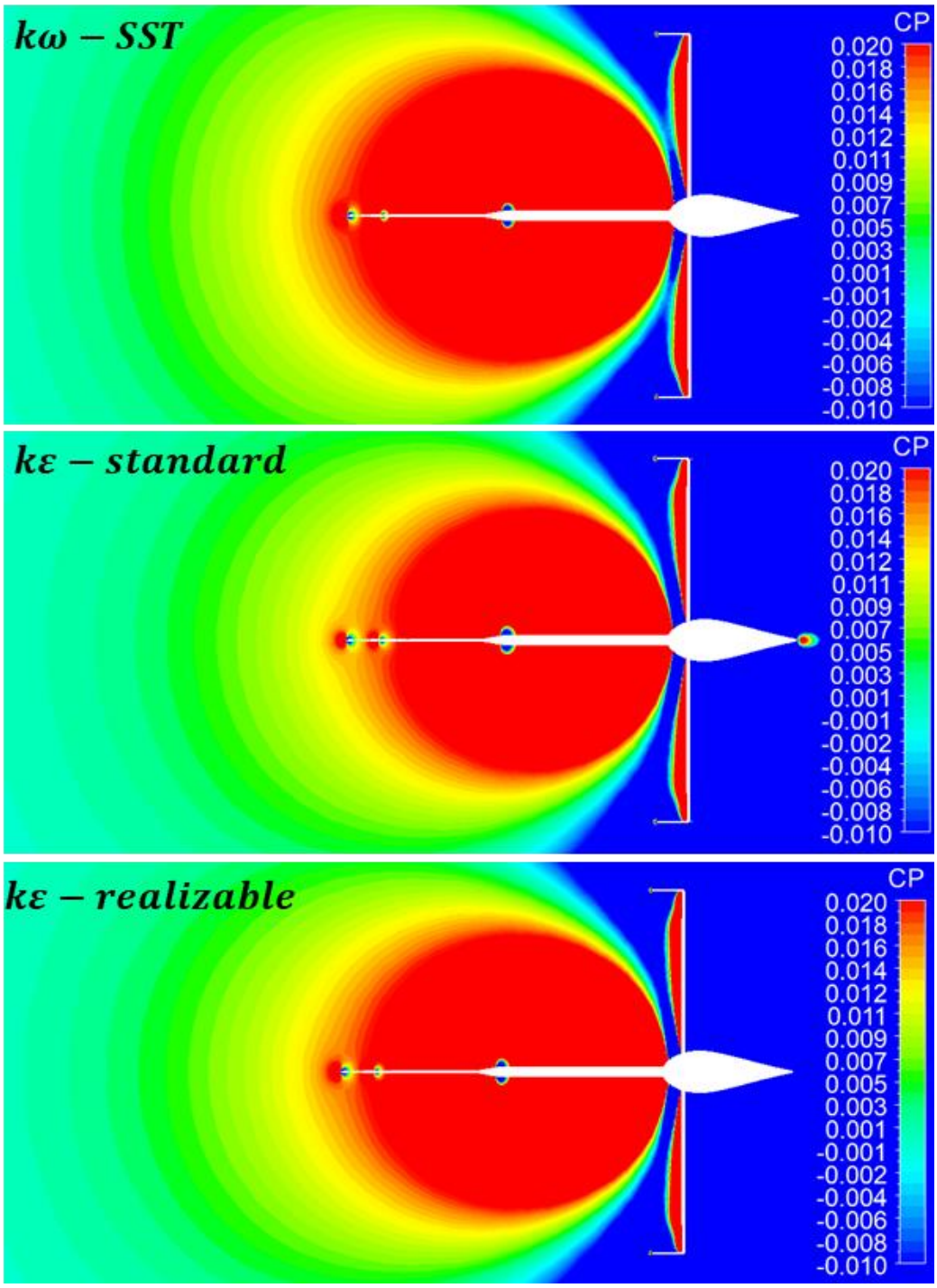

Figure 2.22 Contours of pressure coefficient (C_p) around the probe support obtained by use of different turbulence models

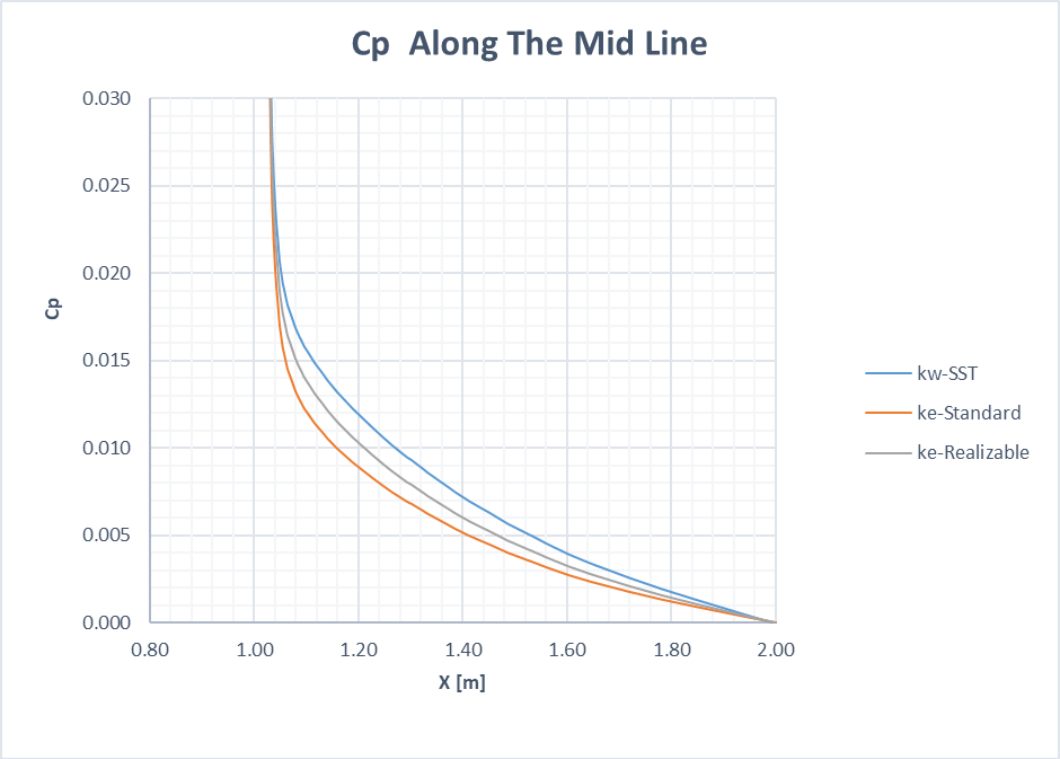

Figure 2.23 Turbulence model differences in C_P data along the midline (X=0 is center of vertical support system and the flow is in the negative X direction)

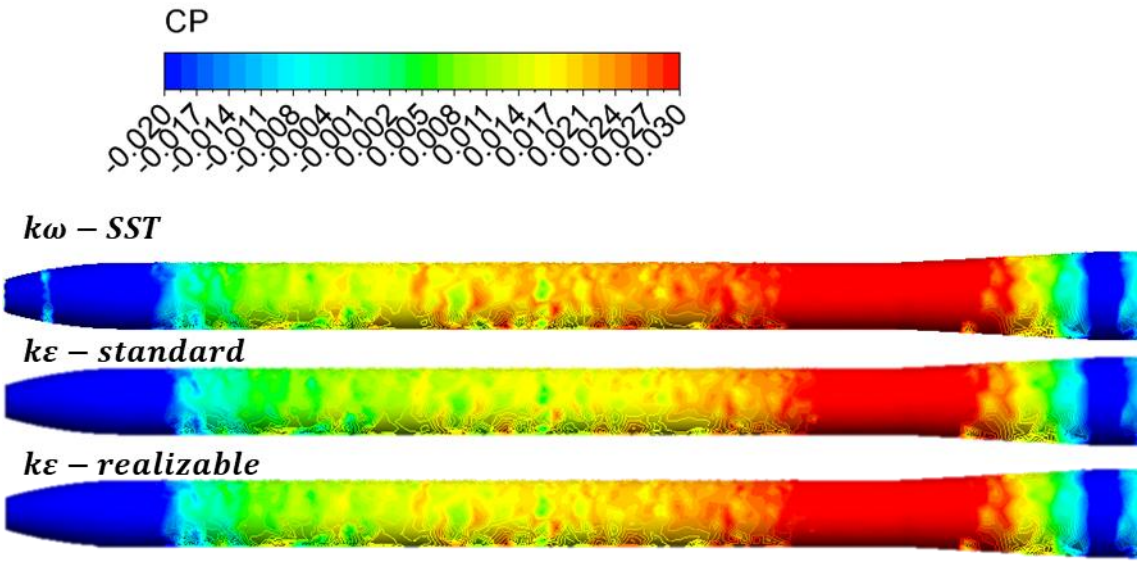

Figure 2.24 C_P Distribution comparison of turbulence models on the probe

2.2.2.6 Convergence Works

The convergence problem in the numerical simulations was investigated using Mesh1 since it has the minimum mesh number, resulting in a minimum convergence duration. The starting point of investigation is to check the inlet and outlet boundary conditions after convergence of the results. In this analysis, the velocity and the pressure distributions at the outlet are shown in Figure 2.25. The outlet condition of analyses seems fair enough to accept the results as converged; however, it is obvious that the support system wake reaches up to the outlet.

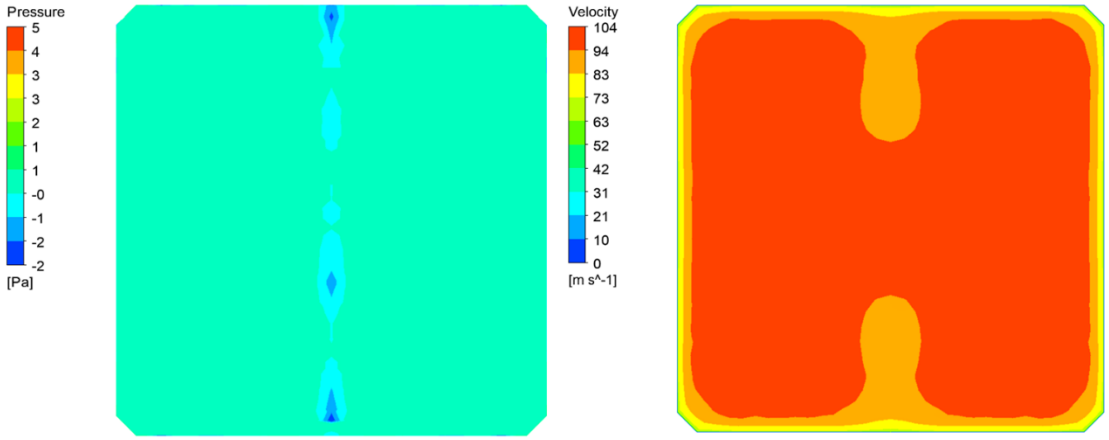

Figure 2.25 Velocity and pressure distribution on outlet

The current CFD domain was extended 15m downstream additionally; see Figure 2.26, without any area variation from the outlet of the test section to check whether the problem is due to downstream length or not. The same mesh parameters were applied to the domain, and analyses were repeated. The residuals history can be seen in Figure 2.27, and it was noted that the convergence issue is not due to downstream length.

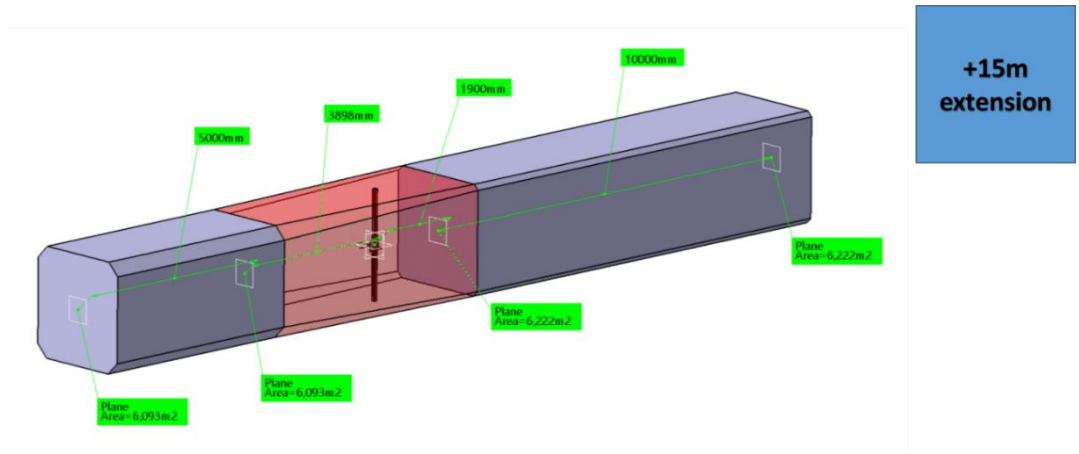

Figure 2.26 CFD Domain extension

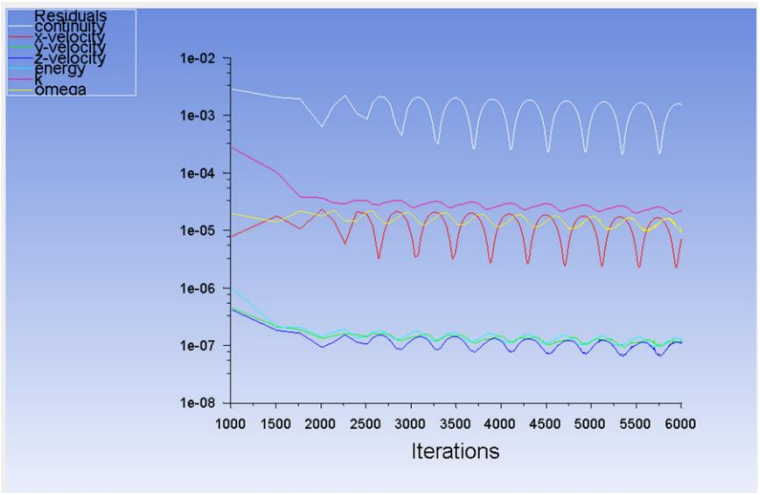

Figure 2.27 Convergence history of extended domain

As a result of this analysis, the wake region of the support does not dissipate up to the outlet, and it naturally causes unsteady flow during the analyses. An unsteady analysis was performed to observe the convergence history in detail. Analyses were run 3000 steps as steady, and then unsteady analyses with the following parameter were continued. For these analyses, mesh4 was preferred because it was decided in the mesh independency phase, and steady mesh analyses should be proven. The iteration number and time steps for unsteady analyses are provided in Table 2.3.

Table 2.3 Solution arrangements of unsteady analyses

Total steps	50
Time steps	0.001 s
Iteration	500

It can be resulted from the residual history that the analyses converge well in the unsteady analyses.

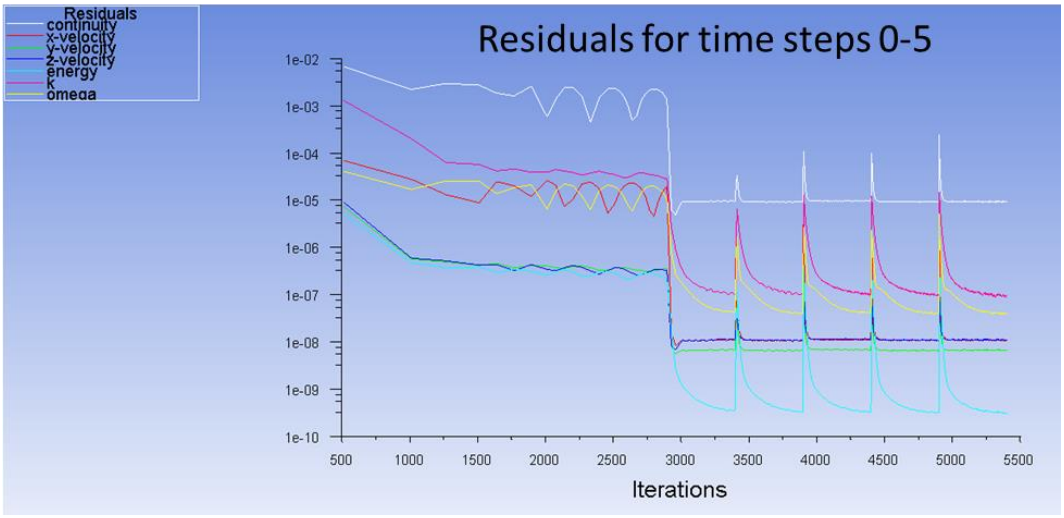

Figure 2.28 Unsteady analysis convergence history

The CFL number for unsteady analyses is around 2 for 100 m/s freestream condition, and the results are shown in Figure 2.29.

$$CFL = u * \frac{\Delta t}{\Delta x} = 100\ m/s * \frac{0.001\ s}{0.05\ m} = 2$$

A line at the mid of the tunnel was used for the data source, and the C_P along the line was provided in Figure 2.29. 0.015 C_P difference should be considered due to unsteadiness of this flow type for 100 m/s condition.

$C_P = 0.015$ resulted from $0.015 * 5500\ Pa = 82.5\ Pa \cong \pm 45\ Pa$

In conclusion, the steady analysis is suitable for evaluating the effect of the support system; however, as an important note from the below graph, ±45 Pa difference for 100 m/s freestream flow condition should be expected erroring relation unsteady variations.

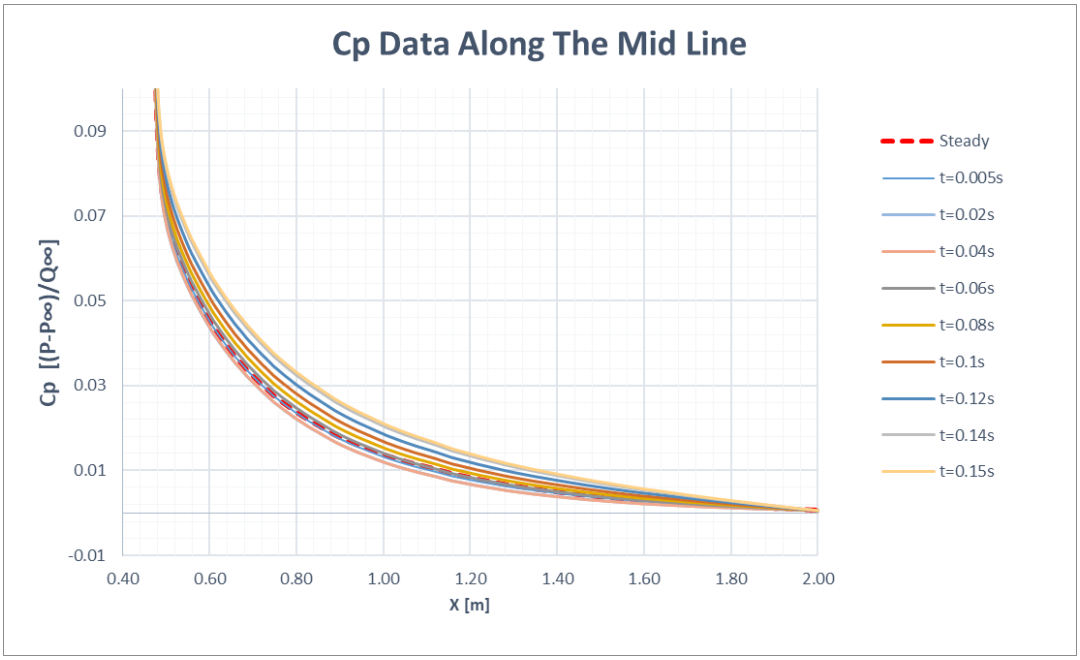

Figure 2.29 C_P Data along the midline (X=0 is center of vertical support system and the flow is in the negative X direction)

2.2.2.7 Simulation Results

The first results are comparisons of rectangular support, partial airfoil and entire airfoil. In these analyses, the stagnation points of probes are at the same location, and the support shapes are only changing parameters. X=0 location was defined as the center of vertical support system. The following figure provides a guide for better evaluating graphs regarding the probe's X, Y, and Z locations.

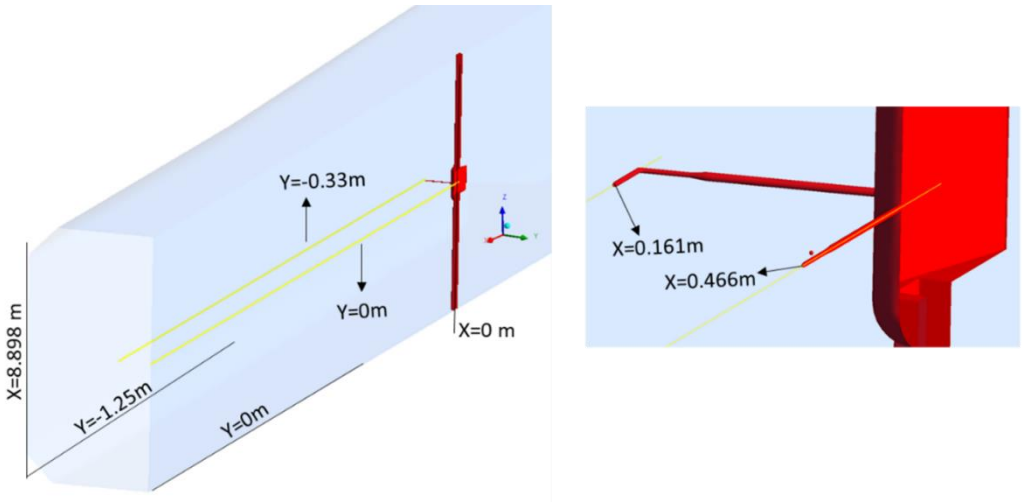

Figure 2.30 Traverse system probe and support system coordinates

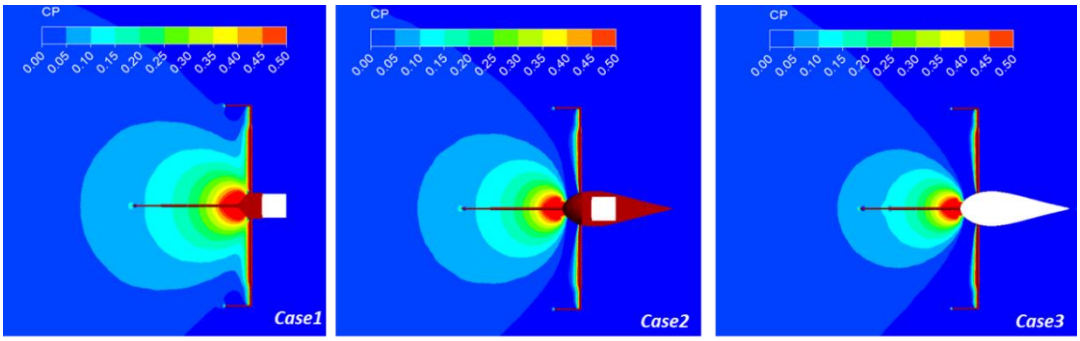

Figure 2.31 Contours of pressure coefficient around the support system plotted in horizontal mid plane of test section

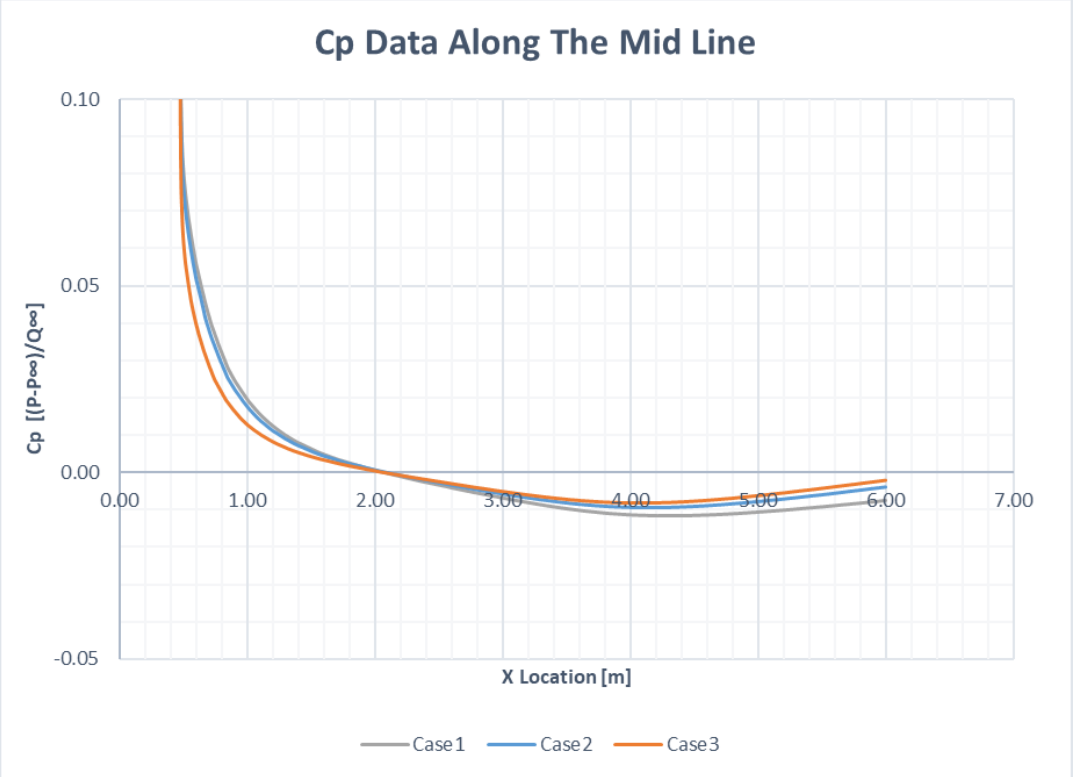

Figure 2.32 C_P Data along the defined midline (X=0 is center of vertical support system and the flow is in the negative X direction)

According to the results,

- The pressure gradient is better for the full profile support (case3), but it has a disadvantage in terms of manufacturability and moving the complete system assembly.
- The partial faring concept (case2) and rectangular support without any fairing (case3) have similar C_P data along the midline except for the X location of 0.5 m to 1.2m which shows the effect of the partial fairing.

The partial faring was evaluated as a better option regarding the disadvantages of manufacturability of the entire support system

Secondly, the results of partial fairing are investigated in detailed for 100 m/s. X=2 m position was chosen as free stream location as shown in Figure 2.33, and C_P

gradient along the midline with respect to the defined freestream static pressure and dynamic pressure is noted on the graph. 120 Pa differences along the test section, 5.8 meters in total, were noted based on empty tunnel analysis, so a 20 Pa difference per meter is expected along the test section. In Figure 2.33, horizontal dashed lines were spotted to notice where the 20 Pa difference exceeds.

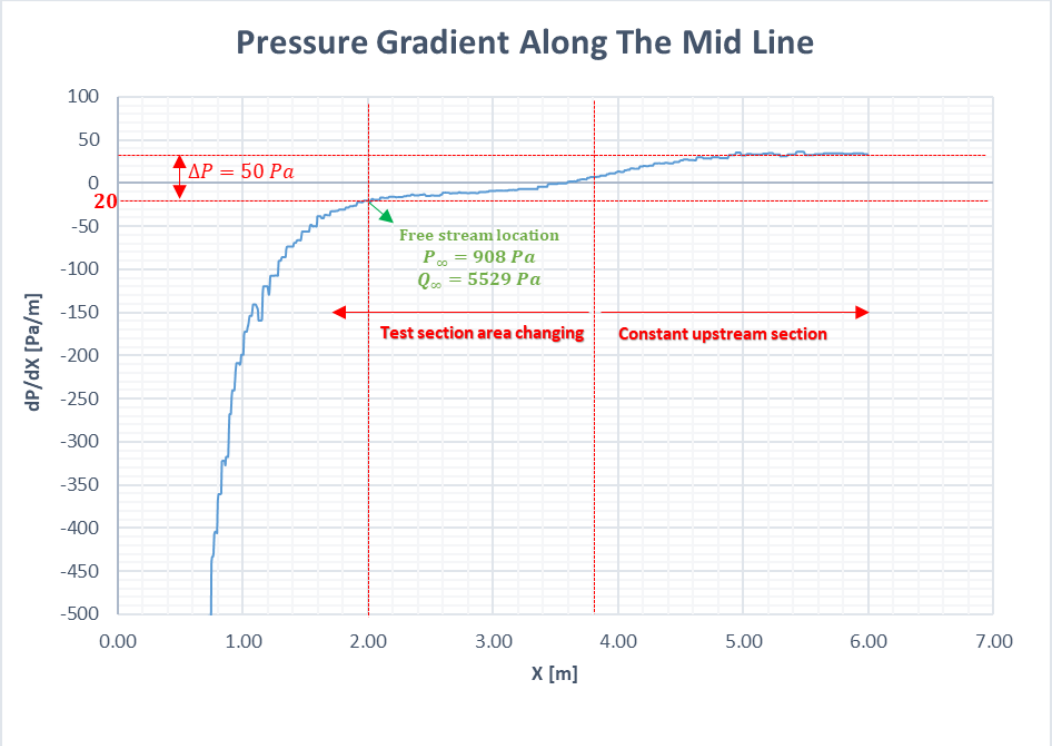

Figure 2.33 Pressure gradient to define the freestream location of ATS at a freestream velocity of 100 m/s (X=0 is center of vertical support system and the flow is in the negative X direction)

For this analysis, the freestream dynamic pressure is 5529 Pa for 100 m/s free stream velocity. 100 Pa difference was chosen as a target to be measured at the mid probe considering that the 20 Pa change is due to the tunnel geometry and the 80 Pa difference is due to the unsteady characteristics of flow. The following criteria was investigated in the mid contour of the analysis.

$$\Delta C_P = \frac{100\ Pa}{5529\ Pa} = 0.018$$

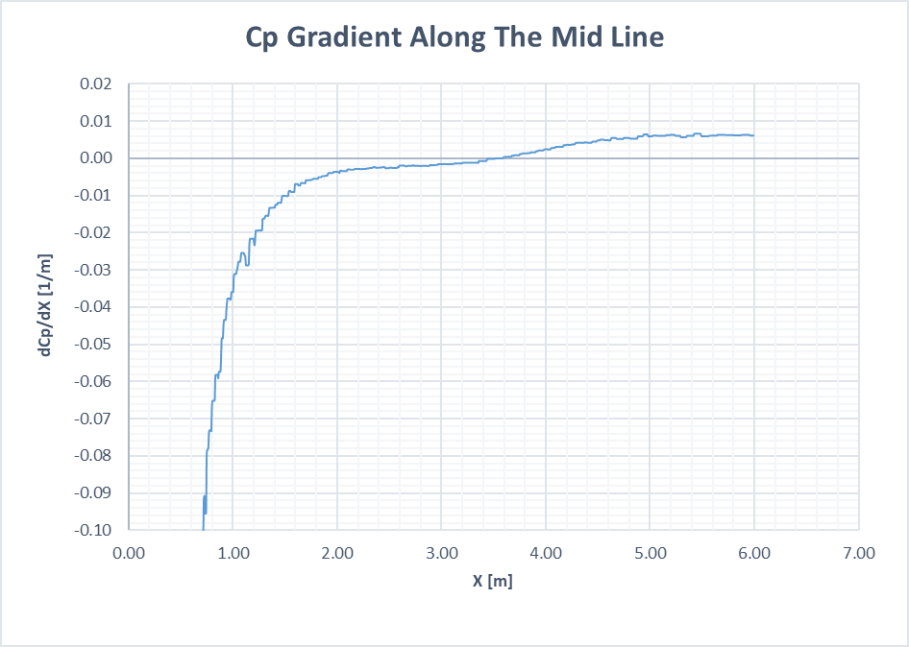

Figure 2.34 C_P Gradient along the midline of ATS at a freestream velocity of 100 m/s (X=0 is center of vertical support system and the flow is in the negative X direction)

The mid C_P contour and midline C_P data are provided in Figure 2.35 and Figure 2.36. According to these results, the mid probe stagnation point should be located at least at X=0.9 m location. For this purpose, the mid probe length should be extended for a minimum of 0.44 m so as not to be affected by the support system. Furthermore, it should be noted from Figure 2.37 that the static pressure measurement of "L" shape probe is not proper to be used for characterization tests regarding it is C_P difference that is higher than 0.5.

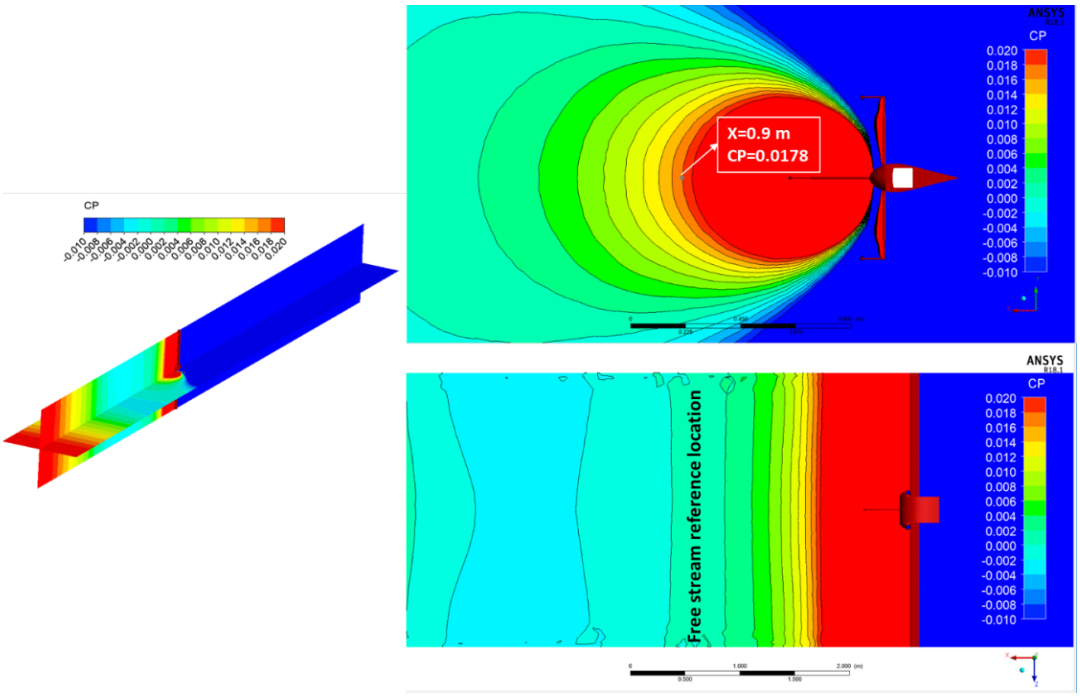

Figure 2.35 C_P Contours of traverse system at ATS at a freestream velocity of 100 m/s

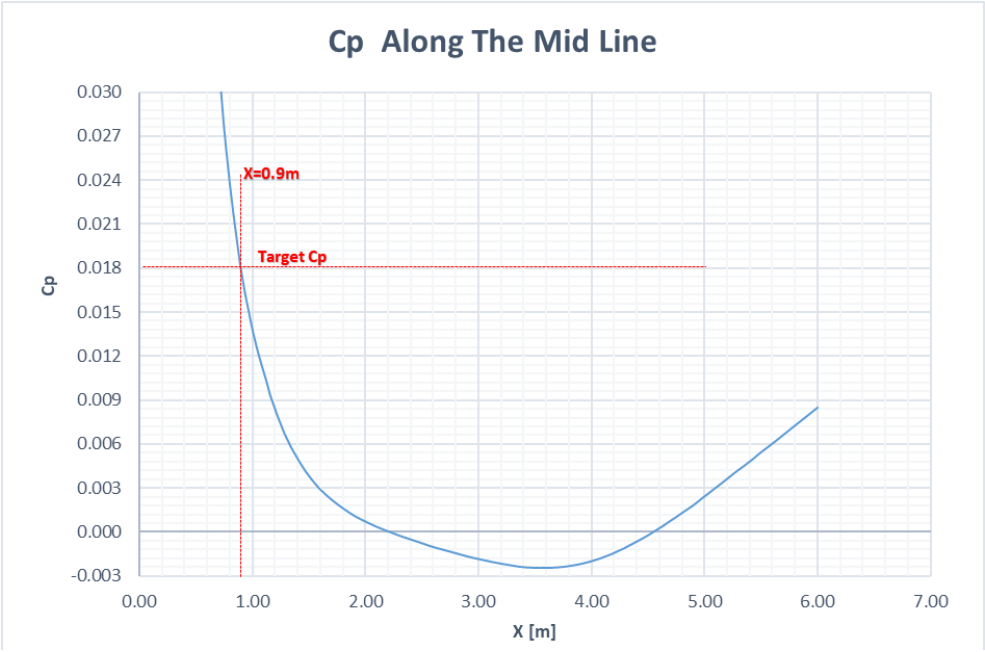

Figure 2.36 C_P Data along the midline of ATS at a freestream velocity of 100 m/s (X=0 is center of vertical support system and the flow is in the negative X direction)

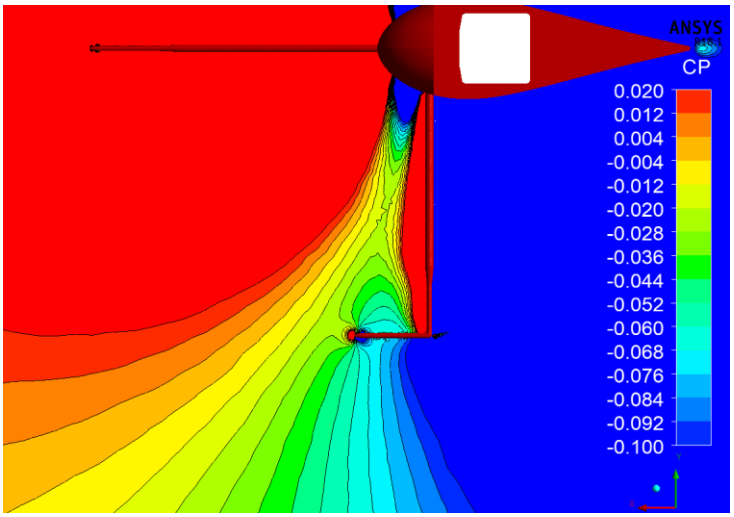

Figure 2.37 C_P Contours in horizontal mid plane of test section for "L" shape probe

The probe length affects the static pressure measurement mainly. It becomes effective on velocity since velocity is calculated from the dynamic pressure. In this situation, the mid probe length was extended for 550 mm, and the analysis was repeated. X=2 m location was used free stream parameter regarding previous results for C_P calculations.

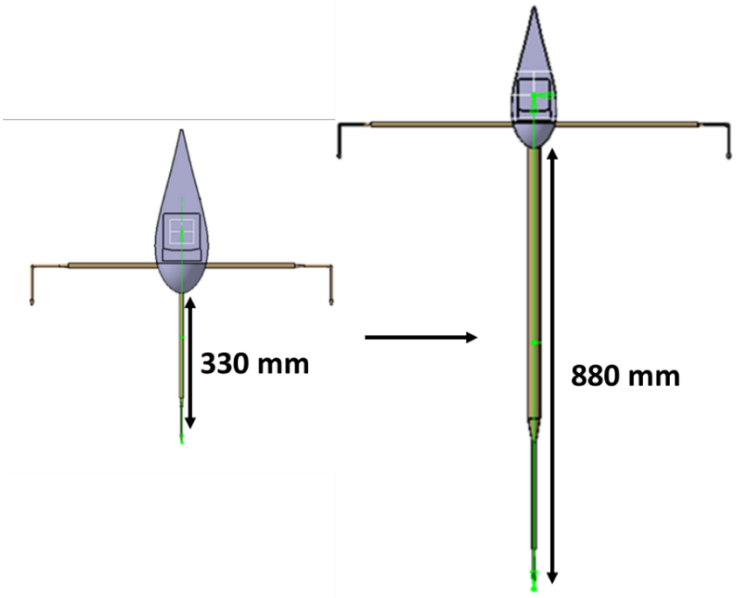

Figure 2.38 Traverse system mid probe length update

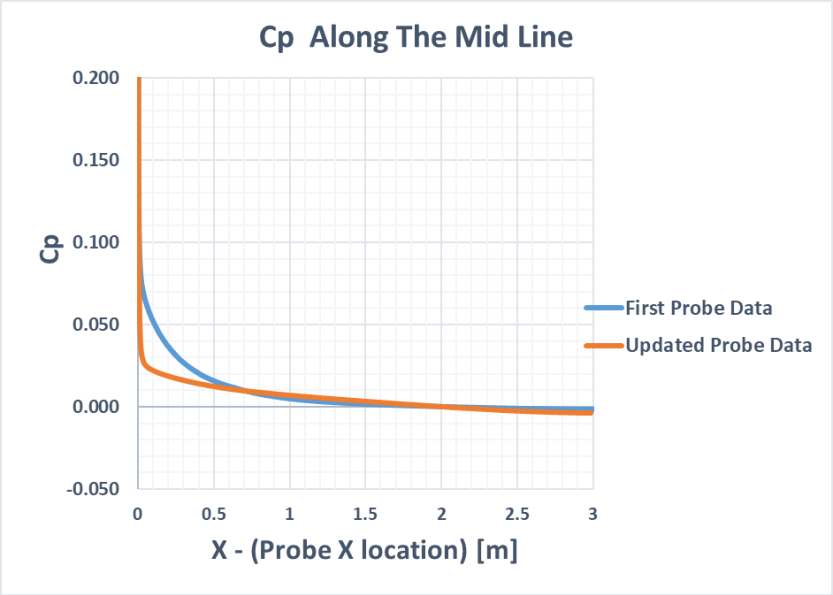

Figure 2.39 C_P Data comparison for first and updated probe length (X=0 is center of vertical support system and the flow is in the negative X direction)

In the first observation in Figure 2.40, it can be concluded that the target C_P was accomplished with the updated arm length. Also, an extension with a larger diameter was added to extend the probe, and its effect was minimal, focusing on the same C_P distribution in Figure 2.40, showing that the main back pressure effects are due to the support system as expected. Figure 2.41 shows the C_P distribution on the probe. It verifies the analyses by showing the stagnation pressure asunity. The main purpose of extending the probe is to avoid the support effect and measure the true static pressure value of the freestream. The C_P should be zero "0" in the ideal case. However, the steady/unsteady effects and empty tunnel distribution were discussed, and noted that ± 0.018 C_P was estimated as an acceptable deviation. The C_P contours on the extended probe and first length probe present that the aim was achieved on the extended probe see Figure 2.42.

In conclusion, this updated probe length should be used on the traverse system according to the analyses which are probe center of tunnel and freestream velocity is 100 m/s condition. The mid probe length is fixed, and then different positions of the

traverse system at various velocity conditions were analyzed to report the effect of the traverse system. On the other hand, freestream is accelerating near the support system due to blockage; hence "L" shape probes are considered not to provide accurate static pressure measurement.

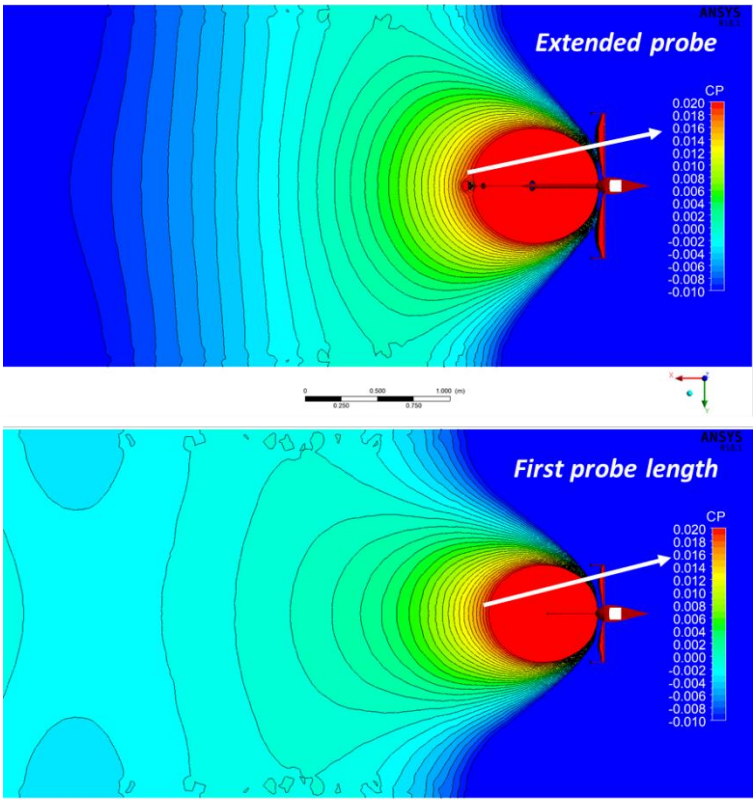

Figure 2.40 C_P Contours of first and updated probes at a freestream velocity of 100 m/s

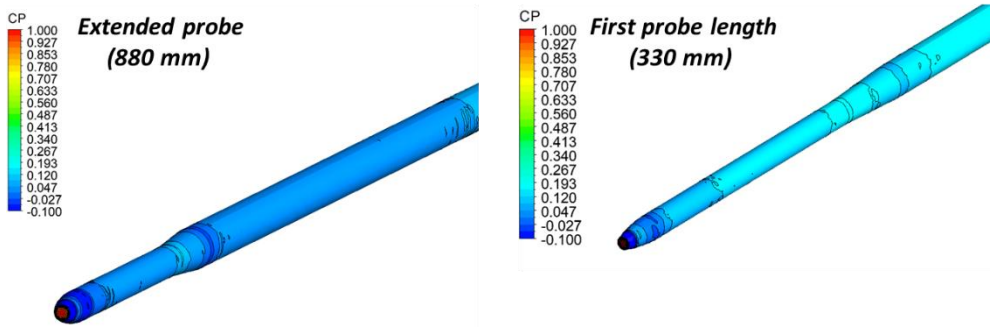

Figure 2.41 C_P Distribution on probes with a length of 880 mm (left) and with a length of 330 mm (right)

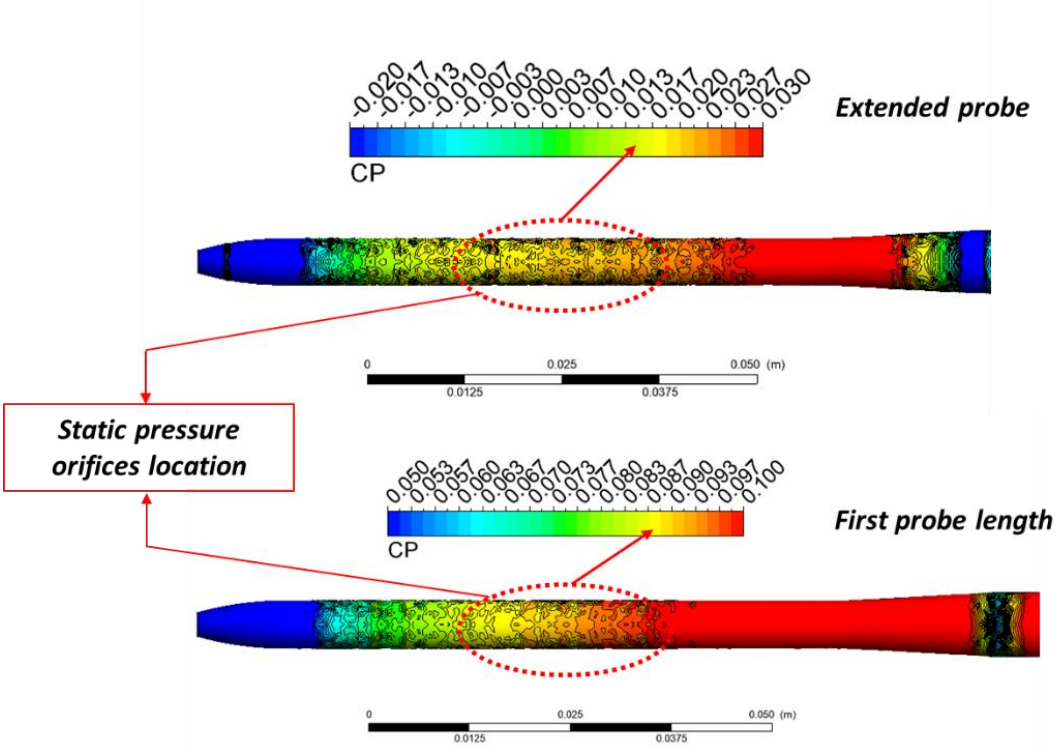

Figure 2.42 C_P Comparison on the first version of the probe (L=330 mm) and the extended probe (L=880 mm)

At the end, the traverse system was analyzed for 9 cases (Table 2.4), and the results are given in Table 2.5. The Figure 2.43 shows the area that used for averaging.

Table 2.4 Case definitions and freestream conditions

		Freestream			
	Probe at	***Q [Pa]***	***Mach***	***V (m/s)***	***Re*10^6 (1/m)***
Case1	Center	5463	0.286	99.6	6.0
Case2	Center	218	0.057	19.9	1.2
Case3	Center	1963	0.172	59.7	3.6
Case4	Bottom	5498	0.287	99.6	6.0
Case5	Bottom	218	0.057	19.9	1.2
Case6	Bottom	1962	0.172	59.7	3.6
Case7	Left	5469	0.287	99.6	6.0
Case8	Left	218	0.057	19.9	1.2
Case9	Left	1962	0.172	59.7	3.6

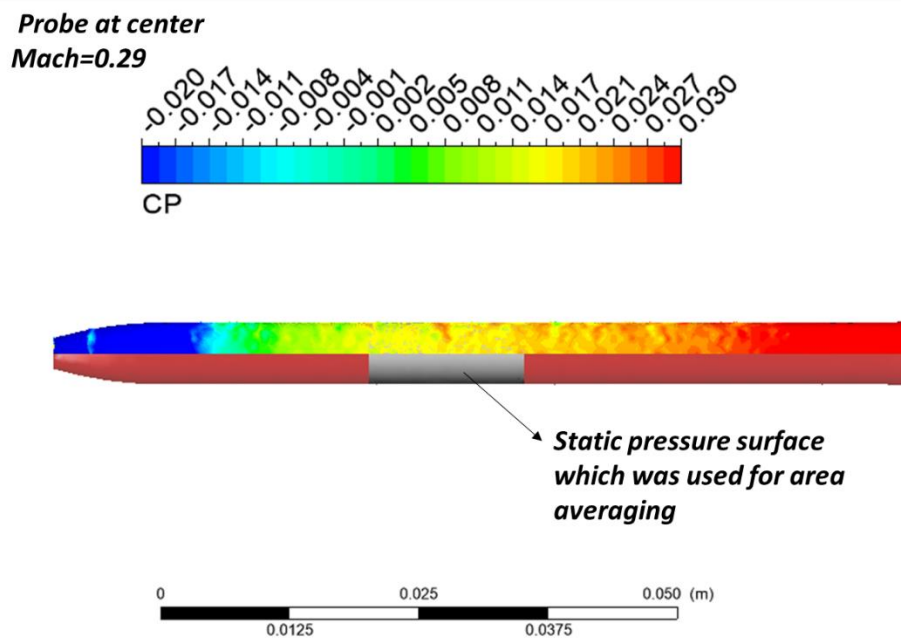

Figure 2.43 Center probe C_P calculations (L=880 mm)

Table 2.5 Traverse system analysis results

	Probe at	*Mach*	*Avr C_P on probe*	*Pressure Difference*	*ΔP/Q %*	*Error on Velocity %*
Case1	Center	0.29	0.018	98	1.8	1.1
Case2	Center	0.06	0.015	3	1.5	0.8
Case3	Center	0.17	0.015	30	1.5	0.9
Case4	Bottom	0.29	0.012	63	1.2	0.8
Case5	Bottom	0.06	0.012	3	1.2	0.7
Case6	Bottom	0.17	0.015	30	1.5	0.9
Case7	Left	0.29	0.024	132	2.4	1.3
Case8	Left	0.06	0.022	5	2.2	1.2
Case9	Left	0.17	0.022	42	2.2	1.3

According to the Table 2.5, when the probe is located at close to the side wall, defined as probe at left on table, the expected errors on velocity measurements is increasing. The changing of Mach number does not cause a dramatic change for error on velocity. Table 2.5 provides the static pressure difference between probe and

freestream. In non-dimensional form ($\Delta P/Q$), 2.4 percentage difference can be caused depending on probe length and position. The differences provided in table should be taken into considerations during the evaluation of experimental results.

Furthermore, the bottom part of traverse system has a horizontal support. This support creates a blockage inside the test section and it has an effect on angularity. 2-Dimensional simulation in ATS was performed to investigate the effect of blockage. The domain is presented in Figure 2.44. A mid plane at the center of tunnel was created. The bottom part of traverse system was subtracted from plane.

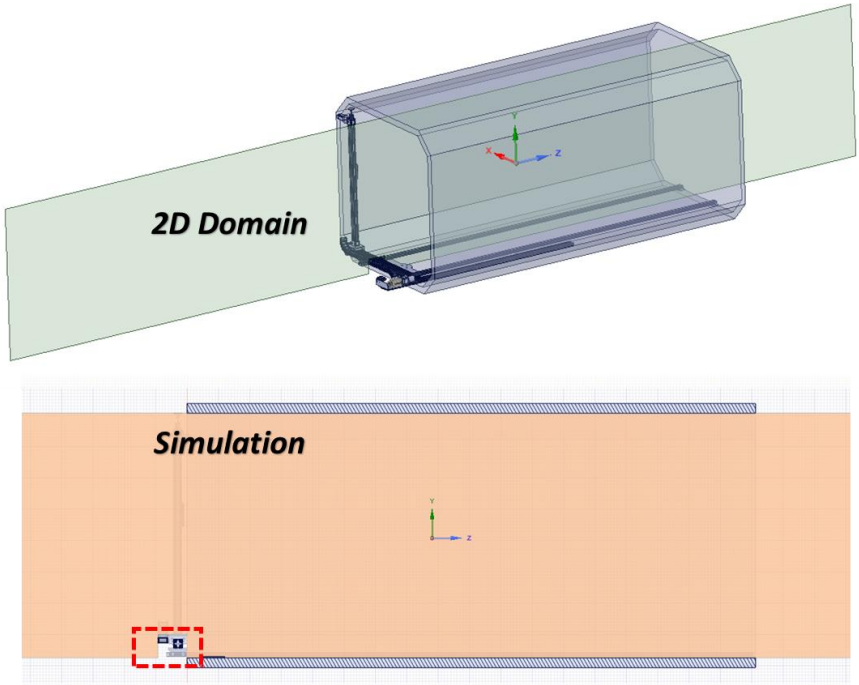

Figure 2.44 2D Simulation domain for blockage effect

The results for a freestream of 35 m/s and 100 m/s are given in Figure 2.45. The graphs present the upwash angle at different vertical locations. According to the results, the magnitude of angle increases at around horizontal support system. For both 35 m/s and 100 m/s freestream conditions, 1° to 3° pitch angle can be observed at current location of probe due to blockage of bottom part of traverse system. It should be taken into account during the characterization measurements.

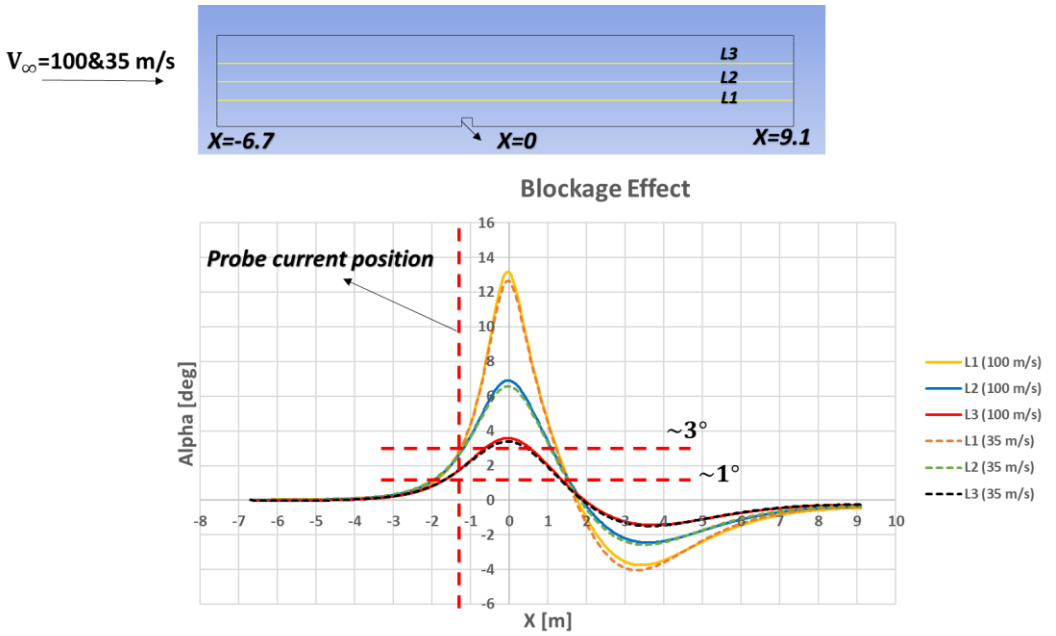

Figure 2.45 2D Flow angularity simulation results (X=0 is leading edge of the rectangular part and the flow is in the positive X direction)

CHAPTER 3

RÜZGEM LARGE SCALE WIND TUNNEL CHARACTERIZATION MEASUREMENTS

3.1 Experimental Setup

3.1.1 Boundary Layer Test Section

The traverse system is assembled to the Boundary Layer Test Section (BLTS) as shown in Figure 3.1. The traverse system is designed to measure the half of the cross-section at a time. After that, the system can traverse the remaining half by rotating the turntable for 180°. It should be noted that when the turntable is moved, it seems like the probe will be placed towards to the downstream however the vertical part of traverse system has also rotational degree of freedom so that the probe can be aligned with the flow easily. Only one plane, named as X=0.75 m location, which traverse was located at centre of test section and the probe position is 900 mm upstream condition with regard to centre of turn table, was defined as characterization plane for boundary layer test section.

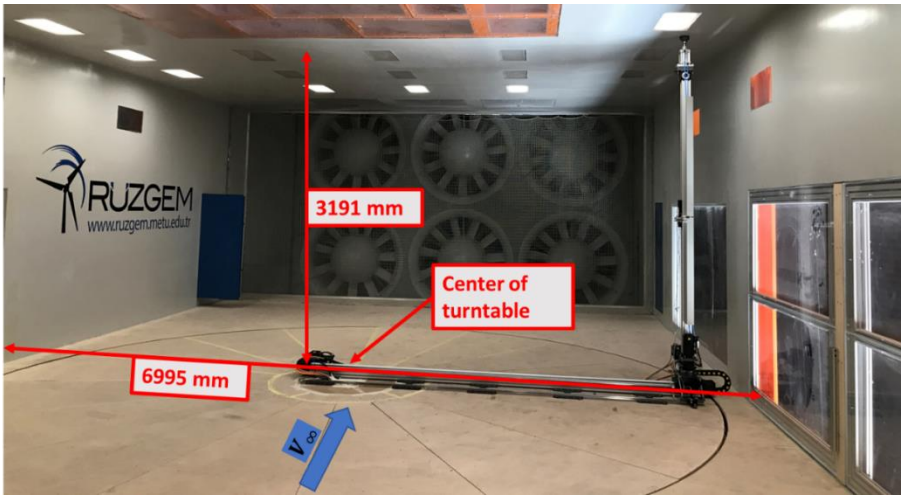

Figure 3.1 Traverse system setup for BLTS

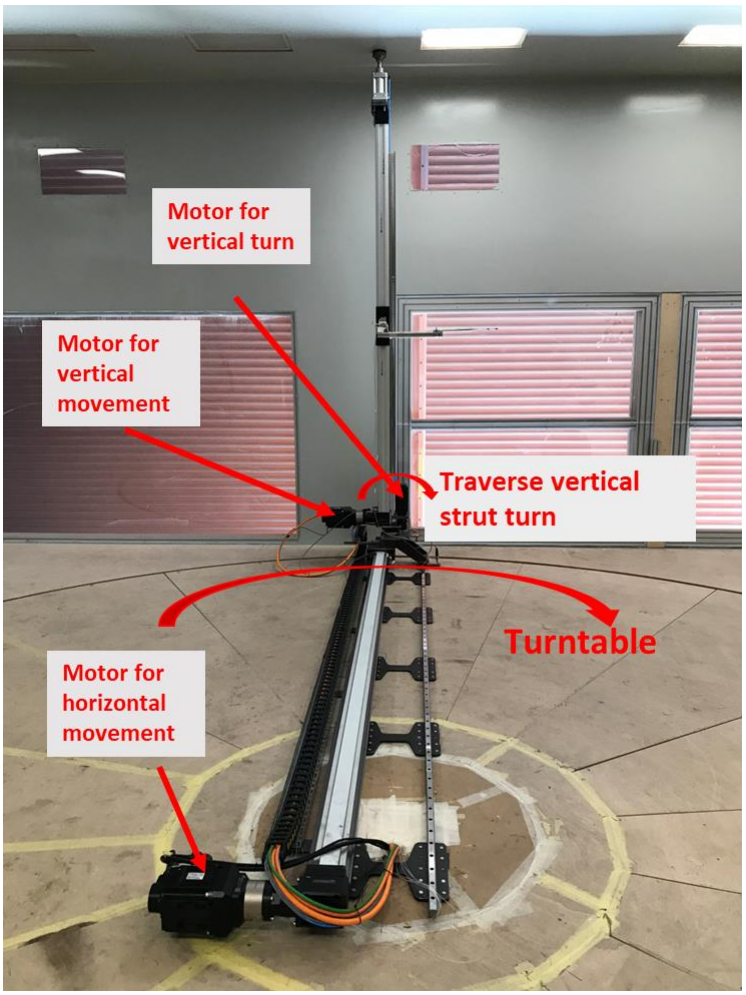

Figure 3.2 Traverse system movement mechanisms

The traverse system probe lengths are discussed in CHAPTER 2 and the required distance with the expected errors are noted. In the preliminary experiments performed in the BLTS, the probe extension part was not ready so that an available sigma aluminium profile is used to attach the five-hole probe to the traverse system. The details of the connection and the resultant lengths are provided in Figure 3.3. The suggested distance from the vertical traverse support is actually 880 mm yet in the preliminary measurements it was recorded as 670 mm roughly.

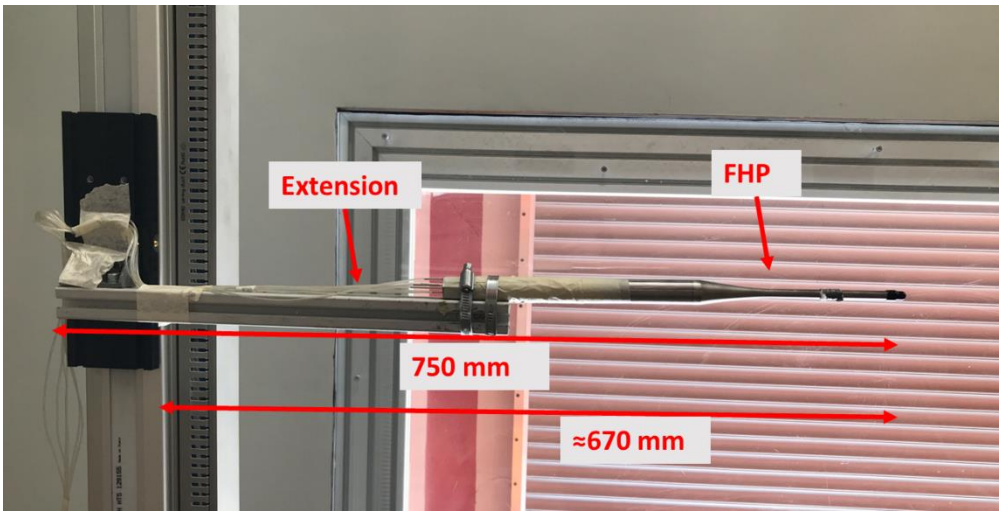

Figure 3.3 FHP Assembling on traverse system in BLTS

The measurements in the BLTS are performed by using a five-hole probe (FHP). The acquired data with the five-hole probe provides information regarding the flow angularity, static pressure and total pressure at the measurement point. The measurement points are shown in Figure 3.4. The measurements conducted in the boundary layer test section are as summarized in Table 3.1.

Table 3.1 Measurements in the BLTS

Dynamic pressure stability	**Flow angularity, total pressure, static pressure, dynamic pressure and velocity distribution.**
FHP, V_∞=14.8 m/s, 500 Hz sampling rate, 5 minutes data duration	FHP, V_∞=14.8 m/s, 500 Hz sampling rate, 30 seconds data duration
At the centre of tunnel (X=0.75, Y=0, Z=0)	Intervals of 400 mm horizontally and vertically. (X=75, ΔY=400 mm, ΔZ=400 mm)
	30 seconds wait after movement of traverse

During the measurements 1 psid Scanivalve MPS4264 type pressure scanner was used. The uncertainty of pressure scanner is ±0.06% of full scale. ±8.3 Pa measurement error should be expected. The measurement intervals are mainly 400 mm; however, a set of data denser at the center of the tunnel was acquired depending on the movement of the turntable, see Figure 3.4.

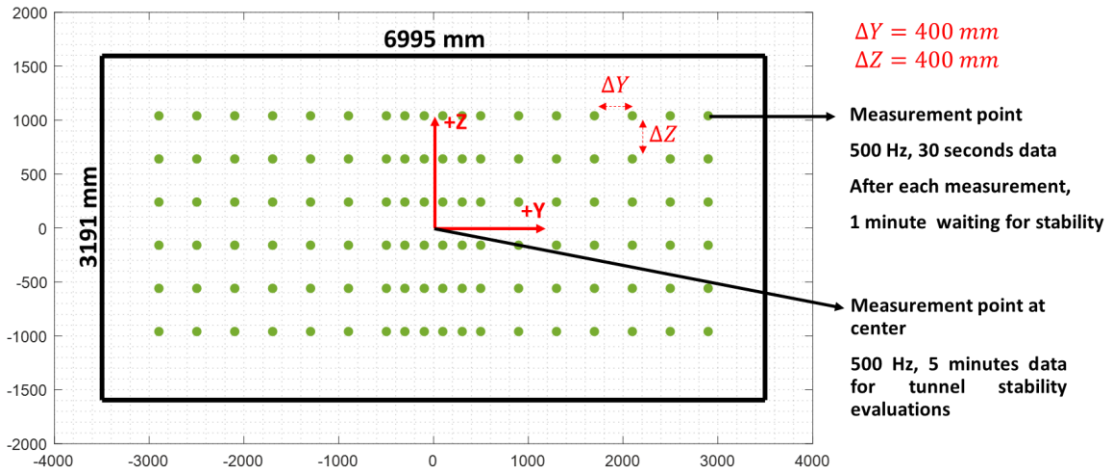

Figure 3.4 Measurement plan for boundary layer test section

3.1.2 Aeronautical Test Section

The traverse system is assembled to the Aeronautical Test Section (ATS) as shown in Figure 3.5 and probe lengths in Figure 3.6. The traverse system probe lengths are discussed in CHAPTER 2 and the required distance with the expected errors are noted. During the experiments of aeronautical test section, the probe extension part was assembled to the system. The total length of probe was recorded as 1350 mm which is 470 mm longer than target of 880 mm.

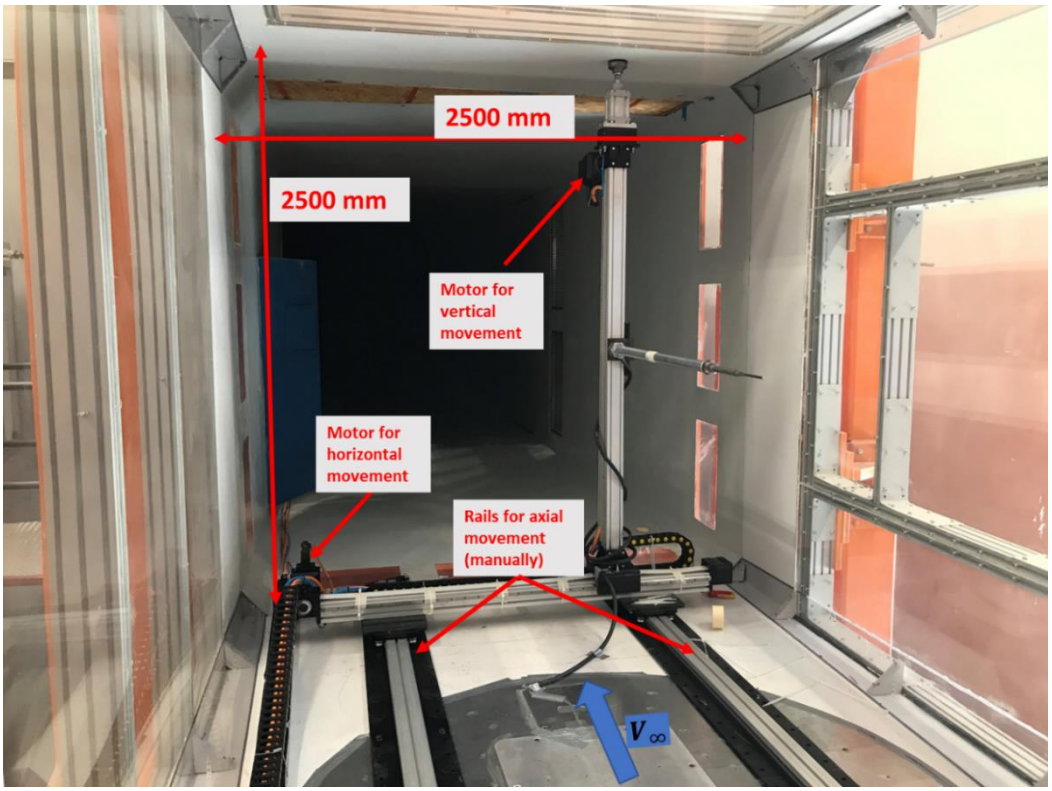

Figure 3.5 Traverse system setup for ATS

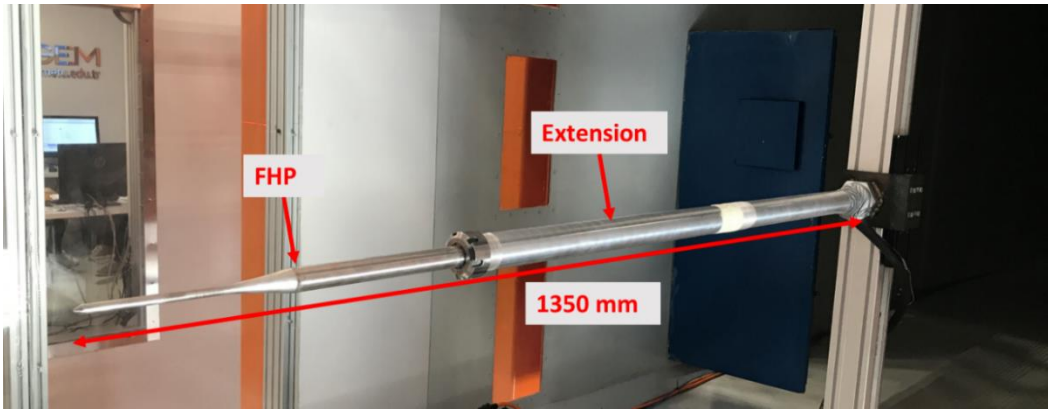

Figure 3.6 FHP Assembling on traverse system in ATS

The characterization tests in the aeronautical test section are performed by using a five-hole probe. The acquired data with the five-hole probe provides information regarding the flow angularity, static pressure and total pressure at the measurement

point. The measurement points are shown in Figure 3.7. Traverse system was located at 1350 mm downstream of tests section in order to acquire data at center of test section. The measurements conducted in the aeronautical test section are as summarized in Table 3.2.

Table 3.2 Measurements in the ATS

Dynamic pressure stability	**Flow angularity, total pressure, static pressure, dynamic pressure and velocity distribution.**
FHP, V_∞=35 m/s and 70 m/s, 500 Hz sampling rate, 2 minutes data duration	FHP, V_∞=35 m/s and 70 m/s, 500 Hz sampling rate, 30 seconds data duration
At the centre of tunnel (X=0.0, Y=0, Z=0)	Intervals of 200 mm horizontally and vertically. (X=0, ΔY=200 mm, ΔZ=200 mm)
	30 seconds wait after movement of traverse

During the measurements 1 psid Scanivalve MPS4264 type pressure scanner was used. The uncertainty of pressure scanner is ±0.06% of full scale. ±8.3 Pa measurement error should be expected.

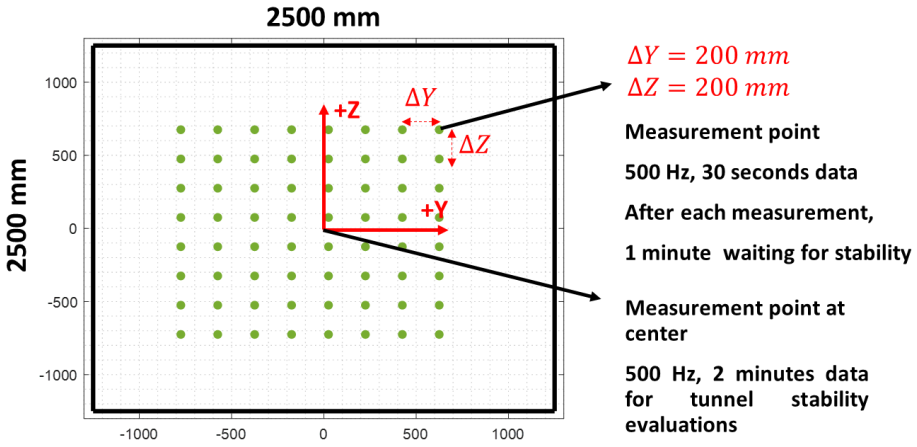

Figure 3.7 Measurement plan for aeronautical test section

For further investigation of effect of traverse system, a support system was assembled in aeronautical test section without any rail and motor systems. Figure 3.8 shows the support system, sting and five-hole probe installation in aeronautical test section.

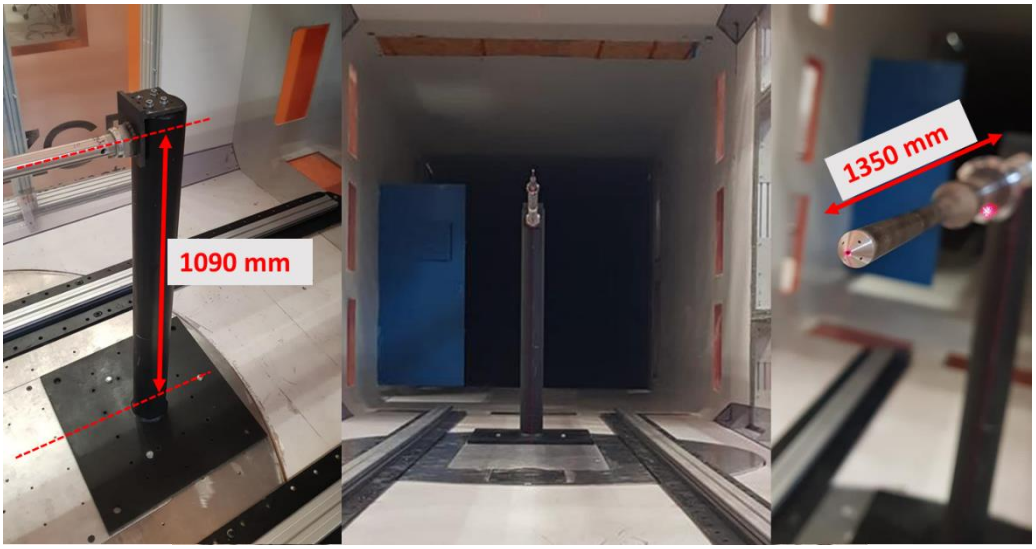

Figure 3.8 Support system installation in aeronautical test section

3.2 Characterization Results

3.2.1 Boundary Layer Test Section

The characteristic of the BLTS of RÜZGEM large scale wind tunnel for a freestream velocity of 14.8 m/s are given in the following figures. The Table 3.3 provides details of measurements. All pressure measurements are provided as gauge pressure. During the experiments, the density of tunnel was acquired from the tunnel data logs and used as input for the calculation of velocity. The data logs of tunnel are given in Figure 3.9. The graphs provide freestream velocity and density changing during the tests. Figure 3.9 provide the log for two days. The reason of the density jump on graph is that the data were acquired at different days. The freestream velocity was defined as 14.8 m/s and density was accepted as constant value of 1.04 according to the logs.

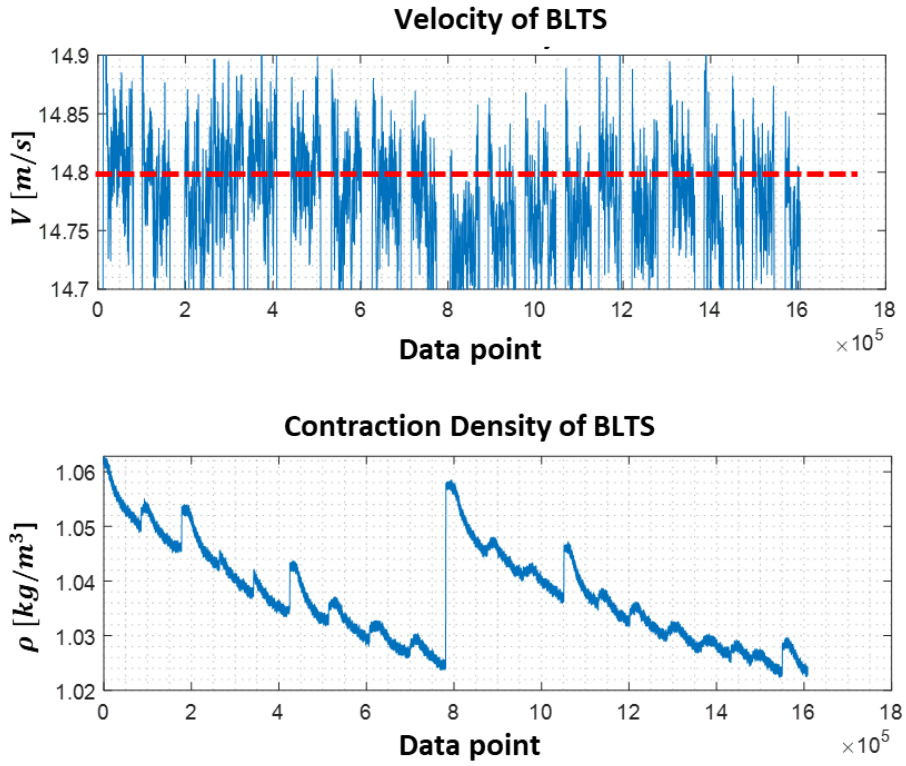

Figure 3.9 Tunnel log data during the characterization measurements of BLTS

Table 3.3 Measurements at the center plane of BLTS for 14.8 m/s

	P_S [Pa]	P_T [Pa]	Q [Pa]	V [m/s]
Minimum	29.3	64.0	41.5	8.9
Maximum	26.8	145.7	121.3	15.3
Mean	23.4	107.3	83.8	12.6
Standard Deviation	1.6	21.4	20.5	1.6

5 Hz low pass filter was applied to the stability measurements in order to avoid the effect of noise. The dynamic stability of BLTS is around ±9% (see details in Figure 3.10). This value is higher than the suggested value of 0.5% [9]. The experiments were performed at freestream velocity of 14.8 m/s. The dynamic pressure is 83.8 Pa as average and this value is small relatively. During these measurements, a pressure

scanner with a range of 1 psid was used, which has an uncertainty range of ±8.3 Pa. The pressure scanner causes 10% uncertainty for a dynamic pressure of 83 Pa. In this dynamic pressure level, small changing on measurements and/or flow causes abrupt changing on stability. The main purpose of BLTS is to perform boundary layer related tests and this level of stability should be taken into consideration during the performing of tests at BLTS.

In Figure 3.11, an upwash angle (pitch angle) of around 4° is observed. This is an unexpected observation for the BLTS. This is probably attributed to the influence of the bottom part of the traverse mechanism. Furthermore, the distance from the vertical traverse was recorded as 670 mm roughly during the measurement. The new extension was not assembled to the traverse system of BLTS yet. The extension of the length of the probe can also help for the acquiring healthier data for flow angularity.

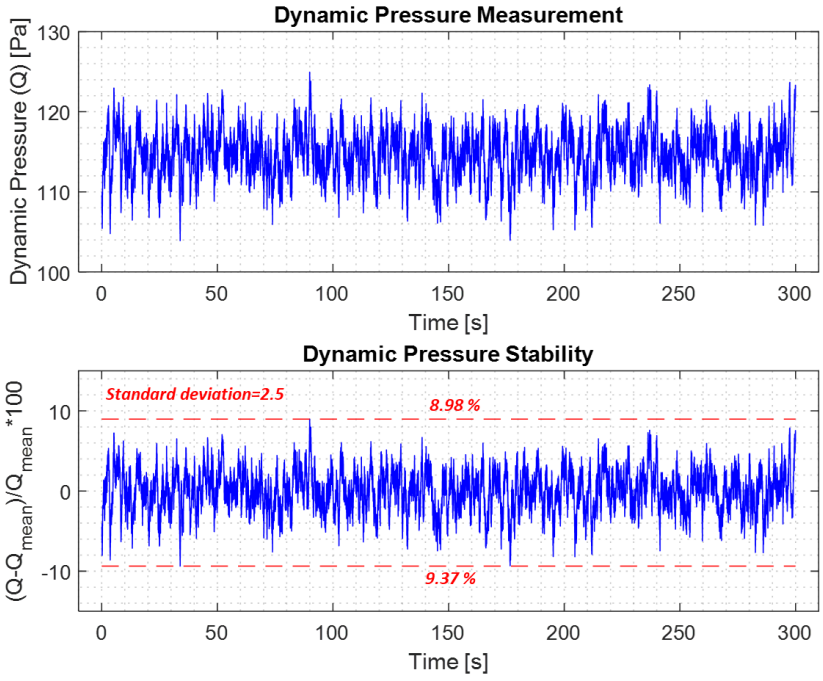

Figure 3.10 Dynamic stability results of BLTS ($V_\infty = 14.8\, m/s$)

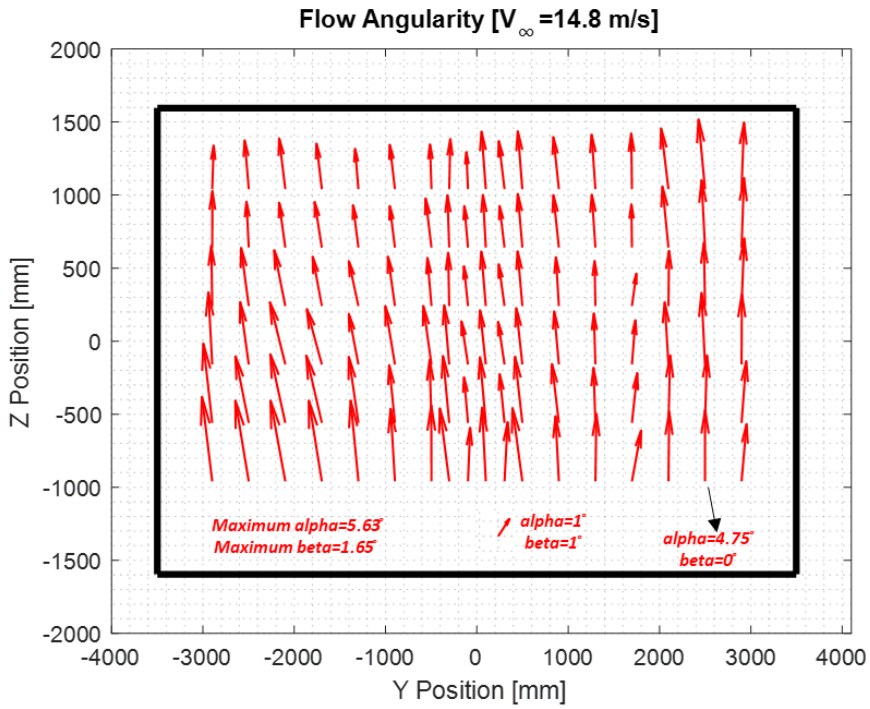

Figure 3.11 Flow Angularity of BLTS

In Figure 3.12, Figure 3.13, and Figure 3.14, the variations of static, dynamic and total pressure are provided respectively. The dynamic pressure and the total pressure variations have identical contours. On the other hand, there is no specific variation on static pressure. The Figure 3.15 gives the velocity distribution of BLTS at a freestream of 14.8 m/s. Both in total pressure and velocity contours, the values are increasing towards to the center of tunnel. In the velocity graph, the center has nearly same velocity with freestream and the velocity is decreasing near around wall. This can be due to boundary layer growth.

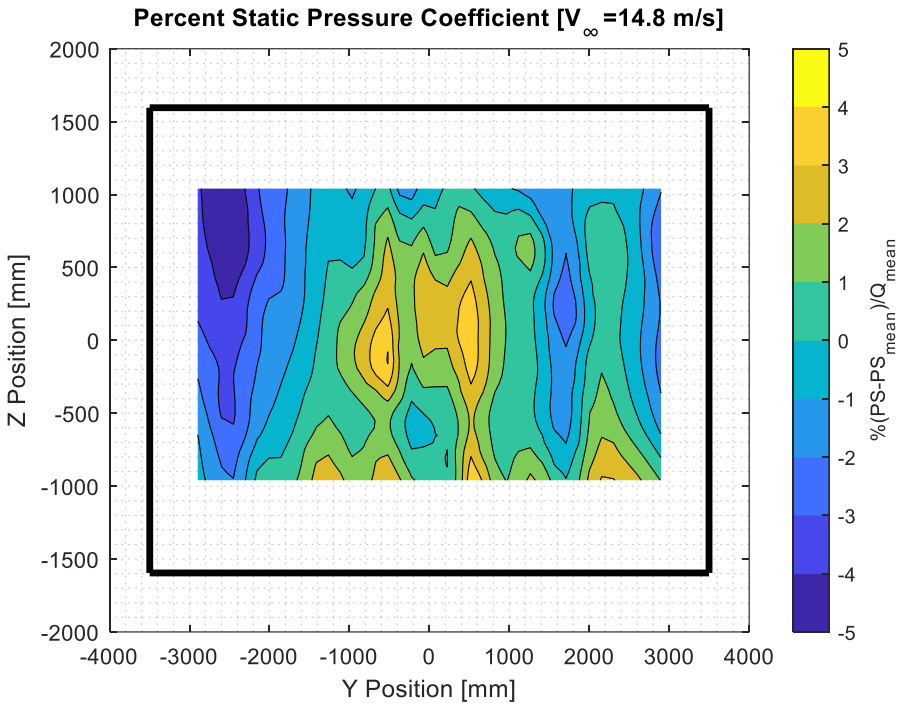

Figure 3.12 Static pressure variation of BLTS

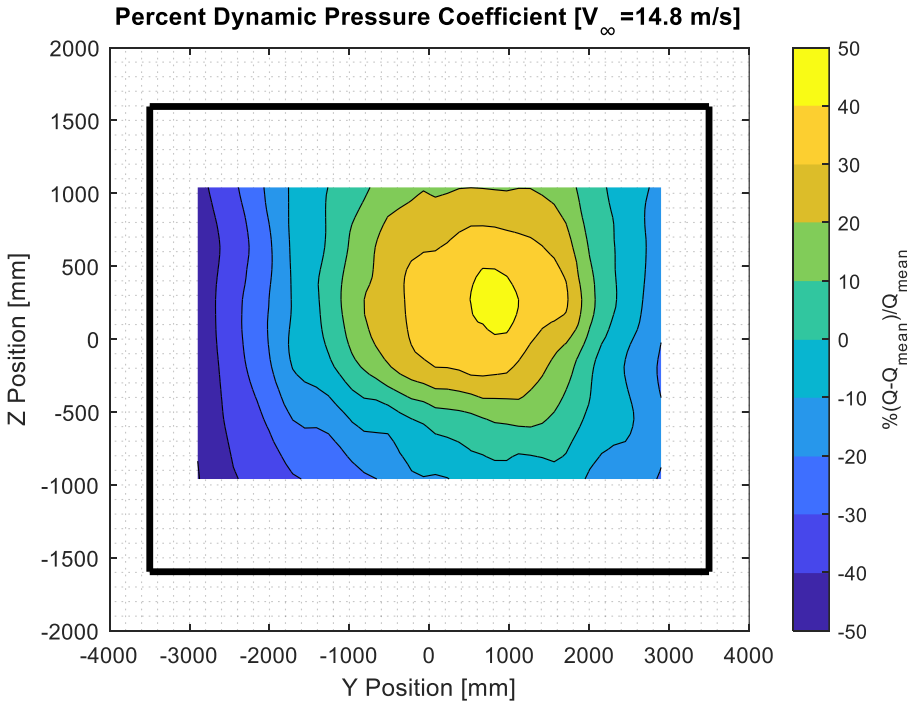

Figure 3.13 Dynamic pressure variation of BLTS

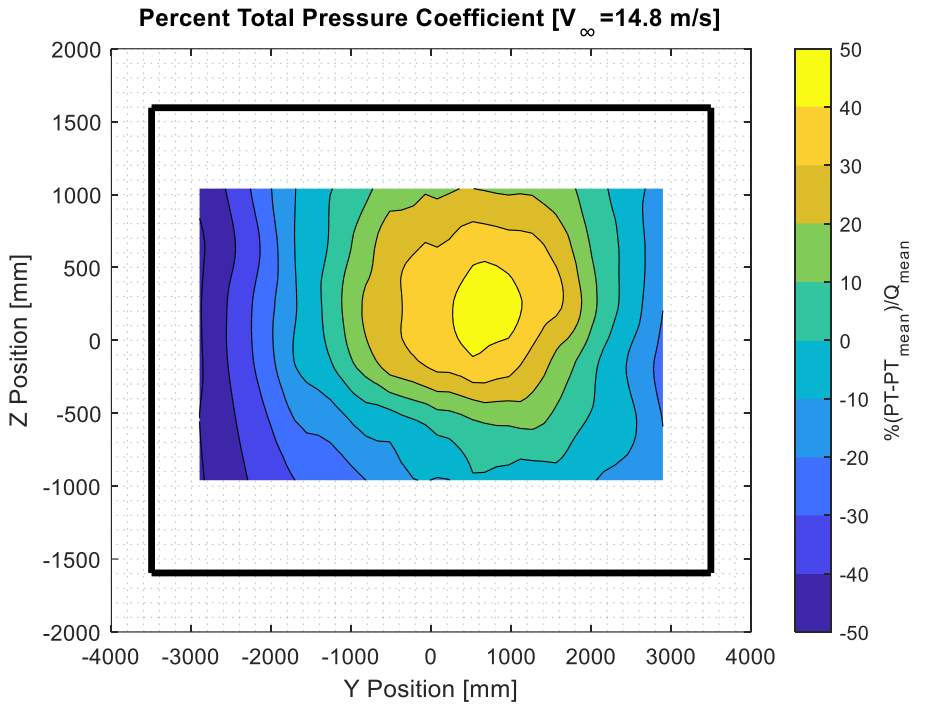

Figure 3.14 Total pressure variation of BLTS

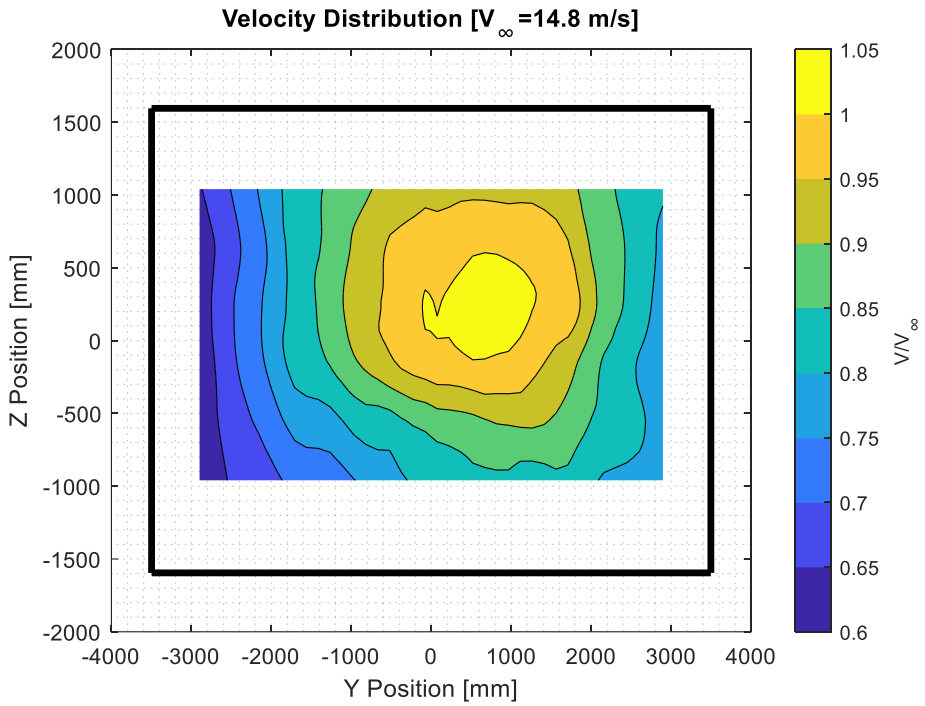

Figure 3.15 Velocity variation of BLTS

3.2.2 Aeronautical Test Section

The characteristic of the ATS of RÜZGEM large scale wind tunnel for various freestream velocities are given in following figures. Table 3.4 and Table 3.5 provide the details of the measurements. All measurements are provided as gauge pressures. During the experiments, the density of tunnel was acquired from tunnel logs and used as input for calculation of velocity. The data logs of tunnel are given in Figure 3.16. The graphs provide freestream velocity and density changing during the tests. The freestream velocity was defined as 35.1 m/s and 70.9 m/s and density was accepted as constant value of 1.034 according to the logs. These freestream velocity values were used for plane measurements. In these measurements, the rpm of tunnel was kept constant. On the other hand, the experiments were aimed to be performed exactly at 35 m/s and 70 m/s for the stability measurement at the center of the wind tunnel test section. However, the values of 34.9 m/s and 70.2 m/s were achieved instead of aims.

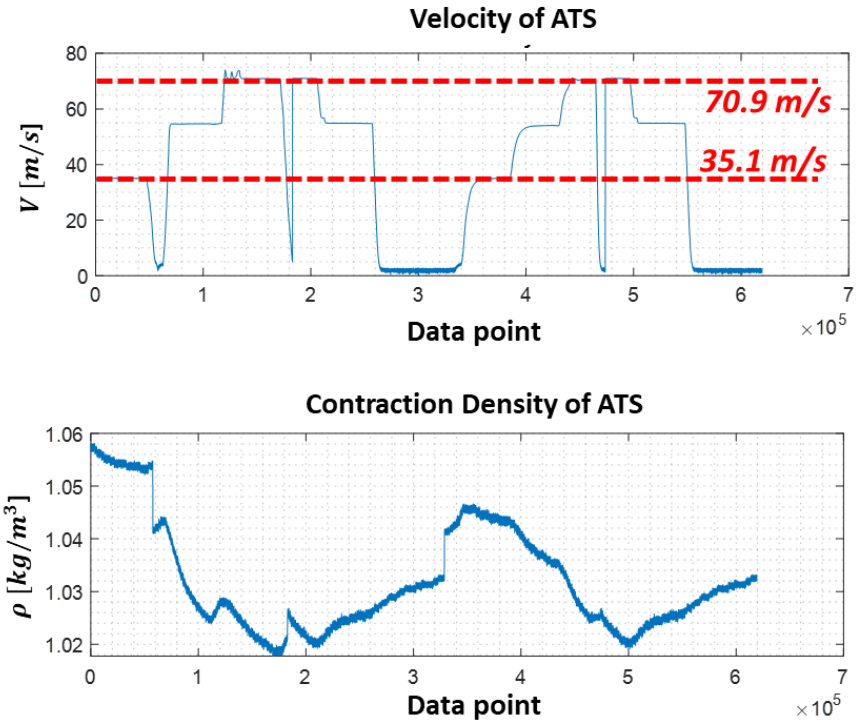

Figure 3.16 Tunnel log data during the characterization measurements of ATS

Table 3.4 Measurements at ATS for a freestream velocity of 35.1 m/s

	P_S [Pa]	P_T [Pa]	Q [Pa]	V [m/s]
Minimum	-75.5	544.6	580.7	33.5
Maximum	-25.5	562.7	622.0	34.7
Mean	-46.6	556.3	602.9	34.1
Standard Deviation	12.4	5.1	10.4	0.3

Table 3.5 Measurements at ATS for a freestream velocity of 70.9 m/s

	P_S [Pa]	P_T [Pa]	Q [Pa]	V [m/s]
Minimum	-279.6	2161.8	2313.0	66.9
Maximum	-98.2	2242.3	2504.3	69.6
Mean	-212.0	2208.2	2420.3	68.4
Standard Deviation	39.1	15.3	44.5	0.6

Similar with the BLTS stability measurements, 5 Hz low pass filter was applied to data. The dynamic stability of ATS is around ±1% and ±0.5% for 35.1 and 70.9 m/s freestream conditions (see details in Figure 3.17 and Figure 3.18). The higher dynamic pressure results in better stability at ATS. Figure 3.19 presents the results of the flow angularity measurements, as one could observe a pitch angle of around 3°. This is an unexpected observation for ATS. The bottom part of traverse system can cause this issue. A 2D simulation was performed to investigated the bottom part of traverse system. According to the 2D simulations, the level of 3° angle is due to blockage of traverse system regarding current position of probe. The whole plane has an upwash flow and the angle is decreasing with an increasing velocity. The measurement of pitch angle is evaluated as not proper. Figure 3.20, Figure 3.21, and Figure 3.22 the variation of static, dynamic and total pressure are provided respectively. The dynamic pressure and static pressure variations have identical contours. The Figure 3.23 gives the velocity distribution of ATS at a freestream of 35.1 and 70.9 m/s. In the velocity graph, the upper part of test section has nearly

same velocity with freestream and the velocity is decreasing near around wall and towards to the bottom. The velocity deviates 5% from freestream in ATS.

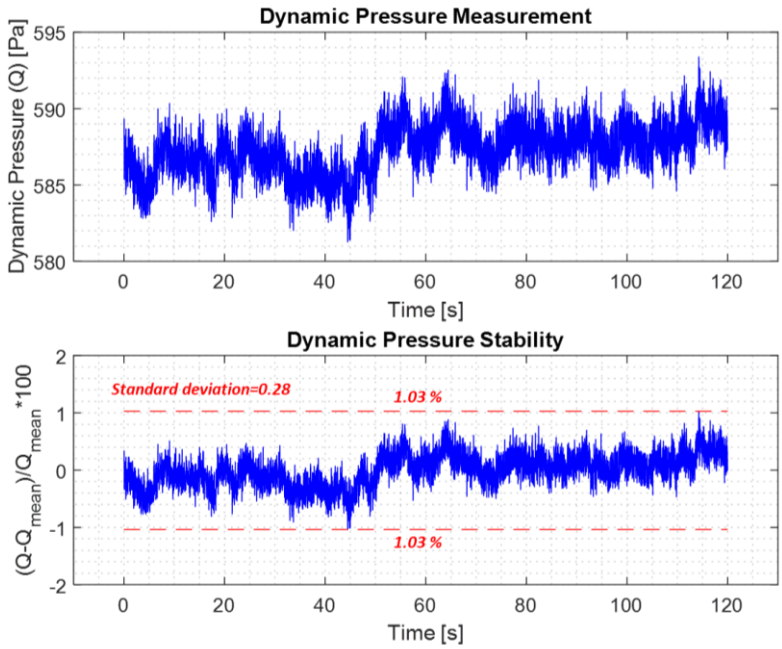

Figure 3.17 Dynamic stability results of ATS ($V_\infty = 34.9\, m/s$)

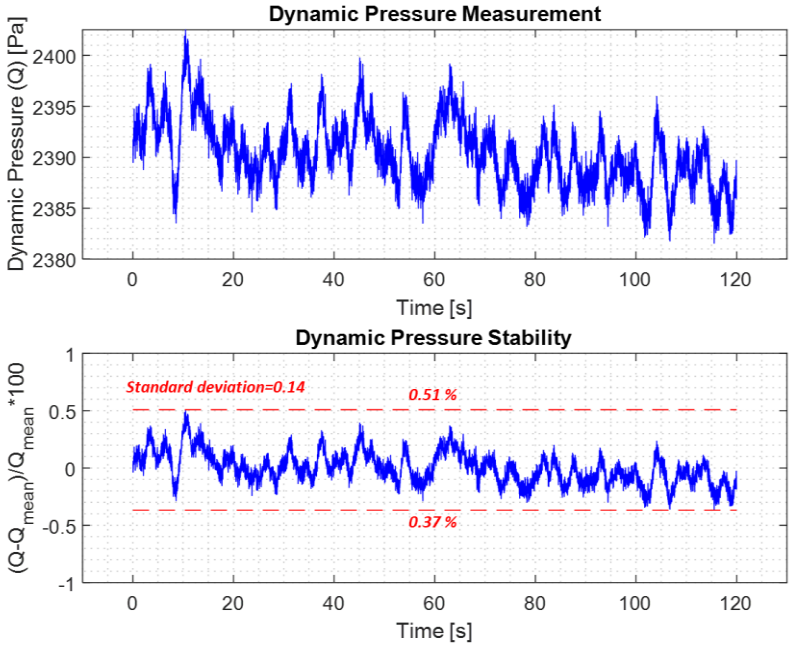

Figure 3.18 Dynamic stability results of ATS for ($V_\infty = 70.2\, m/s$)

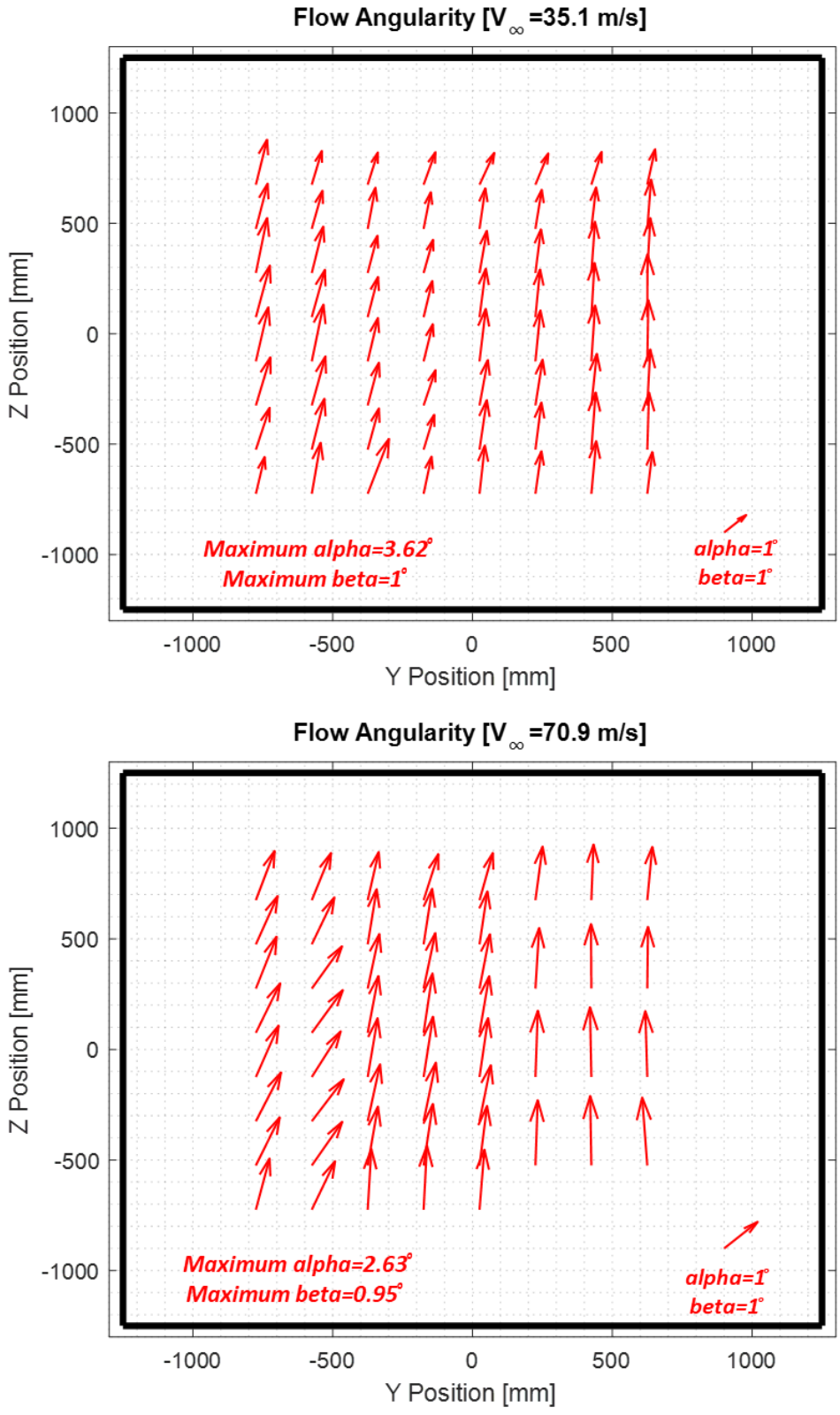

Figure 3.19 Flow Angularity of ATS

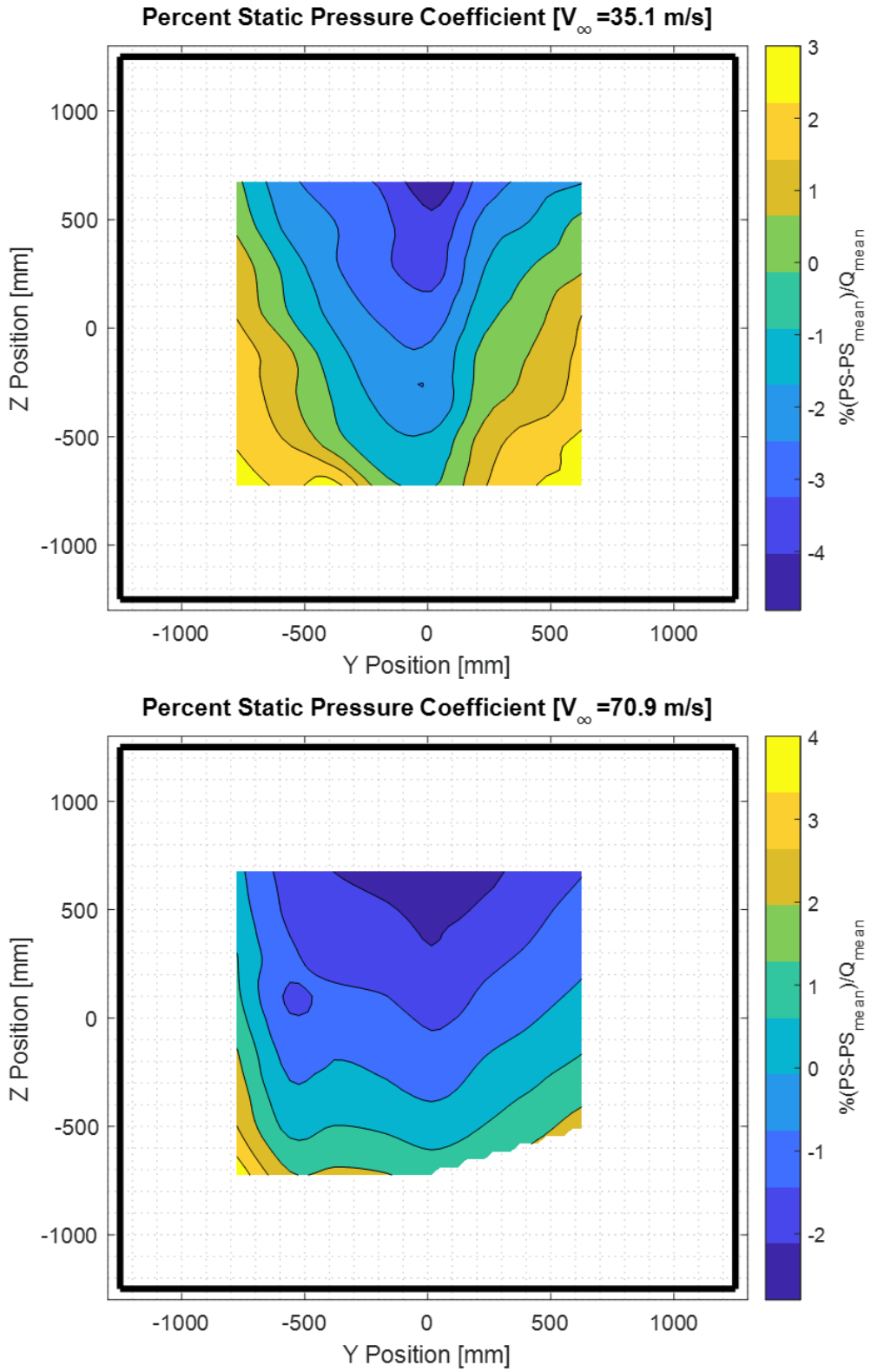

Figure 3.20 Static pressure variation of ATS

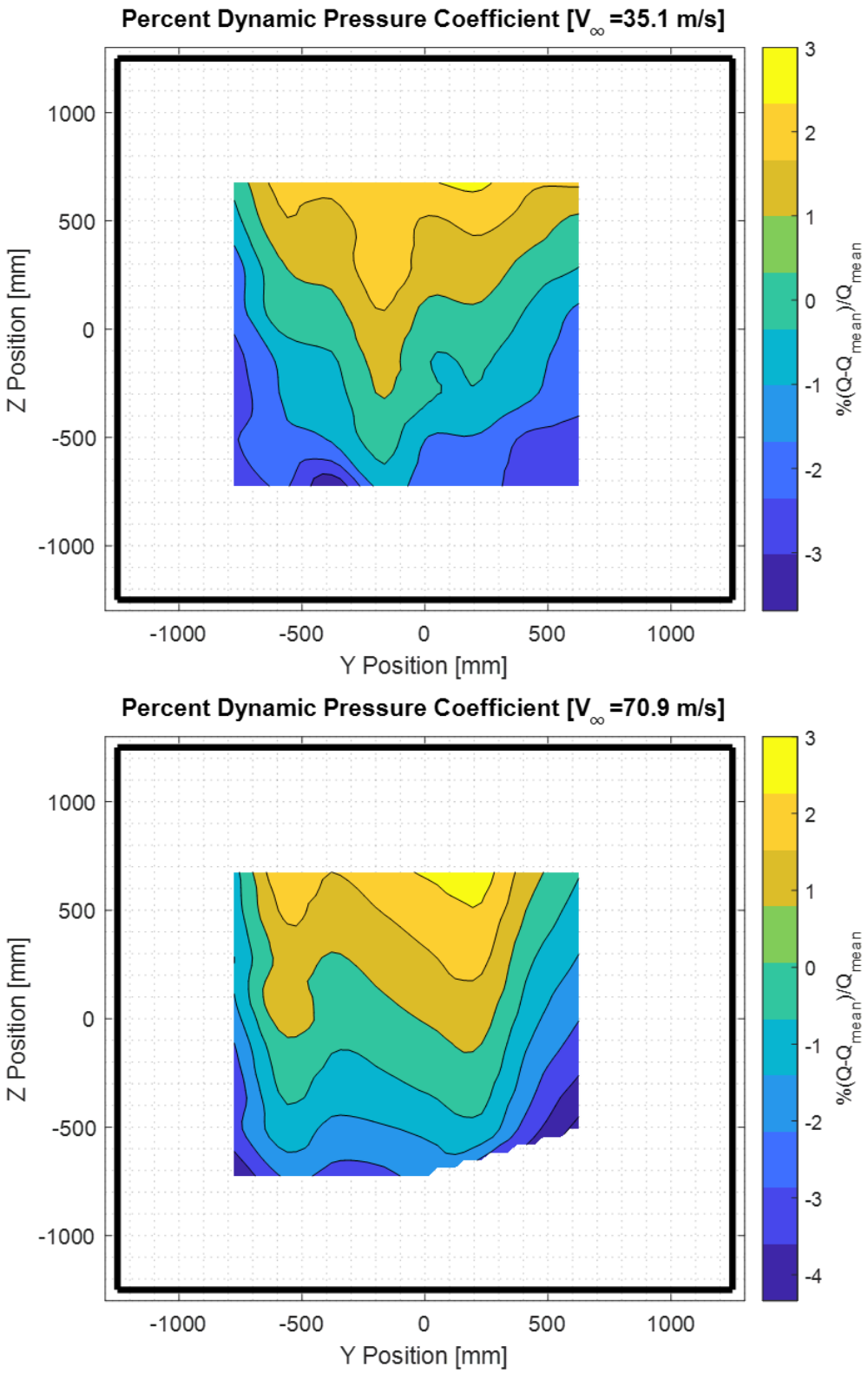

Figure 3.21 Dynamic pressure variation of ATS

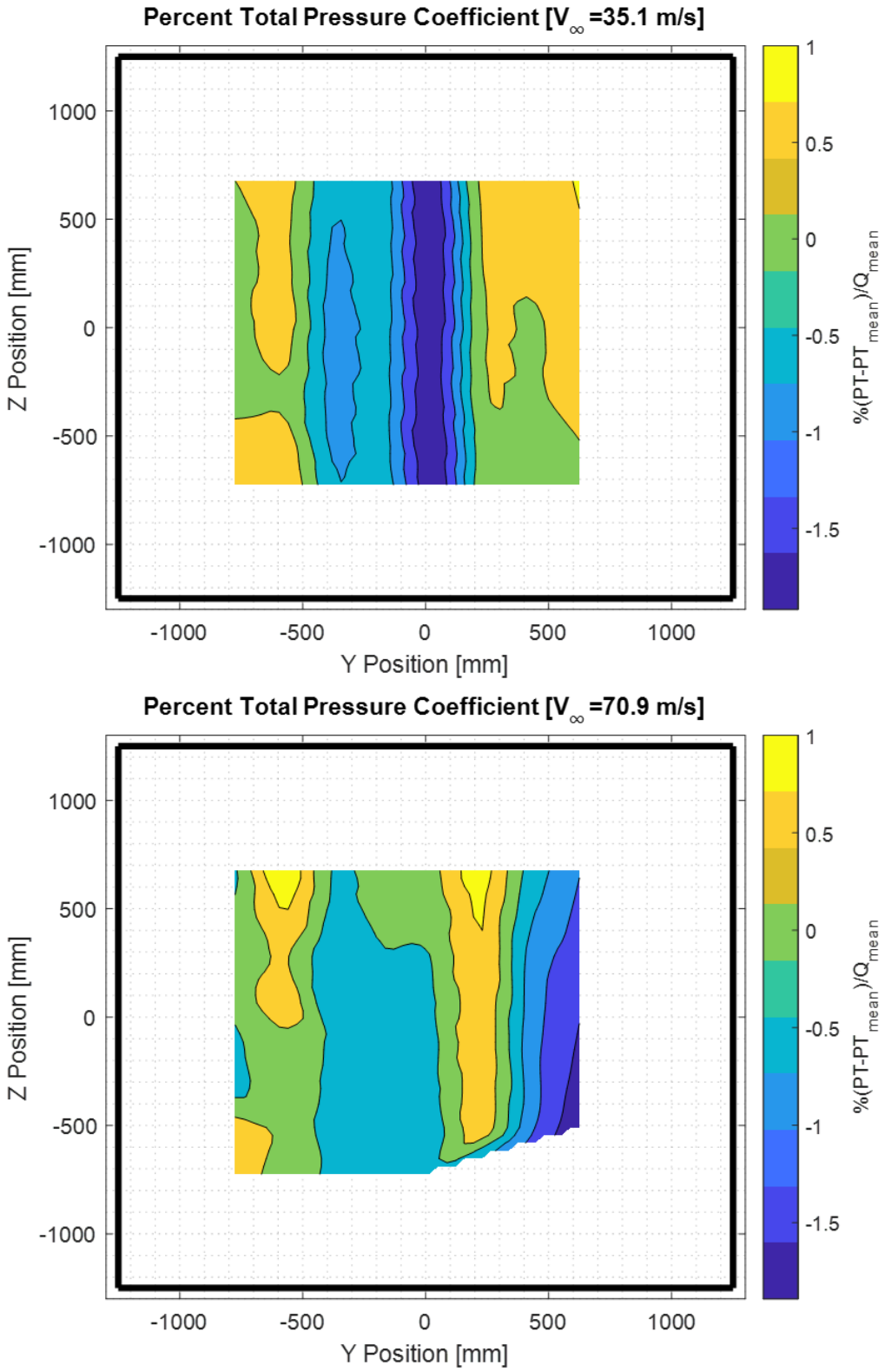

Figure 3.22 Total pressure variation of ATS

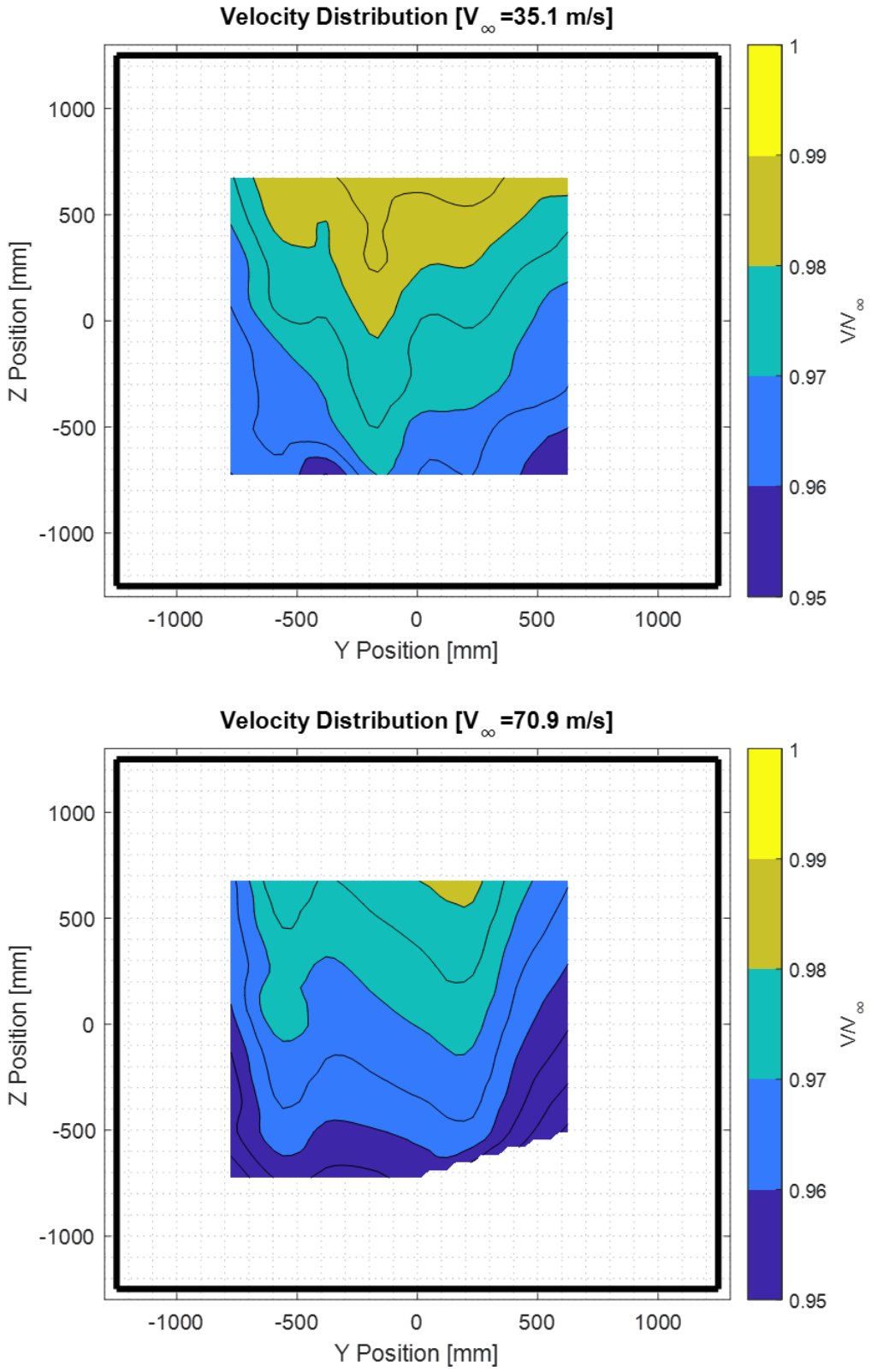

Figure 3.23 Velocity variation of ATS

The results of the flow angularity measurements showed that 3° pitch angle is observed in aeronautical test section due to blockage of bottom part of traverse system. In order to study the effect of traverse system, the measurements were repeated without traverse system, see Figure 3.8. The results are given in Table 3.6. Here the center of tunnel is represented as X=0, Y=0 and Z=0. Figure 3.24 provides the comparison between traverse system and support system measurements. Use of support system results with less pitch angle in the test section. However, there is still 2° pitch angle caused by support system. This experiment proves that bottom part of traverse system has an effect on measurements but the results do not provide true pitch angle measurements or reason of pitch angle in test section. A vertical support system from top wall to bottom wall can provide better results.

Table 3.6 Traverse system and support system angularity measurements

Test system	**X Position (axial)**	**Y Position (horizontal)**	**Z Position (vertical)**	**Velocity [m/s]**	**Alpha [deg]**	**Beta [deg]**
Traverse	0 mm	25 mm	-125 mm	34.1	3.02	-0.28
Traverse	0 mm	25 mm	-125 mm	52.9	2.49	-0.22
Traverse	0 mm	25 mm	-125 mm	68.4	2.23	-0.26
Support	1000 mm	0 mm	-160 mm	34.9	1.96	-0.38
Support	1000 mm	0 mm	-160 mm	56.1	1.89	-0.25
Support	1000 mm	0 mm	-160 mm	77.3	1.70	-0.21

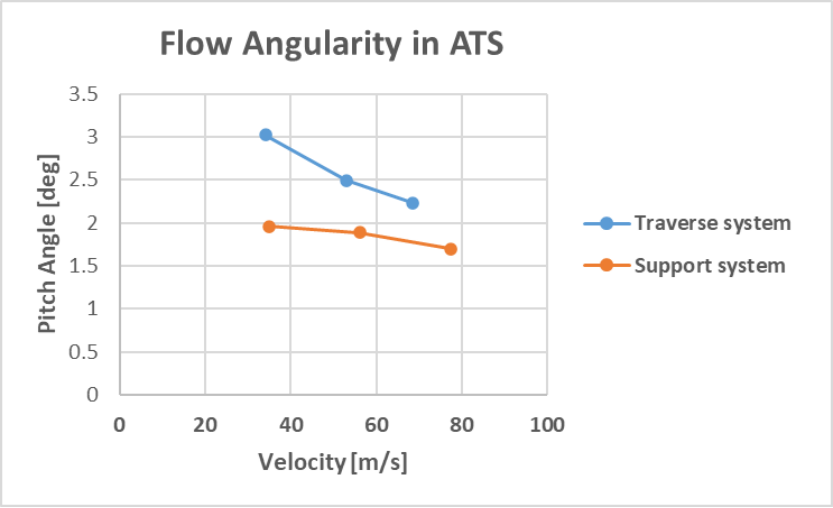

Figure 3.24 Flow angularity difference for traverse system and support system

CHAPTER 4

CONCLUSION

Within the scope of this study, necessary designs and equipment purchases were completed for the test execution of RÜZGEM large-scale wind tunnel characterization tests. Different conceptual traverse mechanisms were designed for the measurement, and their effects on the measurements were examined. It was observed that the use of rectangular support would affect the data acquired from the probes, so it was considered that an appropriate structure with a cross-section similar to and airfoil provides better results. The probe lengths were investigated in detail to determine the most suitable length. Aerodynamic simulations of the traverse system were performed, and expected errors and target probe lengths were shared. The measurement mechanisms and parameters are investigated for different wind tunnels in literature, and the parameters to be measured for RÜZGEM were determined.

The purpose of the BLTS is to execute boundary layer-related tests; its maximum velocity is 30 m/s. In this study, tests at a freestream velocity of 14.8 m/s were performed, and the results were obtained using a 5-hole probe in the BLTS. The dynamic stability of BLTS was measured as ±9% at a freestream of 14.8 m/s. The dynamic stability results of BLTS are nearly the same as uncertainty of the pressure scanner which is 10% for a dynamic pressure of 83 Pa. The measurements in the BLTS should be performed with use of a more sensitive pressure scanner. Pitch angle around 4° was noted. This is an unexpected result for the BLTS. Further investigation is required for pitch angle measurement. The velocity of the BLTS increases towards the center of the tunnel from wall of the test section and reaches the freestream value. Depending on position, a velocity deviation up to 60% should be expected for BLTS.

The purpose of ATS is to perform aeronautical tests, and its maximum velocity is 100 m/s. In this study, tests at a velocity of 35 m/s and 70 m/s were executed, and

the results were obtained using a 5-hole probe in the ATS. The dynamic stability of ATS is around ±1% and ±0.5% for 35.1 m/s and 70.9 m/s freestream conditions. The higher dynamic pressure results in better stability in ATS. The pitch angle around 3° was noted. This is an unexpected observation for ATS. A 2D simulation was performed to investigate the bottom part of the traverse system. According to the 2D simulations, blockage of the bottom part of the traverse system causes a 3° upwash angle around the current position of the probe. The whole plane has an upwash flow, and the angle decreases with an increasing velocity. The measurement of pitch angle is evaluated as not proper. The upper part of ATS has nearly the same velocity as the freestream. The velocity decreases near the wall and towards the bottom. Furthermore, the velocity deviates 5% from the ATS freestream for 35.1 m/s and 70.9 m/s. This study presents the preliminary results for the characterization measurement of the RÜZGEM large-scale wind tunnel. The preliminary measurements provide the opportunity to evaluate the pressure distributions and flow angles in the BLTS and ATS.

The bottom part of traverse system has a negative effect on measurements. Both two-dimensional simulations and measurements with strut type supports system show that the blockage caused by the bottom part of the traverse system affects the flow angle in the test section. For a future work, some suggestions are listed below:

- With this experimental setup, the tests were performed using FHP at a plane of ATS and BLTS of RÜZGEM large-scale wind tunnel. A detailed characterization of the RÜZGEM large-scale wind tunnel should be performed. This thesis states that the turbulent intensity and boundary layer measurements should be performed at various flow conditions and planes. For instance, in a previous study conducted by Abdulrahim [32] where numerical simulations were conducted to assess the boundary layer characteristics inside the BLTS in order to validate the CFD results, can be used as a reference.

- Over then 2-degree pitch angle at the defined plane was observed during the experiments. The reason for this flow should be investigated detailed. The blockage of the bottom part of the traverse system is considered as the main reason. For this purpose, different probe lengths can be tested, and if the upwash decreases, it can be concluded that the measurement of angles is not proper. It can be suggested that the measurements should be repeated without the bottom part of the traverse system, and the difference should be investigated.
- The probe lengths, traverse system geometry and cable channels are more definite currently. To understand the effect of traverse system, CFD simulations can be repeated with detailed geometry.

REFERENCES

[1] https://www. 19fortyfive.com/2021/03/f-16xl-the-super-fighter-the-u-s-air-force - passed-on/, 02.09.2022,18:30

[2] https://www.19fortyfive.com/2021/03/f-16xl-the-super-fighter-the-u-s-air-force -passed-on/, 02.09.2022,18:30

[3] https://www.researchgate.net/figure/The-model-wind-turbine-in-the-wind-tunnel-NTNU_fig1_273898860, 02.09.2022,18:30

[4] https://www.researchgate.net/figure/The-model-wind-turbine-in-the-wind-tunnel-NTNU_fig1_273898860, 02.09.2022,18:30

[5] https://www.researchgate.net/figure/The-model-wind-turbine-in-the-wind-tunnel-NTNU_fig1_273898860, 02.09.2022,18:30

[6] https://www.autoevolution.com/news/automotive-wind-tunnels-making-aerodynamic-cars-23250.html, 02.09.2022,18:30

[7] Melanson M., Arrington A., Cahill D., Best Practices in Wind Tunnel Testing, AIAA Professional Development Course, January 2015.

[8] Melanson M., AIAA Aerospace Sciences Meetings and Exhibit, AIAA-2008-830-483, 7-10 January 2008, Reno, Nevada

[9] Barlow J. B., Rae W. H. and Pope A., Low Speed Wind Tunnel Testing, 3rd Edition, John Wiley and Sons, Hoboken, 1999.

[10] https://www.researchgate.net/figure/Schematic-of-the-University-of- Leeds-UoL-closed-loop-wind-tunnel-system_fig6_267868149, 02.09.2022,18:30

[11] https://www.researchgate.net/figure/School-of-Mechanical-Engineering-USM-open-circuit-wind-tunnel_fig2_233706255, 02.09.2022,18:30

[12] https://www.autoevolution.com/news/automotive-wind-tunnels-making-aerodynamic-cars-23250.html, 02.09.2022,18:30

[13] Anderson J. D., Fundamentals of Aerodynamics, Sixth Edition, McGraw-Hill Education, 2017

[14] AIAA R-093-2003 Recommended Practice, Calibration of Subsonic and Transonic Wind Tunnels, 2003

[15] Lincoln P. Erm, Calibration of the Flow in the Test Section of the Low-Speed Wind Tunnel at AMRL, DSTO-TR-1073, November 2000

[16] Owen K. and Owen A., Measurement And Assessment Of Wind Tunnel Flow Quality, Progress in Aerospace Sciences journel, 10 July 2008

[17] Yeager W.T, Jr., Wilbur M. L. and Mirick P. H., Flow Angularity Measurements in the NASA-Langley Transonic Dynamics Tunnel, NASA/TM-2005-213946, December 2005

[18] Santos C., Jabardo P. J. S., Cardoso M., Taira N.M., Pereira M.T, Characterızatıon Of Low Turbulence Wınd Tunnel, XVIII Imeko World Congress Metrology for a Sustainable Development, September, 17 – 22, 2006, Rio de Janeiro, Brazil

[19] Arnette S. A. Et al, AIAA 2000-0290 Aerodynamic Commisioning Result for the Korea Aerospace Research Instute Low Speed Wind Tunnel, 38th Aerospace Sciences Meeting and Exhibit, 10-13 January 2000, Reno, Nevada

[20] Pope A., Wind Tunnel Calibration Tecqhniques, AGARDograph 54, April 1961

[21] Heely D., Understanding Pressure and Pressure Measurement, AN1573 Rev- 1, 05/2005

[22] Saad M. A., Compressible Fluid Flow, Prentice-Hall, 1985

[23] Vincent T. G., Total Temperature Probe Performance for Subsonic Flows using Mixed Fidelity Modeling, Virginia Polytechnic Institute and State University, March 25, 2019, Virginia

[24] Thangadurai M., Sonu A.K., Singh M., Subhendr*, Kumar V, Singh R.P., Chatterjee P.K., Measurement Of Tubulence Statıstıcs Usıng Hot Wıre Anemometry, DOI: 10.13140/2.1.1178.9768, January 2014

[25] Morrison G.L., Schobeiri M.T., Pappu K.R., Five-hole pressure probe analysis technique, Mechanical Engineering Department, Texas A&M University, June 1998

[26] Town J., Camci C., Sub-Mınıature Fıve-Hole Probe Calıbratıon Usıng A Tıme Effıcıent Pıtch And Yaw Mechanısm And Accuracy Improvements, Proceedings of ASME Turbo Expo Turbine Technical Conference, DOI: 10.1115/GT2011-46391, June 6-10 2011, Vancouver, Canada

[27] https://www.researchgate.net/figure/A-conventional-triple-hot-wire-sensor-with-typical-dimensions-The-normal-wire-diameter_fig2_282975488/download, 02.09.2022,18:30

[28] Bui, T. T., Oates D. L. and Gonsalez J.C., Design and Evaluation of a New Boundary-Layer Rake for Flight Testing, NASA/TM-2000-209014, National Aeronautics and Space Administration, January 200

[29] Schlighting H., Boundary-Layer Theory, Seventh edition, McGRAW-HILL, 197

[30] Perçin M. and Uzol O., Mühendis ve Makine Dergisi, October 2019, pp 4751

[31] http://ruzgem.metu.edu.tr//system/files/tunelbilgi.pdf, 03.01.2021

[32] Abdulrahim A. 2022 Effects of inflow boundary layer on the wake characteristics of a radially non-uniform porous disc Doctoral dissertation (Ankara: Middle East Technical University).

APPENDIX A

L SHAPE AND STRAIGHT PROBES

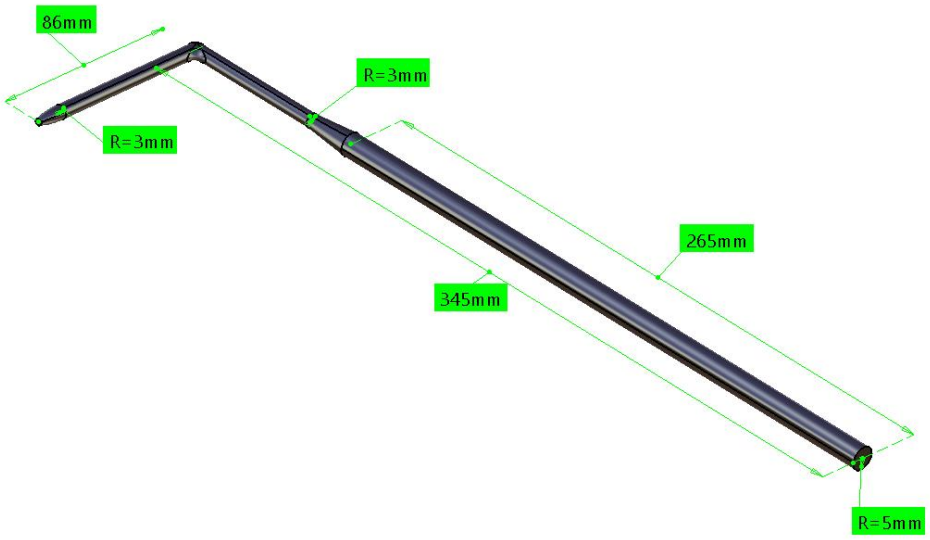

Figure A.1 “L” shape probe dimensions

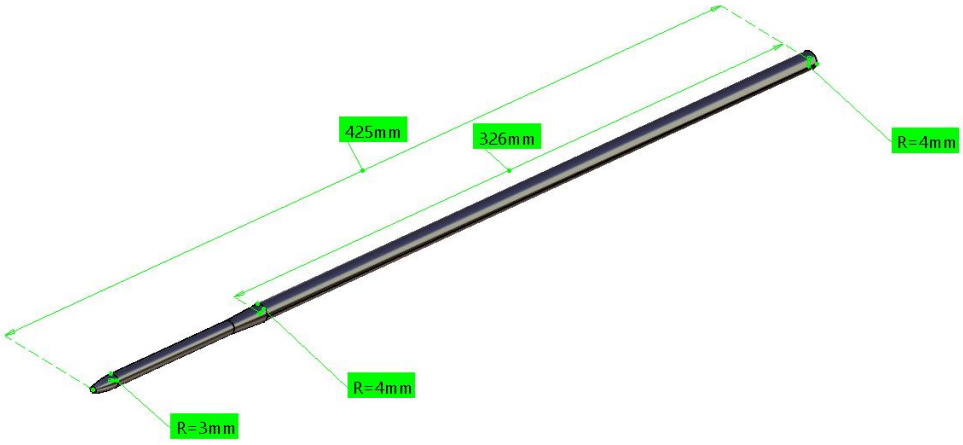

Figure A.2 Straight probe dimensions